Large scale *in vivo* recordings of dentate gyrus granule cells during trace eyeblink conditioning

Dissertation

zur

Erlangung des Doktorgrades (Dr. rer. nat.)

der

Mathematisch-Naturwissenschaftlichen Fakultät

der

Rheinischen Friedrich-Wilhelms-Universität Bonn

vorgelegt von

Fabian Distler

aus

Köln

Bonn, Juni 2023

Angefertigt mit Genehmigung der Mathematisch-Naturwissenschaftlichen Fakultät

der Rheinischen Friedrich-Wilhelms-Universität Bonn

Gutachter 1: Prof. Dr. Heinz Beck

Gutachter 2: Prof. Dr. Michael Pankratz

Tag der Promotion: 05.12.23

Erscheinungsjahr: 2024

Acknowledgments

I would like to express my deepest gratitude to my first supervisor, Prof. Dr. Heinz Beck, for his unwavering support throughout this project. He provided me with a lot of freedom to pursue my ideas and offered valuable feedback and guidance at every stage of the process. I have learned a great deal from his expertise and am grateful for his mentorship.

I would also like to thank my second supervisor, Prof. Dr. Michael Pankratz, for his insightful feedback and thought-provoking questions that helped me to refine my ideas and methodology.

I also thank the members of my IMPRS thesis advisory committee, Prof. Dr. Cristian Henneberger, Prof. Dr. Tobias Rose, and Dr. Marcel Oberländer, for their valuable feedback and advice throughout the project.

Special thanks go to Dr. Martin Pofahl, who trained me in dentate gyrus imaging and wrote most parts of the imaging readout pipeline, network event detection, and cell tracking algorithm. His expertise and guidance were invaluable to the success of this project.

I am also grateful to Dr. Kurtulus Golcuk, who wrote the program for the blink detection and CR readout and helped to set up a head-fixed variant of tEBC.

I extend my appreciation to André Haubrich for his support with the virus injections and fiber implantations for the inhibition experiments and his contribution to the experimental design of the inhibition experiments. I also thank Elisa Fernández, who did the surgeries, histology, and behavioral experiments for the inhibition cohorts.

I also thank Dr. Oliver Braganza for proposing the idea to try combining tEBC with dentate gyrus imaging experiments and for his contributions to the experimental design, statistics questions, and overall scientific support.

I would like to thank Olga Zabashta for her work in histology for the imaging cohorts and Dr. Nicola Masala for being great company during the lonely lab days during the Covid lockdown and for providing additional animals that were not included in this thesis. I also thank Dr. Negar Nikbakht for sharing her wisdom about behavioral experiments and surgeries with me and for providing animals to establish the head-fixed tEBC task.

I am grateful to Margit Reitze and Nicole Schönfelder for always having an open ear and their tremendous support with administrative tasks and orders. I would also like to thank Lea Keller for doing a great job with breeding the needed animals.

I thank Kristian Reichelt for providing IT support while pretending my bad jokes are actually funny.

I owe a debt of gratitude to Dr. Tony Kelly and Dr. Thoralf Opitz, whose experience, advice, and humor were really important to me.

I want to thank the Beck Group for creating a great working environment that made my time here a memorable experience.

I am grateful to Ezgi Bulca for always being there to help and for her outstanding support in career planning and project management questions.

I thank everyone in IMPRS for Brain and Behavior for creating a stimulating and supportive environment for my Ph.D.

I am also grateful to Eike Töllner and Uli Arenbeck who were a huge support with figure design and text formatting.

Finally, I thank my family and friends for their constant support and encouragement throughout my Ph.D. journey.

Abstract

The dentate gyrus (DG) is known to play a role in associative learning, but the precise contribution of individual granule cells (GC) to this process remains unclear. In this study, we established a head-fixed trace eyeblink conditioning (tEBC) task that enabled simultaneous calcium imaging of the DG GC population to investigate their role in learning.

Using longitudinal tracking of individual cells, we identified specific stimuli responses in a subgroup of the imaged GC population that were higher than chance but found that these responders were relatively unstable over time. Moreover, we observed sizeable synchronous population activity of the dentate GCs, referred to as network events, which grew in size during training sessions and had a significantly higher proportion of task-responding cells compared to nonresponders during late learning. Responder cells were also more likely to participate in network events with other responder cells.

To address critical questions regarding the role of the DG in tEBC, we investigated the necessity of the DG GCs and examined how task-associated activity and synchronous offline activity changed during learning. Our results demonstrated that the DG GCs are essential for tEBC and that the activity of these cells changes over time, with synchronous offline activity increasing during training sessions.

Overall, this study provides novel insights into the role of the DG GCs in associative learning, highlighting the importance of network events and individual cell responses during tEBC. The findings contribute to a better understanding of the neural mechanisms underlying associative learning and have implications for developing therapies for disorders affecting learning and memory.

Content

1 Introduction

Among the last big questions in neuroscience are how the biological basis of behavior and memory are composed (Kandel et al. 2000). How can millions of neurons enable us to learn new tasks and help us remember, for instance, what we ate at our favorite restaurant yesterday? One of the underlying brain structures crucial for memory is the hippocampal formation (Andersen 2007, pp. 4–5; Scoville and Milner 1957; Squire 1998, 2004; Bliss and Lømo 1973; O'Keefe 1976). Not only is the hippocampus involved in spatial learning, but it also seems to provide a neural basis for associative learning and linking temporal segregated stimuli (Andersen 2007, p. 539; Modi et al. 2014; Tseng et al. 2004; Miller et al. 2022; Moyer, JR et al. 1996; Matthew D. McEchron and John F. Disterhoft 1997).

The DG is seen as the first processing step of the hippocampal formation. This makes the DG an exciting region to study. Besides its function during spatial learning, the DG is essential for discriminating similar inputs (pattern separation) (Kesner 2013b, 2018; Kesner et al. 2015; Rolls and Kesner 2006; Treves et al. 2008; Rolls 2013b; Marr 1971). Pattern separation is the process in which a network forms distinct representations from similar inputs (van Dijk and Fenton 2018; Leutgeb et al. 2007; Rolls 2013b).

During the last two decades, more evidence emerged, indicating a role of the DG in sequence learning and associative conditioning (Scharfman 2007a, pp. 574–575; Miller et al. 2022; Kimberly M. Christian and Richard F. Thompson 2003; Miller et al. 2019; Madroñal et al.). However, most of these studies recorded data from a few DG cells and could not track them over days. Further research is needed to elucidate how the DG facilitates associative learning on a population level. The current gap in understanding poses the need for data from larger populations of dentate principal cells during an associative learning task over days.

A well-established model of associative learning is classical eyeblink conditioning. This paradigm uses paired presentations of a conditioned stimulus (CS, e.g., a tone) and an unconditioned stimulus (US, e.g., an air puff to the cornea). Eventually, the animal develops a conditioned response and starts blinking to the previously neutral CS (Takehara-Nishiuchi 2018; Woodruff-Pak and Disterhoft 2008; Kimberly M. Christian and Richard F. Thompson 2003). Classical eyeblink conditioning relies on computations in the cerebellum (Yeo and Hesslow 1998). Learning-related activity has been found in the neostriatum, thalamus, trigeminal nucleus, and other brain stem areas (Steinmetz 2000; Clark and Lavond 1996; Desmond and Moore 1991; Sears et al. 1996; White et al. 1994). This task becomes hippocampus-dependent when a stimulus-free trace period is introduced between conditioned and unconditioned stimuli. This paradigm is called tEBC (Moyer et al. 2015; Walker and Steinmetz 2008; Tseng et al. 2004; Weiss et al. 1999). It has been shown that the DG plays a vital role in this behavioral task (Nokia et al. 2017; Madroñal et al. 2016; Miller et al. 2019, 2022; Suter et al. 2018). Nevertheless, it

remains unclear what the exact computational function of the DG during tEBC is. A better understanding of the mechanisms involved in associative learning in the hippocampus can serve as a model to better understand the effects of drugs, age, and disease on learning and memory.

1.1 The hippocampal formation

The hippocampal formation has been the focus of many studies over the last decades (Andersen 2007, p. 3). In a famous case study, Patient H.M. received a bilateral temporal lobectomy. This intervention included the removal of the hippocampal formation. After the surgery, H.M. developed anterograde and limited retrograde amnesia (Andersen 2007, p. 3; Scoville and Milner 1957). This generated significant interest in the involvement of the hippocampal formation in memory. Since the early days of hippocampal research, different key features of hippocampal formation have been unrevealed. Tolman introduced the concept of the hippocampal formation serving not only as a spatial but a cognitive map. He hypothesized the hippocampal formation to be an integrative outline combining different environmental information types (Tolman 1948). Subsequently, so-called place cells in the hippocampus were found. These cells encode specific environmental locations (O'Keefe 1976; Morris et al. 1982). Novelty detection and memory of facts are associated with the hippocampal formation (Strange et al. 1999). Additionally, spatial navigation (Buzsáki and Moser 2013) and time coding (Eichenbaum 2014) were investigated. More details will be presented in the following chapters.

The hippocampal formation is part of the temporal lobe and consists of different brain regions. These are the hippocampus proper (with its subdivisions CA1, CA2, and CA3), DG, subiculum, presubiculum, parasubiculum, and entorhinal cortex (EC) (Amaral 1999; Amaral and Witter 1989). There are three main fiber pathways in the hippocampal formation. First, the angular bundle conveys information from the EC to the other parts of the hippocampal formation. The fimbria-fornix pathway forms connections to the basal forebrain, hypothalamic, and brain stem regions. Lastly, the dorsal and ventral commissures connect the hippocampal formation of both hemispheres (Andersen 2007, p. 44; Amaral and Witter 1989)
There are differences in the volume and thickness of the hippocampus in humans compared to other species like rats. However, the hippocampal formation has high structural similarity across phylogeny. Humans, monkeys, and rats all share the same basic hippocampal architecture (Andersen 2007, p. 39; Burwell and Witter 2002; Burwell et al. 1995; Gertz et al. 1972; Amaral and Witter 1989).

1.1.1 Functional anatomy of the hippocampal formation

The so-called trisynaptic circuit describes the main flow of information in the hippocampal formation. The different stations of this connection are the EC, DG (synapse 1), CA3 (synapse 2), and CA1 (synapse 3) (Andersen et al. 1971; Andersen et al. 1966). The EC can be seen as the first station of information flow since most of the neocortical input reaching the hippocampus passes through it **(**Figure 1**-1)**. Originating in the superficial layers of the EC, the perforant path forms a unidirectional input into the DG (Witter 2007b; Andersen 2007, pp. 38–39). The axons of the DG GCs, so-called mossy fibers, form strong projections onto the pyramidal cells of the CA3 subfield (Andersen 2007, pp. 38–39; Amaral et al. 2007). While initially thought to be unidirectional, more and more studies report a back-projection from CA3 to the DG (Swaminathan et al. 2018; Sun et al. 2017; Vivar et al. 2012; Wittner et al. 2007; Kneisler and Dingledine 1995a; Li et al. 1994). The CA3 pyramidal cells form the primary input to the CA1 subfield, called the Schaffer collateral axons (Witter 2007a). The CA1 field projects to the subiculum and EC. Hereafter, the subiculum gives rise to inputs to the pre-, and parasubiculum and closes the hippocampal loop by also connecting to the EC (Andersen 2007, pp. 38–39; Amaral and Witter 1989). While hippocampal connectivity has more intricacies, this serves as a general overview.

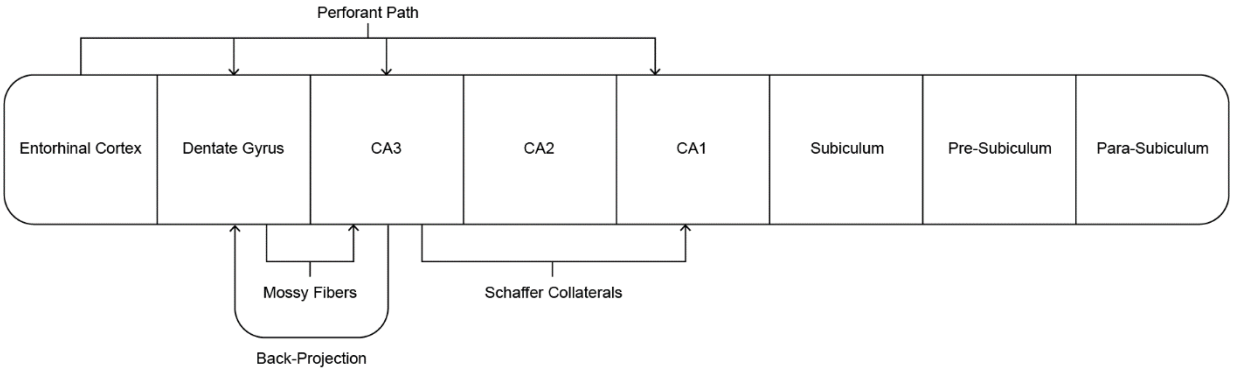

Figure 1-1: Simplified circuit of the hippocampal formation (Andersen 2007, p. 38). Overview of how the different parts of the hippocampal formation are connected.

1.2 The dentate gyrus

The DG is a „V“, or „U“ shaped cortical region with three laminae. Structurally, the DG is not typically divided into subregions. It has a similar structure in all levels of the hippocampal formation (Andersen 2007, pp. 42–43; Amaral and Witter 1989). However, more recent work points to differences along the long axis of the hippocampal formation (Strange et al. 2014). The three layers of the DG are the molecular layer, the granule cell layer, and the polymorphic layer, or hilus. Mostly cell-free, the molecular layer contains the dendrites of the principal cells, the dentate GCs. Furthermore, the perforant path fibers originating in the EC terminate here. The granule cell layer is densely packed with GCs. The cell bodies of the dentate pyramidal basket cells can be found at the border of the granule cell layer and polymorphic layer. In the polymorphic layer, the second principal cell type, the dentate mossy cells, have their somata (Amaral et al. 2007; Scharfman 2016).

1.2.1 Cell types of the dentate gyrus

The dentate GC is elliptical with an approximate diameter of 10 µm in the rat (Amaral et al. 2007; Claiborne et al. 1990). Neurogenesis of adult-born GCs can be found in most mammalian species during adulthood, including humans. One exception are cetaceans like whales (Amaral et al. 2007; Patzke et al. 2015; Hainmueller and Bartos 2020; Spalding et al. 2013; Charvet and Finlay 2018). There are about 500.000 GCs per hemisphere in the murine brain (Bonthius et al. 2004).

The axons of the dentate GCs, the mossy fibers, form glutamatergic projections to the CA3 subregion and the polymorphic layer (Amaral et al. 2007; Claiborne et al. 1986; Gaarskjaer 1986; Blackstad et al. 1970). In the rat, each GC forms a single mossy fiber that connects to 11-15 CA3 pyramidal cells. Additionally, they connect to a similar number of mossy cells and about 100-150 hilar GABAergic interneurons (Hainmueller and Bartos 2020; Acsády et al. 1998). The ratio of GCs to CA3 pyramidal cells is estimated to be around 12:1 at septal levels and around 2:3 at the temporal pole (Amaral et al. 2007; Gaarskjaer 1978). Dentate GCs exhibit very sparse activity with rates from 0.01–0.48 Hz (Jung and McNaughton 1993; Senzai and Buzsáki 2017).

The dentate mossy cell is the second principal cell type in the DG. They are larger than GCs (25-35 µm) and of triangular or multipolar shape. Dendritic branches of mossy cells are mostly confined to the polymorphic layer but sometimes enter the molecular layer (Amaral et al. 2007; Scharfman 2016, 2018). Rarely, mossy cell axons can enter the CA3 region, but a monosynaptic connection between mossy cells and CA3 has not been found (Soltesz et al. 1993; Hainmueller and Bartos 2020). A hallmark characteristic of the mossy cells are the so-called thorny

excrescences. These are large and complex spines covering their proximal dendrites (Amaral et al. 2007; Scharfman 2018).
The inner molecular layer gets exclusive input from neurons in the polymorphic layer, including the mossy cells. In the rat and mouse, this input stems from both hemispheres and is called the associational/commissural projection. The commissural portion of this connection does not seem to exist in the primate brain (Amaral et al. 2007; Amaral and Witter 1989). Since mossy cells are immunoreactive for glutamate, the associational/commissural projection is deemed excitatory (Soriano and Frotscher 1994; Scharfman 1994, 1995).

The dentate pyramidal basket cells are inhibitory interneurons that reside at the border of the granule cell and polymorphic layer. They are about the same size as mossy cells. Pyramidal basket cells form inhibitory contacts with the apical dendrites of GCs. One basket cell is assumed to influence up to 1% of the total GC population (Amaral et al. 2007; Sik et al. 1997; Struble et al. 1978).

Other dentate cells include the so-called MOPP (molecular layer perforant path-associated cell) and the axo-axonic cell in the molecular layer (Amaral et al. 2007; Soriano and Frotscher 1989; Freund and Buzsáki 1996). In the polymorphic layer are different fusiform cells. These include the HIPP (hilar perforant path-associated cell) cells and HICAP (hilar commissural-associational pathway-related cell) cells (Amaral et al. 2007; Freund and Buzsáki 1996). Hilar interneurons of the DG are generally very diverse (Sik et al. 1997; Hainmueller and Bartos 2020; Hosp et al. 2014; Freund and Buzsáki 1996).

1.2.2 Afferent and efferent information flow in the dentate gyrus

The dorsal DG receives inputs from all sensory modalities via the perirhinal and lateral entorhinal cortex (LEC) (Hargreaves et al. 2005; Wang et al. 2018; Deshmukh and Knierim 2011; Woods et al. 2020). Additionally, input from the medial entorhinal cortex (MEC) sends spatial information from entorhinal grid cells (Kesner 2018, p. 5; Rolls and Kesner 2006; Hafting et al. 2005; Moser et al. 2008). The medial perforant path (MPP) forms the primary input to the DG, predominantly arising from layer II neurons in the EC. A minority of this projection origins in layers V and VI of the EC (Amaral et al. 2007; Deller et al. 1996; Steward and Scoville 1976). Entorhinal inputs to the DG are restricted to the outer two-thirds of the molecular layer. Furthermore, the perforant path can be subdivided into a lateral perforant path (LPP) and MPP, stemming from the LEC and MEC, respectively. The LPP arrives at the most superficial layer of the molecular layer and the lateral part in the middle molecular layer (Amaral et al. 2007; Amaral and Witter 1989). Presumably, the medial perforant part contains spatial and the lateral part non-spatial (e.g., objects, odors) information (Scharfman 2007a, p. 567; Strange et al. 2014; Hargreaves et al. 2005; Høydal et al. 2019). The MPP relies on NMDA receptors. The LPP

information is partially conveyed by opioid receptors (Kesner 2018; Hargreaves et al. 2005; Witter et al. 1989; Bramham et al. 1988).

There is increasing evidence for a back-projection from CA3 to the DG. This projection runs in the opposite direction of the mossy fibers. It has been shown to form connections with hilar inhibitory neurons and mossy cells (Kneisler and Dingledine 1995b; Swaminathan et al. 2018; Ishizuka et al. 1990; Li et al. 1994; Wittner et al. 2007; Vivar et al. 2012; Sun et al. 2017; Shi et al. 2019). Even though there seems to be strong evidence for the anatomical presence of this back-projection, its physiological and behavioral functions remain elusive. In 1994, Li et al. injected biocytin into CA3 pyramidal cells *in vivo* using adult rats. They found collaterals of CA3 pyramidal cells in the polymorphic layer. This was the case for all parts of CA3 (be it CA3a, b, or c). This being said, the most proximal part of CA3 to the polymorphic layer, CA3c, was found to have the most collateralizations in the polymorphic layer, especially in the ventral hippocampus.

Furthermore, CA3 pyramidal cells were found to have axons entering the granule cell layer and collateralizing in the inner molecular layer. This was a specific feature of ventral CA3c pyramidal cells. This finding led to the assumption that pyramidal cells in this area might directly activate dentate GCs (Scharfman 2007b; X.-G. Li, P. Somogyi, A. Ylinen, AND G. Buzsáki 1994).

Caveats of older studies are small n numbers and potential variability across species and age (Scharfman 2007b, p. 629). Two newer studies, however, reported direct anatomical connections from CA3 pyramidal cells to dentate GCs using retrograde tracing methods in mice (Vivar et al. 2012; Sun et al. 2017). There might also be a developmental-related change in how the back-projection from CA3 elicits activity in the DG (Shi et al. 2014).

Future experiments are needed to investigate the physiological properties of this connection and determine its role on a behavioral level.

Other inputs to the DG emanate from the presubiculum, parasubiculum, hypothalamus (including the supramammillary area), locus coeruleus, ventral tegmental area, and raphe nuclei (Amaral et al. 2007; Köhler 1985; Wyss et al. 1979; Vertes and McKenna 2000).

1.2.3 The function of the dentate gyrus

Two main functions of the DG are conjunctive encoding of multiple sensory inputs and spatial pattern separation (Rolls and Kesner 2006; Rolls 1996; Scharfman 2007a, p. 567). As mentioned, the DG receives spatial and non-spatial information via the LPP and MPP. Kesner argues that combining spatial and visual information using conjunctive encoding leads to a unique spatial representation in the DG (Scharfman 2007a, p. 568; Hunsaker et al. 2007; Kesner et al. 2015).

One of the other proposed functions of the DG is pattern separation. A process in which ambiguous sensory inputs are converted to nonoverlapping neuronal patterns (Hunsaker and Kesner 2013). Rolls hypothesizes that pattern separation is supported by the sparse connections between dentate GCs to CA3 pyramidal cells (Rolls and Kesner 2006; Rolls 1996). This sparse connectivity leads to a low likelihood of one mossy fiber relaying information to the same two CA3 neurons. One reason is the ratio of GCs to CA3 pyramidal neurons. There are about 2.5x more GCs in the murine brain than CA3 pyramidal neurons (Bonthius et al. 2004). As summarized in the following, pattern separation has been investigated in rodents, monkeys, and humans. In one study, rats were placed into a morphing arena. While recording activity from dentate GCs, the arena was slowly transformed into a different shape. Despite the gradual arena reshaping, the GCs expressed distinct representations of each intermediate step of the arena transformation. This decorrelation suggests that the DG can form distinct representations of similar sensory inputs with a limited pool of cells (Leutgeb et al. 2007). Another paradigm to study behavioral pattern separation is an object relocation task. Only very slightly displaced objects would not be detected as displaced by dentate-disrupted mice, while further displaced objects would still be inspected for longer (Pofahl et al. 2021).

In monkeys, pattern separation can be probed in a visual discrimination task. While recording from dentate/CA3 cells, monkeys were trained to discriminate whether a presented picture was new, similar, or repeated. Interestingly, the recorded cells reacted to similar lure pictures in a comparable way as to new pictures. This discrete representation of similar visual inputs is believed to be a form of pattern separation (Sakon and Suzuki 2019).

Participants had to discriminate a sequence of two akin pictures in a human study. The goal was to only react to the third repetition of the correct picture while avoiding the lure. Brain activity was scrutinized during the task using fMRI. The authors found a significantly higher representation of lures in the DG area than in other brain regions. Additionally, a classifier had the highest accuracy for lure trials when trained with the DG data (Berron et al. 2016). The presented studies show strong evidence for the DG as a pattern separator in multiple species.

Another potential role of the DG might be temporal processing. For example, disruption of neurogenesis in the DG impairs learning during tEBC. However, impaired neurogenesis does not affect delay eyeblink conditioning, water maze spatial navigation, or contextual fear conditioning(Shors et al. 2002; Miller et al. 2019; Scharfman 2007a, p. 574). Furthermore, the back-projection from CA3 to the DG might enable the coding of short-term memory across seconds and facilitate the recall of sequences (Scharfman 2007a, p. 574; Lisman 1999).

1.3 The CA3 subfield

The principal cell layer of CA3 is the pyramidal cell layer. Below the pyramidal layer lays the stratum oriens. This layer contains the basal dendrites of the pyramidal cells and different classes of interneurons. The next adjacent layer is the alveus, which is thin and fiber-rich. Compared to CA1, in CA3, a thin cell-free zone, called the stratum lucidum, is located above the pyramidal cell layer. The stratum lucidum contains the mossy fibers arriving from the DG. Just above the stratum lucidum lays the stratum radiatum, which harbors associational connections between CA3-CA3 and CA3-CA1 Schaffer collateral connections. Finally, t stratum lacunosum-moleculare forms the most superficial layer (Andersen 2007, pp. 67–68; Amaral and Witter 1989). Topographically, CA3 can be subdivided into three parts. The CA3c subfield is the portion proximal to the DG. The CA3a subfield is proximal to CA1, with the CA3b subfield lying between them (Andersen 2007, p. 156; Amaral and Witter 1989).
The CA3 pyramidal cell is the principal neuron type of CA3. These cells express a large variability in size and dendritic length (Andersen 2007, p. 68; Ishizuka et al. 1995). Besides pyramidal cells, many different interneuron types reside in CA3 (Andersen 2007, pp. 68–71; Blackstad et al. 1970).

A hallmark characteristic of CA3 are recurrent connections between CA3 pyramidal neurons (associational connections). These recurrent connections also connect the two CA3 regions of both hemispheres (commissural connections) and project to the contralateral CA1 (Witter 2007a; Andersen 2007, p. 71). CA3 projections to CA1 constitute the Schaffer collaterals. Furthermore, the EC has connections that terminate in the distal dendrites of CA3 pyramidal cells and interneurons. Like the DG, CA3 gets inputs from layer II cells of the EC (Andersen 2007, p. 71; Witter 2007a). The mossy fibers of the DG form connections over the entire transverse or proximodistal extent of CA3 (Witter 2007a; Blackstad et al. 1970; Swanson et al. 1978; Gaarskjaer 1986; Claiborne et al. 1986). As described before, strong anatomical evidence exists for a back-projection from CA3 to the DG (Witter 2007a; Ishizuka et al. 1990; Buckmaster et al. 1993; Li et al. 1994; Scharfman 2007b).

The functional role of CA3a, b seems to be the acquisition of spatial information within a short-term memory time scale. Additionally, CA3 potentially performs rapid encoding of especially spatial information and novelty detection. Another function of CA3a, b is pattern completion (Kesner 2013a). Pattern completion is the ability of a network to reconstruct a familiar neuronal representation from an incomplete input pattern (Wilson 2009). The CA3c region is hypothesized to support the DG in pattern separation processes (Kesner 2013a). Moreover, it has been stated that CA3 is involved in working memory processes in associating temporally separated stimuli by acting as an attractor network (Kesner 2013a, 2013a; Rolls 2013a).

This interplay between the DG and CA3 is believed to play a vital role in episodic memory (Rolls 2013a). The sparse connectivity between the two regions leads to nonoverlapping representations in CA3. This is possible by the randomizing effect provided by the DG input (Rolls 2013a). This process is essential for encoding new memories. The likelihood of two pyramidal cells getting activated by the same DG GCs is assumed to be very low (Rolls 2013a). One hypothesis is that the DG-CA3 path is vital for learning new associations, and the direct perforant path-CA3 connection is more involved in the retrieval of information (Kesner 2013a).

1.4 The CA1 subfield

The CA1 subfield has a very similar laminar structure as the CA3 subfield. However, the pyramidal cell layer is more tightly packed, with no stratum lucidum (Andersen 2007, pp. 67–68; Amaral and Witter 1989). The CA1 pyramidal cells have an average diameter of 15 µm. Hence they are smaller than CA3 pyramidal cells (Andersen 2007, p. 68; Amaral and Witter 1989). Compared to CA3 pyramidal cells, the principal cells of CA1 are more homogenous in their dendritic trees (Andersen 2007, p. 68; Pyapali et al. 1998). Besides the CA1 pyramidal cells, many different interneurons are spread over all layers of CA1 (Andersen 2007, pp. 68–70; Freund and Buzsáki 1996).

The two primary inputs into CA1 are the Schaffer collateral arising from CA3 and direct inputs from the EC (Andersen 2007, p. 74, 2007, p. 71). The associational and commissural projections of CA1 are much weaker than those of CA3 (Andersen 2007, p. 76; Amaral and Witter 1989). Eventually, CA1 gives rise to its two main hippocampal outputs. These terminate in the subiculum and the EC (Andersen 2007, p. 76, 2007, p. 71; Naber et al. 2001). Contrary to the canonical connectivity of the CA1 subregion, there is evidence for a CA1 to CA3 back-projection, which seems to be GABAergic (Witter 2007a; Sik et al. 1995; Sik et al. 1994). Furthermore, a back-projection from the subiculum to CA1 seems to exist (Xu et al. 2016).

One primary function of CA1 is the formation of episodic memory (La Prida 2020). One of the hallmark features of CA1 is the presence of so-called „place cells“, which fire at specific places in space (Igarashi et al. 2014a; O'Keefe 1976). Beyond that, there have been reports of other feature-coding cells in CA1 that encode floor texture, odors, color, and shapes, the passage of time, and motivational states (Igarashi et al. 2014b; MacDonald et al. 2011; Komorowski et al. 2009; Pastalkova et al. 2008; Leutgeb et al. 2005; Moita et al. 2004; Wood et al. 1999; Markus et al. 1995; Young et al. 1994; Igarashi et al. 2014a). Another potential function of CA1 is its involvement in coding tEBC. While the hippocampus does not seem necessary for delay conditioning, it is crucial for trace conditioning (Gruart and Delgado-Garcia 2007; Tseng et al. 2004; Weiss et al. 1999). CA1 firing seems to correlate with an increase in the percentage of conditioned responses (Gruart and Delgado-Garcia 2007). While it does not correlate with the kinetics of the conditioned eyelid closure (Gruart and Delgado-Garcia 2007), there are specific

cellular responses to all parts of a trial. This means cells specifically code the CS, trace period, and US (Múnera et al. 2001; Mount and Sridhar 2021; Modi et al. 2014; Moyer, JR et al. 1996; Matthew D. McEchron and John F. Disterhoft 1997).

1.5 Associative learning and memory in the hippocampus

Learning is generally defined as gathering knowledge about one's environment. Memory, on the other hand, entails encoding, storing, and later retrieving this information (Kandel et al. 2000). While there is an ongoing debate on how to categorize different forms of memory, long-term memory can generally be separated into two forms. Firstly, implicit, or non-declarative memory, and secondly explicit, or declarative memory. Implicit memory involves unconscious learning, like perceptual skills, motor learning, or classical conditioning. Explicit memory is the memory of facts, such as people, places, and things. It is a more conscious form of memory (Kandel et al. 2000). Implicit memory can be subdivided into associative and nonassociative learning. Nonassociative learning involves a single type of stimulus. Standard forms are habituation and sensitization. Associative learning, on the other hand, requires a relationship between two stimuli. Typical forms of associative learning are operant and classical conditioning (Kandel et al. 2000). During classical conditioning, a CS (e.g., a tone) gets repetitively paired with an US (e.g., an air puff to the cornea). After multiple repetitions, the previously neutral CS elicits a reaction that would otherwise only be caused by the US (Kandel et al. 2000). This is called the conditioned response. If the US gets presented alone repetitively after the subject has learned, eventually, the response will be unlearned again. This is called extinction. Extinction is an important mechanism to avoid environmental stimuli's excessive, maladaptive association (Kandel et al. 2000).

Interestingly, the temporal contiguity of two stimuli is insufficient to cause conditioning. Therefore, pairing any two stimuli does not necessarily lead to a conditioned response. This leads to the notion that the brain must somehow be able to infer whether the relationship between two stimuli is relevant (Kandel et al. 2000). Some theories state that the involvement of the hippocampus is essential to code the context in which certain stimuli occur. This might be a way to determine if two stimuli have a meaningful connection in a given environment or situation (Andersen 2007, p. 658).

1.5.1 Trace eyeblink conditioning as a model of associative learning in the dentate gyrus

Eyeblink classical conditioning has been well-studied as a model for associative memory in mammals (Takehara-Nishiuchi 2018; Woodruff-Pak and Disterhoft 2008; Kimberly M. Christian and Richard F. Thompson 2003). In this paradigm, the animal is supposed to associate a neutral CS with an aversive US that evokes an eyeblink. Typically, the CS consists of an auditory,

visual, or somatosensory stimulus. The US, an air puff to the cornea or electric shock near the eye, provokes a defensive eyelid closure in trained and naive animals. After repeated paired presentations of the CS with the US, the subject shows an eyelid response to the previously neutral CS. This is called the conditioned response (Takehara-Nishiuchi 2018). The kinematics and underlying circuit of a conditioned response differ from those of spontaneous blinks and the unconditioned eyelid closure (Gruart et al. 2000; Gruart et al. 1995; Schade Powers et al. 2010; Takehara-Nishiuchi 2018). To determine whether the animal learned, the eyelid movement gets read out. Subsequently, the fraction of stimuli presentations with conditioned responses gets computed. A single trial of eyeblink conditioning is short. The CS is often shorter than a second, and the US is about a hundred milliseconds long (Takehara-Nishiuchi 2018).

A variant of eyeblink classical conditioning is tEBC. Instead of simultaneously presenting the stimuli, the CS is followed by a stimulus-free trace period. The resulting sequence is CS, trace interval, and US. Usually, the trace period is no longer than 500 milliseconds in rodents studies (Takehara-Nishiuchi 2018, pp. 298–299). While classic eyeblink conditioning does not rely on the hippocampus, the addition of a trace period makes the hippocampus relevant to learn the task (Moyer et al. 2015; Tseng et al. 2004; Weiss et al. 1999; Takehara-Nishiuchi 2018; Izquierdo et al. 2016; Woodruff-Pak and Disterhoft 2008; Kimberly M. Christian and Richard F. Thompson 2003; Madroñal et al. 2016).

The longer the trace interval, the more the disruption of the hippocampus decreases learning performance in tEBC (Tseng et al. 2004; Walker and Steinmetz 2008; Takehara-Nishiuchi 2018). It is assumed that the hippocampus is needed to somehow link the temporally separated stimuli in trace learning and predict how likely the US can occur at a specific moment. As (Miller et al. 2022) argued, this poses the need for a mechanism in the hippocampus that compares the learned stimuli sequence with incoming stimuli sequences. Possibly, this mechanism is reliant on pattern separation because other stimuli might be very similar, and excessive generalization of conditioned responses is problematic (Miller et al. 2022). Furthermore, the hippocampus links context and spatial information with the presented stimuli. Changing the conditioning chamber can disrupt the previously acquired conditioned response. This effect gets negated by lesioning the hippocampus (Takehara-Nishiuchi 2018; Penick and Solomon 1991). The hippocampus shows sequential firing with specific cells responding to the US, trace period, and US (Modi et al. 2014; Miller et al. 2022). There is also some evidence that this firing behavior is linked to specific contexts and only occurs therein (Penick and Solomon 1991).

This led to the assumption that the hippocampus performs two main computations during tEBC. Firstly, code the sequence of the US, trace, and US in a specific context. Secondly, use the learned temporal stimuli sequence and predict how likely the present stimuli presentation leads to the US (Takehara-Nishiuchi 2018).

Many studies lesioned the whole hippocampus or the entire hippocampal formation. Thus, it is not well understood what specific role the individual parts of the hippocampal formation play in tEBC (Takehara-Nishiuchi 2018; Kimberly M. Christian and Richard F. Thompson 2003; Woodruff-Pak and Disterhoft 2008; Izquierdo et al. 2016). However, in recent years, cutting-edge approaches, like tetrode recordings, calcium imaging, new transgenic models, and pharmacological inhibition became available. These allowed for studying the role of specific parts of the hippocampal formation, like the DG and the CA1 subfield, during tEBC (Miller et al. 2022, 2019; Suter et al. 2018; Nokia et al. 2017; Madroñal et al. 2016; Mount and Sridhar 2021; Hattori et al. 2015; Modi et al. 2014).

The following is a summary of studies that scrutinized the role of the DG during tEBC using these new techniques. Miller (2022) conducted trace eyeblink experiments while recording DG cells with tetrodes. The authors could segregate cells into dentate GCs, mossy cells, and interneurons. As in previous studies, they found an increase in the firing rate of GCs during the CS. Mossy cells, on the other hand, decreased firing during the trace period and the US. Finally, dentate interneurons seemed to either increase or decrease activity in a longer-lasting fashion, starting with the onset of the CS (Miller et al. 2022).

When investigating neurogenesis during trace eyeblink, the number of newborn GCs in the DG increased (Kimberly M. Christian and Richard F. Thompson 2003). Additionally, the ablation of newborn GCs decreased performance in trace conditioning (Miller et al. 2019).

Disrupting the dentate GC population during training led to an unlearning effect in a pharmacological mouse model. Interestingly, this effect was only present if the GC inactivation was paired with training in mice that had already learned tEBC (Madroñal et al. 2016). These studies did not investigate how population activity in the DG changes during tEBC. However, some evidence shows that population activity in the DG, like dentate spikes (DSs) plays an important role in tEBC (Nokia et al. 2017). This raises the question of how the population code in the DG may change during tEBC.

Moreover, other brain regions are relevant for tEBC. For example, cerebellar dentate interpositus nuclei lesions led to abolishing the conditioned response. Additionally, stimulation of these areas in a separate cohort of animals elicited the learned eyeblink response (McCormick and Thompson 1984; Lincoln et al. 1982).

Inducing lesions in the caudal medial prefrontal cortex impeded trace eyeblink learning in rabbits (Kronforst-Collins and Disterhoft 1998; Weible et al. 2000; McLaughlin et al. 2002). Another study investigated how the infusion of a GABA agonist and an NMDA antagonist into the medial prefrontal cortex affects tEBC. The GABA agonist retarded learning when applied right before training. The GABA agonist reduced the learned response when applied shortly after successful learning. Infusion with the NMDA antagonist before training hindered learning as well. This led

the authors to conclude that the medial prefrontal cortex is vital for early learning and consolidation during tEBC (Takehara-Nishiuchi et al. 2005).
Bilateral lesions of the entorhinal cortices disrupted learning-related activity in the CA1 region and decreased learning performance in trace conditioning (Ryou et al. 2001). Another study reported that lesioning the peri-, and postrhinal cortices, but not the LEC disturbs trace conditioning (Suter et al. 2013). On the contrary, in another study, the acquisition of tEBC relied on cholinergic signaling of the LEC (Tanninen et al. 2015).
In a whisker trace eyeblink paradigm, lesions of the barrel cortex disrupted acquisition and retention (Galvez et al. 2007). In addition, bilateral inactivation of the visual cortices in rats prevented the acquisition and retention of tEBC (Steinmetz et al. 2013).
Bilateral lesions of the caudate nucleus prevented acquisition and retrieval after consolidation. Furthermore, neurons in the caudate nucleus showed learning-related activity changes in a separate cohort of animals (Flores and Disterhoft 2013, 2009).
Thalamic lesions also disrupted learning of tEBC (Oswald et al. 2007; Powell and Churchwell 2002).
How these brain regions functionally interact during tEBC is not understood yet (Takehara-Nishiuchi 2018).

1.6 Oscillations and population events in the hippocampal formation

1.6.1 Oscillations

A common feature of electrophysiological recordings of the brain are rhythmic oscillations. The neuronal activity of neurons induces voltage fluctuations. These can be picked up by local field potential measurement or other recording methods (Nokia and Penttonen 2022; Buzsáki et al. 2012; Andersen 2007, p. 477). Interpreting the electrophysiological signal of the hippocampus has led to two assumptions. The first notion states that information is parsed between single cells, representing distinct computing elements (O'Keefe 1976; Jung and McNaughton 1993; Miller et al. 2022). An alternative view is that a more extensive network or population code contains the processed information (Barnes et al. 1990; Bland and Oddie 2001; Nokia et al. 2017). This code might be reflected in large synchronous cellular activity that can be picked up in electrophysiological recordings (Arnolds et al. 1980). The current theory is that the hippocampus deploys both strategies to process information (Andersen 2007, p. 475).

The canonical view separates frequencies in the brain into different categories. Alpha (8-13 Hz), beta (13-30 Hz), delta (0.5-4 Hz), and Theta (4-7 Hz) (Kandel et al. 2000; Nokia and Penttonen 2022; Andersen 2007, p. 477). These categories have been associated with different behavioral states and differ slightly across species (Kandel et al. 2000; Andersen 2007, pp. 477–479). For

example, Theta occurs during movement, rapid eye movement, sleep, and immobile arousal in the rat. Gamma is present during odor sniffing, and beta has been associated with predator-linked odor sniffing. Alpha waves have been detected during relaxed wakefulness in human EEG. Delta waves can be present during drowsiness and early slow-wave sleep. Theta can be further distinguished into two components. One component involves cholinergic signaling and plays a role in arousal and attention. The other component is not affected by cholinergic drugs and is involved in translational movement (Andersen 2007, p. 480).

1.6.2 Sharp-wave ripples in CA3/1

A common population phenomenon that can be found in CA1 are the so-called sharp waves. They are typically 50-100 ms long and can have an amplitude of over 1 mV. CA1 sharp waves are caused by synchronous activity in CA3, which propagates to CA1 via the Schaffer collaterals (Andersen 2007, p. 483; Buzsáki 2015). It has been shown that sharp waves from the hippocampus proper can spread to other brain regions (Buzsáki 2015). Two *in vitro* studies reported the activation of dentate GCs, mossy cells, and interneurons during sharp-wave ripples (Swaminathan et al. 2018; Szabo et al. 2017). This might be part of an essential mechanism of how sharp-wave ripples modulate activity in the DG.

Connected to sharp waves, another type of population event in CA1 are high-frequency oscillations called ripples. Ripples occur around the negative peak of a sharp-wave at frequencies of 120-200 Hz for ~100ms with a peak amplitude in the CA1 pyramidal layer (Andersen 2007, p. 483; Nokia and Penttonen 2022). During sharp-wave ripples, neuronal sequences of remote experiences get replayed while the subject is sleeping (Buzsáki 2015; Liu et al. 2019). Sharp-wave ripples are assumed to be controlled by excitatory and inhibitory neurons of the CA2 and CA3 regions (Oliva et al. 2016; Csicsvari et al. 2000; Nokia and Penttonen 2022). These sharp-wave ripples are most frequent during non-rapid eye movement sleep and are assumed to play a role in memory consolidation (Nokia and Penttonen 2022; Klinzing et al. 2019). Sharp-wave ripple-contingent tEBC led to higher learning rates and retarded extinction (Nokia et al. 2010).

1.6.3 Offline states of the dentate gyrus

Like other hippocampal regions, the DG exhibits specific population events. These are DSs, dentate sharp waves, and network events. DSs are short (<30 ms) synchronous discharges of GCs and interneurons of large amplitude (2-4 mV) (Bragin et al. 1995; Penttonen et al. 1997). Two types of DSs have been reported. The LPP drives DS type 1whereas DS type 2 events are triggered by MPP activity (Bragin et al. 1995; Dvorak et al. 2021). Rates of DSs vary between 12-60 events/minute in rats (Dvorak et al. 2021; Headley et al. 2017; Bragin et al. 1995). In one study, DS1 co-occurred with decreased firing rates of dentate GCs and dentate

interneurons, while CA1 and CA3 pyramidal cells were unaffected. CA3/1 interneuron rates were higher during DS1. DS2, on the other hand, coincided with higher GC, mossy cell, and CA3 cell firing rates, as well as interneuron rates in the DG, CA1, and CA3 (Dvorak et al. 2021). DSs occur predominantly during quiet rest and sleep (Headley et al. 2017). One study reported differences between DS1 and DS2. According to the authors, DS1 and DS2 get modulated by speed differently. This resulted in a higher event rate for DS2 at higher running speeds (Dvorak et al. 2021).
DSs inhibit sharp-wave ripples for up to 200ms (Bragin et al. 1995).
While the behavioral role of DSs is unknown, they might play a role in memory consolidation (Nokia et al. 2017). Nokia and Penttonen hypothesized that DSs play a role in reorganizing neural representations in the hippocampus during memory consolidation. They argue that DSs might be necessary for merging similar representations during rest and sleep. Furthermore, disruption of DSs during eyeblink conditioning curbed learning. This led to the conclusion that DSs might be involved in associating temporally separated stimuli (Nokia and Penttonen 2022; Nokia et al. 2017).

Dentate sharp waves are a novel type of population event in the DG introduced by a recent study. These dentate sharp waves are characterized by a source in the outer molecular layer and granule cell layer and a sink in the inner molecular layer. Cells in the dentate GC layer and CA1 express increased activity right before a dentate sharp-wave.
Dentate sharp waves occur independently or together with sharp-wave ripples. The dentate sharp-wave rate was increased following two hippocampus depended learning tasks (Meier et al. 2020).

A recent imaging study detected similar large population events of the dentate GCs. Network events were associated with MPP activity. These events predominantly happened during wakeful rest at a rate of about 4 events/minute. However, how these network events were linked to DSs, dentate sharp waves, or other electrophysiological phenomena remained unclear as electrophysiological validation was missing (Pofahl et al. 2021).
Inhibiting the GC population during rest in a pattern separation task disrupted learning in an object relocation task (Pofahl et al. 2021). This adds to the hypothesis that synchronous population events of the GC population are essential for learning and memory consolidation.

More studies will be needed to elucidate the exact role of population events in the DG during learning. This requires recording a large sample of cells over multiple days during associative learning. Improving our understanding of the computations involved in tEBC in the DG can serve as a model to better understand the effects of drugs, age, and disease on learning and memory.

1.7 Key questions

While several studies indicate that the DG is important for associative learning, many are based on lesions that lack precise conclusions. Furthermore, studies using the targeted disruption of the dentate GC during tEBC are few (Madroñal et al. 2016; Miller et al. 2019) and vary in results. To this day, no published study recorded data from a more extensive set of GCs during tEBC, let alone tracking them over days. Therefore, I asked the following key questions:

1. Is the DG necessary for tEBC?
2. How does task-associated activity change during learning?
3. How does synchronous offline activity change during learning?

2 Materials and Methods

Animals and procedures: All animal experiments were conducted in accordance with European (2010/63/EU) and federal law (TierSchG, TierSchVersV) on animal care and use and approved by the county of North-Rhine Westphalia (LANUV AZ 81-02.04.2019.A192). We used 6-8 weeks-old Thy1-gCaMP6 mouse line (GP4.12Dkim/J) mice for imaging experiments expressingCaMP6s in most hippocampal neurons (Dana et al. 2014). In addition, for optogenetic inhibition of the DG GCs, we used heterozygous Prox1-Cre animals (Tg(Prox1-cre)SJ39Gsat/Mmucd) as well as wildtype Prox1-Cre animals as illumination controls, obtained from MMRRC UC Davis as cryopreserved sperm and rederived in the local facility. In total, n=37 animals were used for experiments.

Window implantation procedure: Cranial window surgery was performed to allow imaging of the hippocampal DG. 30 minutes before induction of anesthesia, the analgesic buprenorphine was administered for analgesia (0.05 mg/kg body weight), and dexamethasone (0.1 mg/20 g body weight) was given to inhibit inflammation. Mice were anesthetized with 3-4% isoflurane in an oxygen/air mixture (25/75%) and placed in a stereotactic frame. Eyes were covered with eye-ointment (Bepanthen, Bayer) to prevent drying, and body temperature was maintained at 37°C using a regulated heating plate (TCAT-2LV, Physitemp) and a rectal thermal probe. Further anesthesia was carried out via a mask with a reduced isoflurane dose of 1-2% at a gas flow of about 0.5 l / minute. After removing the head hair and superficial disinfection, the scalp was removed about 1 cm^2 around the middle of the skull. The surface was locally anesthetized with a drop of 10% lidocaine, and after 3–5 min, residual soft tissue was removed from the skull bones with a scraper and 3% H2O2/NaCl solution. After complete drying, the cranial sutures were clearly visible and served as an orientation to mark the craniotomy site with a surgical pen. Optibond (Optibond 3FL; two component, 48% filled dental adhesive, bottle kit; Kerr; FL, USA) was then applied thinly to the skull to aid the adhesion of dental cement. Subsequently, a flat custom-made head post ring was applied with dental cement (Tetric Evoflow), and the surrounding skin was adapted with tissue glue, adapting the surrounding skin with tissue glue. A circular craniotomy (Ø 3 mm) was opened above the right hemisphere hippocampus using a dental drill. Cortical and CA1 tissue was aspirated using a blunted 27-gauge needle until the blood vessels above the DG became visible. A custom-made cone-shaped silicon inset (Upper diameter 3 mm, lower diameter 1.5 mm, length 2.3 mm, RTV 615, Movimentive) attached to a cover glass (Ø 5 mm, thickness 0.17 mm) was inserted and fixed with dental cement. Postoperative care included analgesia by administering buprenorphine twice daily (0.05 mg/kg body weight) and ketoprofen once daily (5 mg/kg body weight s.c.) on the three consecutive

days after surgery. Animals were carefully monitored twice daily for the following 3 days and recovered from surgery within 24-48 hours, showing regular activity and no signs of pain.

Imaging and treadmill system: We used a commercially available two-photon microscope (A1 MP, Nikon) equipped with a 25x long-working-distance, water-immersion objective (N.A.=1, WD=4 mm, XLPLN25XSVMP2, Olympus) controlled by NIS-Elements software (Nikon). GCaMP6s was excited at 940 nm using a Ti:Sapphire laser system (~60 fs laser pulse width; Chameleon Vision-S, Coherent). Emitted photons were collected using gated GaAsP photomultipliers (H11706-40, Hamamatsu). Movies were recorded using a resonant scanning system at a frame rate of 15 Hz and a duration of 20 minutes per movie. Mice were head-fixed, awake, and allowed to move freely on a linear track. Two weeks before the measurements, mice were habituated to the head fixation. Initially, mice were placed on the treadmill without fixation for 5 minutes. Subsequently, mice were head-fixed but immediately removed if signs of fear or anxiety were observed. These habituation sessions lasted 5 minutes each and were carried out thrice daily, flanked by 5 minutes of handling. During the following 3-5 days, sessions were extended to 10 minutes each. The treadmill was a self-constructed linear horizontal treadmill, with no spatial cues added to the belt beyond the texture of the belt itself. Each animal was recorded on an individual belt, and the treadmill setup was cleaned entirely between recordings. Belt position and running speed were measured by modified optical computer-mouse sensors. All stimulation and acquisition processes were controlled by custom-made software written in LabView (National Instruments, USA).

Trace eyeblink conditioning in head-fixed mice: tEBC was achieved using a tone (350 ms, 7 kHz, ~ 70 dB) as the CS, while a 100 ms air puff (output pressure 1.5 bar at pipette tip) given to the cornea served as US. The air puff was applied through a pipette tip with a 1-2 cm distance to the left cornea and was positioned in a way to elicit explicit aversive blinking behavior. The trace period separated the CS and US, with the air puff starting 250 ms after the end of the tone. A total of two habituation, four conditioning, and one extinction sessions were carried out, with each session lasting 20 minutes. For habituation and extinction, the unpaired tone was presented 30 times in a pseudorandom fashion with 35-45 s between trials. A conditioning session consisted of 25 paired tone air puff trials, with five tone only trials at the end of the session. An offline eyeblink detection was used to analyze behavioral responses to tEBC.

A close-up video of the left eye was recorded using a high-speed IR camera (Basler Pilot, Basler, Germany) at a frame rate of 100 Hz. The video frames were processed using a custom-written program in Matlab (Mathworks, USA). First, the video frames were loaded as grayscale images. Next, a circular ROI was drawn around the eye so that only the eye was included in the image-processing steps. Then each frame was filtered using a 2D Gaussian smoothing kernel

with a standard deviation of 1 for digitally removing whiskers and thresholded for binary image conversion. After applying morphological image-processing operations, the binary image's geometrical parameters (i.e., major and minor axis, area, and Feret diameter) were calculated for generating eyelid traces. The minor axis length was chosen as the momentary distance between the upper and lower eyelids for each frame. Finally, the eyelid traces were normalized between 0 (fully open eye) and 1 (fully closed eye) to get the eye closure metric. A successful CR was defined as a relative change in the eye closure value of more than 10% during the 350 ms tone compared to a 2-second pre-tone baseline. Dr. Kurtulus Golcuk wrote the blink and CR detection program.

Data analysis of imaging data: All analyses on imaging data and treadmill behavior data were conducted in Matlab using standard toolboxes, open access toolboxes, and custom-written code. To remove motion artifacts, recorded movies were registered using a template-matching approach (Pnevmatikakis and Giovannucci 2017). Next, individual cell locations and fluorescence traces were identified using a constrained nonnegative matrix factorization-based algorithm, and afterward, Ca^{2+} events were identified with a constrained deconvolution algorithm (Pnevmatikakis et al. 2016). All components were manually inspected, and only those that showed the shape and size of a granular cell and at least one Ca^{2+}-event amplitude two standard deviations above noise level in their extracted fluorescence trace were kept. Finally, we binarized individual cell fluorescence traces by converting the onsets of detected Ca^{2+} events to binary activity events.

Responder detection: We determined GCs responsive to learning by identifying those responding at a higher level than chance during the tone-trace period. The sum of total events during the tone-trace interval for each cell was computed for all paired trials. This value was compared to a shuffling distribution. To get this distribution, the binarized onset vector for each cell was shuffled 1000x. The p value was calculated by computing the chance of each shuffle vector having more onsets during the tone-trace interval than the actual cell. We flagged cells with a p value of 0.05 or less as statistically significant tone-trace responders. Cells with a p value over 0.05 were categorized as nonresponders.

Network activity: To define events of synchronized activity, we used binarized data that marked the onset of each significant Ca^{2+} event. First, we searched for events co-occurring in several GCs within a moving time window of 200ms corresponding to 1±1 frames in our recordings, where multiple events in one cell were counted as one. Using a shuffling approach, we then defined the distribution of synchronous events that could arise by chance in each session.

For every individual cell, the event onset times were redistributed to random times, conserving the mean event frequency per cell but destroying temporal correlations. This was done for every cell and repeated a thousand times to create a null distribution of population behavior. To ascertain how robustly the data differed from the null distribution, we identified the number of synchronous events for different network event size thresholds ((Pofahl et al. 2021), see **Supplementary Fig. 5a** for six individual representative examples). We then set the minimal threshold for network events in each session at that number of synchronously active GCs where less than 5% of events could be explained by chance. The threshold was then increased by one more count. This led to a p value of less than 0.1% ($p<0.001$) for all investigated sessions. Dr. Martin Pofahl wrote the network detection program.

Tracking and stability detection: First, the FOVs between successive sessions were aligned to follow individual cells over days. To this end, a 2D cross-correlation approach was utilized using standard Matlab image registration procedures. Next, the FOV of each session was mapped onto the FOV of the former session using an affine transformation which allowed translation, rotation, and stretching transformations. The resulting transformation matrix could then be combined with other session combinations to allow a mapping throughout several days. Utilizing this transformation matrix, all cell-ROI of each session could be mapped to reference session so that the same cell should be at similar positions in the FOV of each day. ROIs with a maximal distance of five pixels (4.55 µm) on day 1 and day 2 were considered as putatively the same cell. Since this method could not exclude absent cells, e.g., through z-shift in the recording plane, distance alone was no sufficient criterion to identify the same cell. To validate putative candidates, the cross-correlation between their spatial footprints was computed. Two candidates were considered the same cell if cross-correlation reached a minimum threshold of 0.5.

Additionally, the first 60 components for every animal were manually inspected over all seven sessions. CD27 and CD28 showed sufficient FOV alignment for seven-session tracking. For CD20, T1, and T3, and for CD23, T1, and T2 were excluded due to poor alignment of the FOV. Two animals had to be excluded entirely from tracked analyses due to shifts in the z-plane. If the FOV of a session was correctly aligned, this applied to all 60 investigated components. This approach led to a pool of about 1000 active components tracked over at least two sessions. Dr. Martin Pofahl wrote the initial tracking program.

Silent cell classification: To inspect if inactive cells were in FOV and z-plane in a given session, the spatial component of the closest session in which the cell was active was transformed on the averaged GCaMP FOV of the current session. By doing that, we could manually inspect if a cell was present and could have been detected by NNMF. We visually ensured the correct alignment of the FOV as described above. The resulting trackable but inactive cells were included in tracked data analyses as entirely inactive. Only cells active in at least one of the seven sessions were added that way. This approach increased the pool of components to about 2000 **(Table 1)**.

Table 1: *Overview of how many components could be tracked over 2-7 sessions. Upper part shows results without and lower part with silent cell addition.*

Sessions tracked	2	3	4	5	6	7	Total
Number of active components	410	238	136	74	41	40	939
Silent cells included							
Sessions tracked	2	3	4	5	6	7	
Number of components	0	0	1	8	769	1159	1937

Virus injections and optical fiber implantation for optogenetic experiments: Mice were injected with buprenorphine (0.05 mg/kg BW) 30 minutes before inducing anesthesia using 3.5 % isoflurane for induction and 1-1.5 % for maintenance. Mice were placed in a stereotactic frame (Kopf Instruments), and their eyes were covered with eye-ointment (Bepanthen, Bayer) to prevent drying. The scalp was opened with surgical scissors after disinfecting it with an iodine solution and applying local anesthetic (10% lidocaine). The skull was thoroughly cleaned using 2% H_2O_2, covered with a thin layer of two component dental adhesive (Optibond), and the surrounding wound was sealed with tissue glue (Vetbond). Small craniotomies were performed above the target sites, and 500 nl virus suspension (rAAV-hSyn-GFP for illumination controls, rAAV2/1-EF1a-DOI-eNpHR3-eYFP for non-illuminated controls, and experimental animals) was bilaterally injected using a 34 G syringe (Nanofill Syringe, World Precision Instruments, Inc.) at a speed of 50 nl/min. After each injection, the syringe was kept in place for 5 minutes to ensure permeation of the virus into the parenchyma. Coordinates for viral injections into dorsal DG were: (from bregma): AP: -2.3; ML: -/+ 1.6 and 150 nl each at DV: -2.3 mm, DV: -2.2 mm, and DV: -2.1 mm). Afterward, a flat custom-made head ring was glued to the skull with dental cement (Tetric Evoflow). Subsequently, fiber optic cannulae of 200 µm diameter (NA: 0.39, CFMLC12, Thorlabs) were bilaterally implanted at (from bregma): AP: -1.7; ML: -/+ 1.35 and DV: 1.7 and fixed to the skull with a layer of flowable opaque composite (Tetric Evoflow) topped by multiple

layers of dental cement (Paladur, Heraeus). Finally, antibiotic cream (Refobacin, Almirall) was applied to the wound, and the animals received ketoprofen (5 mg/kg BW) s. c. Analgesia was applied post-surgery by injecting ketoprofen (5 mg/kg BW) s. c. after 24, 48, and 72 hours. All mice recovered for at least 3 weeks after surgery before the start of behavioral experiments. Elisa Fernández and André Haubrich did the virus injections and optical fiber implantations.

Optogenetic behavioral experiments: the control and the experimental animals were subjected to tEBC (as previously described) while being optogenetically stimulated during all sessions. The non-illuminated controls underwent tEBC with an attached patch cord but no illumination. Using a dual patch cord (NA: 0.39, Doric lenses, Quebec, Canada), 561 nm laser light (OBIS/LS FP, Coherent, Santa Clara, CA) was bilaterally delivered via the implanted light fibers. Pulsed laser light was applied at a frequency of 20 Hz, and the laser power output was around 5mW at the tip of the fiber probes. Elisa Fernández did the optogenetic behavioral experiments.

Illumination control and non-illuminated controls were pooled after statistical analysis revealed no significant difference between the two groups (**Supplementary Fig. 1d**, 2way ANOVA, Holm-Šídák's multiple comparisons test, Illumination control vs. non-illuminated control H1-T4 $p>0.3063$, illumination control n=9, non-illuminated control n=10)

Histology and microscopy: Histology was carried out to verify successful viral expression and light fiber position. Animals were deeply anesthetized with ketamine (80 mg/kg body weight) and xylazine (15 mg/kg body weight), and they were intracardially perfused with cold phosphate-buffered saline (PBS) followed by 4% paraformaldehyde (PFA) in PBS. Mice were decapitated, and the brain was removed and stored in 4% PFA in PBS solution at 4°C for at least two days. Brains were washed thrice with PBS for 10 minutes and cut on a vibratome (Leica) to generate 50 µm coronal hippocampus slices. Those slices were stained with DAPI (Biotium, cat: 40043, 1:1000) for 25 minutes, washed thrice with PBS for 10 minutes, and mounted. Brain slices were mounted on glass microscopic slides (Thermo Scientific) with Aqua-poly/mount (Polysciences) and covered with a coverslip (Thermo Scientific). Microscopy was performed in a spinning disc microscope (Visitron VisiScope) in the Microscopy Core Facility of the Medical Faculty at the University of Bonn. The brain slices were checked for eNpHR-eYFP or GFP expression using the 488 channel and for DAPI using the 405 channel with objectives 5x, 10x, and 20x. The images were processed with ImageJ (Wayne Rasband). Elisa Fernández and André Haubrich did histology of the light fiber cohorts.

3 Results

3.1 Trace eyeblink conditioning in head-fixed mice

With simultaneous two-photon imaging experiments, we have established a behavioral paradigm for trace eyeblink conditioning in head-fixed mice. This task requires the association of a non-spatial, CS (a tone) with an US (an aversive air puff to the eye) presented with a stimulus-free trace interval (**Supplementary Fig. 1a**). Robust tEBC was obtained in head-fixed mice using a tone (350 ms, 7 kHz, ~ 70 dB) as CS, while a 100 ms air puff (output pressure 1.5 bar at pipette tip, calibrated to avoid startle responses) given to the cornea served as the US (see Methods). The initial habituation sessions presented unpaired tones with no eyelid closure response (***Fig. 1a, b***). On four successive days, the training sessions pair tones with a delayed US (25 trials, ***Fig.1a, b***). At the end of each training session, five tone only trials are presented (Probe phase), which clearly show robust learning (**Fig. 1b**). This was apparent in the fractional eyelid closure (FEC, **Fig. 1c,** Friedman test, p=0.004, Friedman statistic 22.38, Dunn's post-test baseline vs. T_1 p = 0.0101, baseline vs. T_2 p=0.003, baseline vs. T_4 p=0.0436, n=6 mice**,** **Supplementary Fig. 1b**). When the presence of a conditioned response was defined as a FEC above a threshold (10% FEC), we found a marked increase of conditioned responses during learning (**Fig. 1d**, Friedman test, p=0.005, Friedman statistic 22.31, Dunn's post-test baseline vs. T_1 p=0.0101, baseline vs. T_2 p=0.0019, baseline vs. T_3 p=0.0436, n=6 mice).

To determine if mice form a persistent memory of the CS-US association over days, we examined the first tone presentation on the session either during habituation sessions (no previous learning) or following any training session on the previous day (post-learning). The FEC was larger post-learning (**Fig. 1e**, Mann-Whitney test p=0.0057, n=11 mice pooled). Likewise, conditioned responses were present in significantly more first trials post-learning (Fisher's exact test, p=0.0371).

To elucidate the role of DG GCs during tEBC, we inhibited GCs during the entire tEBC protocol in a separate cohort of animals (**Supplementary Fig. 1c, d**). Inhibiting DG GCs led to a decrease in both average FEC and CR of the inhibition group on T_1 and T_2, and T_4 compared to the control (**Fig. 1f**, **top**, 2-way ANOVA, interaction p=0.0619, day and group p<0.0001, Holm-Šídák's multiple comparisons test, control vs. inhibition T_1 p = 0,0038, control vs. inhibition T_2 p = 0,0040, control vs. inhibition T_4 p = 0.0175, **Fig. 1f**, **bottom**, 2-way ANOVA, interaction p=0.0402 day and group p<0.0001, Holm-Šídák's multiple comparisons test, control vs. inhibition T_1 p=0.0006, control vs. inhibition T_2 p=0.0018, control vs. inhibition T_4 p =0.0344, control n=19, inhibition n=12 for all days except T_1, n=11, missing data due to technical difficulties). When analyzing the first tone response as in Fig. 1e, inhibition led to a decreased

average FEC response to the first tone after learning in the inhibition group (**Fig. 1g**, 2-way ANOVA, interaction p=0.0727, day p<0.0001, group p=0.0543, Holm-Šídák's multiple comparisons test, control vs. inhibition Pre p=0.9294, control vs. inhibition post p = 0.0114)

In summary, these data show robust learning, with a stable association of tone and air puff stimulation and the involvement of DG GCs during tEBC.

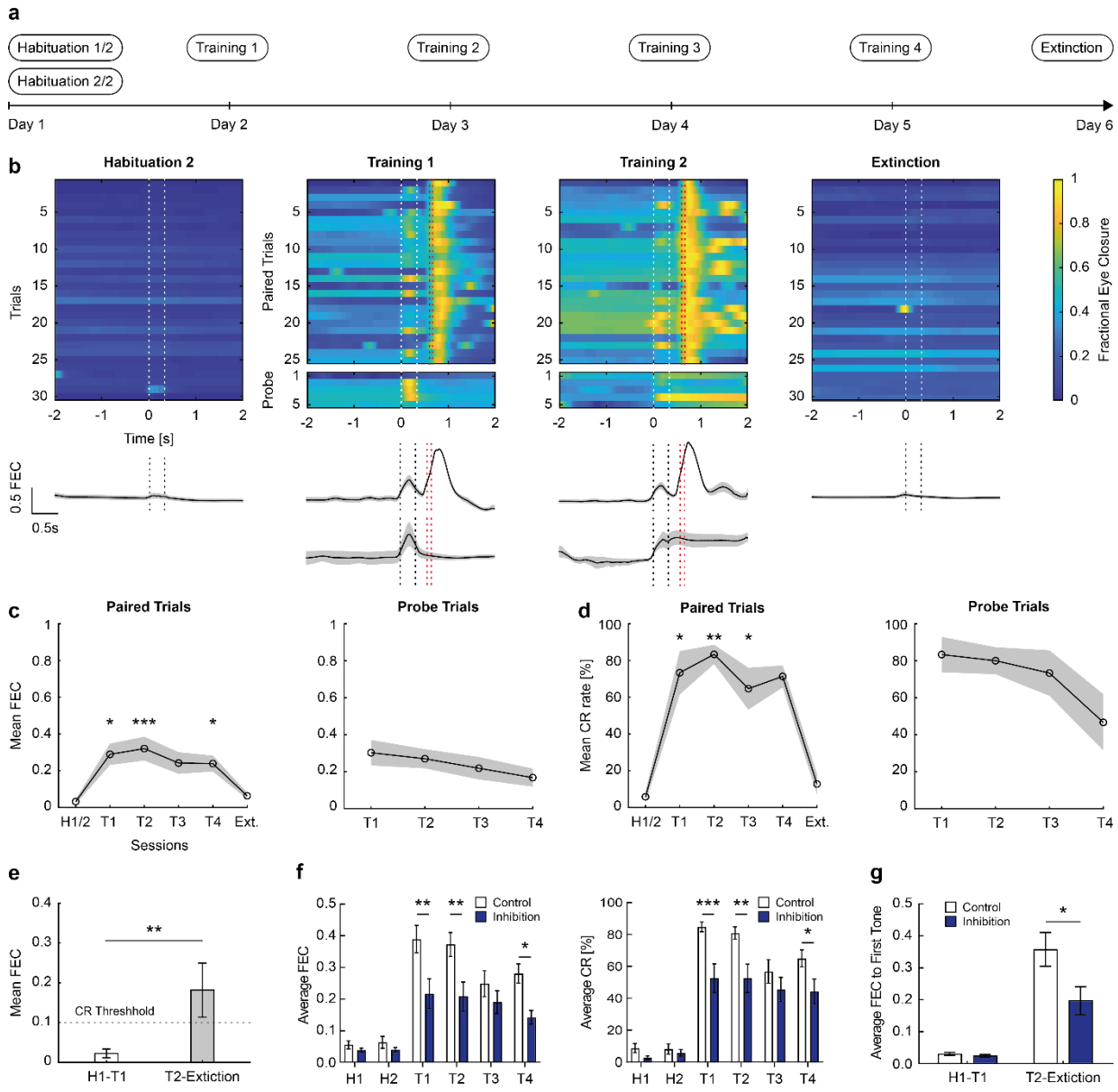

Fig. 1: tEBC protocol in head-fixed mice during 2-photon imaging. a, *Schematic of the experiment.* ***b,*** *Representative heatmaps from an individual mouse indicating fractional eyelid closure (FEC) measured for each trial (upper panels), or averaged traces (lower panels) for habituation sessions with tone only (left), two examples of paired training sessions with tone and air puff (Training 1 and 4), and the extinction session. A FEC of 0 and 1 describe a fully open or closed eye.* ***c,*** *Mean FEC in paired and probe trials.* ***d,*** *Conditioned response measured as responses >10% during either the paired (left) or the five probe stimulations (tone only, right).* ***e,*** *day-to-day memory of the tone air puff association, evaluated by the first tone presentation in sessions following any training session.* ***f,*** *optogenetic inhibition of GCs (white: control group, grey: inhibited group). Top: Average FEC over days. Bottom: Average conditioned response rate over days.* ***g****, day-to-day memory of the tone air puff association of the control and the inhibited group.*

3.2 Online task-related neuronal activity during associative learning

We imaged the activity of large populations of hippocampal dentate GCs using a Thy1-GCaMP6s mouse line (GP4.12Dkim/J, **Fig. 2a-d, Supplementary Fig. 2** (Dana et al. 2014))

during associative learning. A subset of GCs responded during the tEBC protocol (**Fig. 2c**). To determine which GCs respond at a higher level than chance during the tone-trace period (responder GCs), we used a shuffling approach (**Fig. 2d**). The fraction of significant tone-trace responders was not enhanced during training, as well as in the extinction session (**Fig. 2e**, Chi-Square test p=0,2973). Within the tone-trace responder category, responses were increased during learning, as evidenced by the dF/F traces and the event frequencies (**Fig. 2f,** for grand averages of dF/F, onsets and average running speed. See **Supplementary Fig. 3** for all sessions and probe data. **Fig. 2g**, 2-way ANOVA, interaction/day/cell type p<0.0001, Holm-Šídák's multiple comparisons test, nonresponder baseline vs. T1-T4 p<0.05, responder baseline vs. T_1-Ext. p<0.0001, responder vs. nonresponder Baseline-Ext. p<0.0001, n=6 mice). This increase was partly caused by a significant increase in the reliability of GC activity to tone presentation, but not the nonresponder population (**Fig. 2h**, **Supplementary Fig. 2g**). There was a significant increase in the fraction of trials causing at least one Ca^{2+} event onset during the tone-trace period (**Fig. 2h** inset: Kruskal-Wallis test, p < 0.0001, Dunn's multiple comparisons test, Baseline vs. T_2-Ext p<0.0002). Of note, the responding GCs were generally more active cells than nonresponding cells, with significantly higher event frequencies outside the trial interval (**Supplementary Fig. 2e**, Kruskal-Wallis test, p<0.0001, Dunn's multiple comparisons test, Baseline vs. T_1-Ext p < 0.0001, **Supplementary Fig. 2f (top)**, 2-way ANOVA, interaction/day/cell group p<0.0001, Holm-Šídák's multiple comparisons test, Nonresponder vs. Responder baseline vs. T_1-T_4 p<0.0229, **Supplementary Fig. 2f (bottom)**, 2-way ANOVA, Nonresponder vs. Responder interaction p=0.0003, day/cell group p<0.0001, Holm-Šídák's multiple comparisons test, baseline vs. T_1-Ext. p<0.0001, n=6 mice).

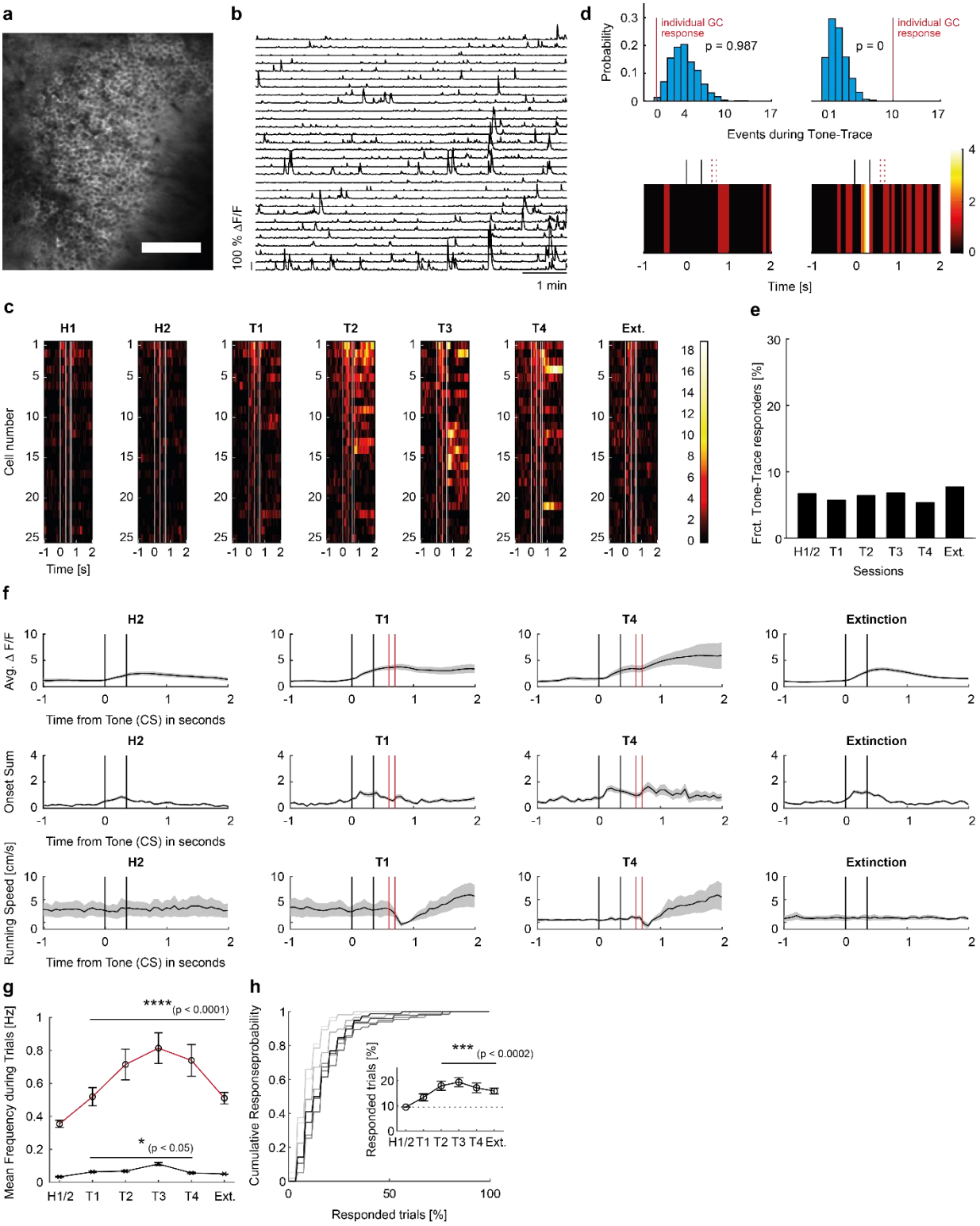

Fig. 2: Activity of GCs during tEBC learning, key data for c and d shown. a, *Representative example of a field of view (FOV) during in vivo two-photon imaging of GCs.* ***b,*** *Activity obtained from a subset of GCs in panel a.* ***c,*** *Heatmaps of the activity of cells sorted by the response magnitude during the tone-trace interval pooled over all mice across sessions.* ***d,*** *Examples illustrating the shuffling procedure to determine GCs responding above chance level. Blue bar distributions indicate shuffled data, red vertical line illustrates the response of individual GCs.* ***e,*** *Fraction of GCs that respond significantly during the tone-trace interval.* ***f,*** *Grand averages of Δf/f and onset frequencies for significant tone-trace responders and average running speed (examples shown for sessions H2, T1, T4, and Ext., for all sessions and probe response see* ***Supplementary Fig. 3****).* ***g,*** *Changes in activity for responders and nonresponders during the first second after tone onset.* ***h,*** *Cumulative distributions of the fraction of trials in which tone-trace responding GCs fire at least once during the tone-trace interval. Inset shows the average % of trials during which significantly tone-trace responding GCs show at least one Ca^{2+} event.*

3.3 Stability of task-responsive granule cell ensembles during associative learning

We next examined how stable the integration of individual GCs is over learning. We first examined whether GCs respond stably in successive sessions on consecutive days. To this end, we tracked GCs over successive sessions (see Methods, **Supplementary Fig. 4**). This enabled us to study the stability of tone-trace responders during learning in more detail (**Fig. 3a** for examples). In consecutive sessions, we identified all GCs that were responders in either or both sessions. Of these GCs, the stable responders active in both sessions were a minority (<10%, **Fig. 3b**). More than 90% of GCs were either nonresponders in previous sessions or converted back to nonresponders in the consecutive session (indicated as NR-R and R-NR in **Fig. 3b**). Vanishingly few GCs were significantly active during more than two learning sessions (one out of 123 training responder cells was a responder on three training days, n=4 mice). The fractions of unstable responders were decreased for the T_4-Ext. transition and increased for the de novo responder group (**Fig. 3b**, Chi-square test, p=0.0005, Holm-Šídák post-test, NR-R Baseline vs. T_1-Ext. p=0.0143, R-NR Baseline vs. T_1-Ext. p=0.0072, n=4 mice).

We examined if task-responsive GCs are more active in previous or subsequent sessions, even if they are not significant responders as determined by shuffling (**Fig. 3c**). We found that task-related activity both prior and after being a responding GC was much lower and not significantly different from the activity in habituation trials (**Fig. 3e (left and middle)**, Kruskal-Wallis test, p<0.0001, see supplements for multiple comparisons results, n=4 mice). However, the activity increase observed when GCs become responders was higher during training than during habituation (**Fig. 3e**, **(right)**, Kruskal-Wallis test, p<0.0001, Dunn's multiple comparisons test, p=0.0007, n=4 mice).

We already established that task-responsive GCs are generally more active than unresponsive GCs, even outside of conditioning trials (**Supplementary Fig. 2f**). When tracking GCs, this was also apparent. The T_0 non-trial activity (defined as activity during 20 seconds before tone onset) was increased for both habituation and training responsive GCs (**Fig. 3f, (left, middle),** Kruskal-Wallis test, p < 0.0001, see supplements for multiple comparisons results, n = 4 mice). This increase did not vary significantly during associative learning (**Fig. 3f, (right)** Kruskal-Wallis test, p<0.0001, Dunn's multiple comparisons test, p=0.2748, n=4 mice). The T0 trial rates were higher than the T0 non-trial rates for habituation and training (**Fig. 3e, f (right)**, indicated by §, Kruskal-Wallis test, p<0.0001, Dunn's multiple comparisons test, trial baseline vs. non-trial baseline, p=0.0002, trial training vs. non-trial training, p<0.0001, n=4 mice).

These data show that a subpopulation of GCs displays increased activity and reliability in the tone-trace interval during learning. Most GCs switch to a high-activity state with significantly higher task-related and non-task-related activity when they become responders and switch back to a low-activity regime after that. A relatively small subset of 4-7% of GCs exhibits stable task-related activity from session to session.

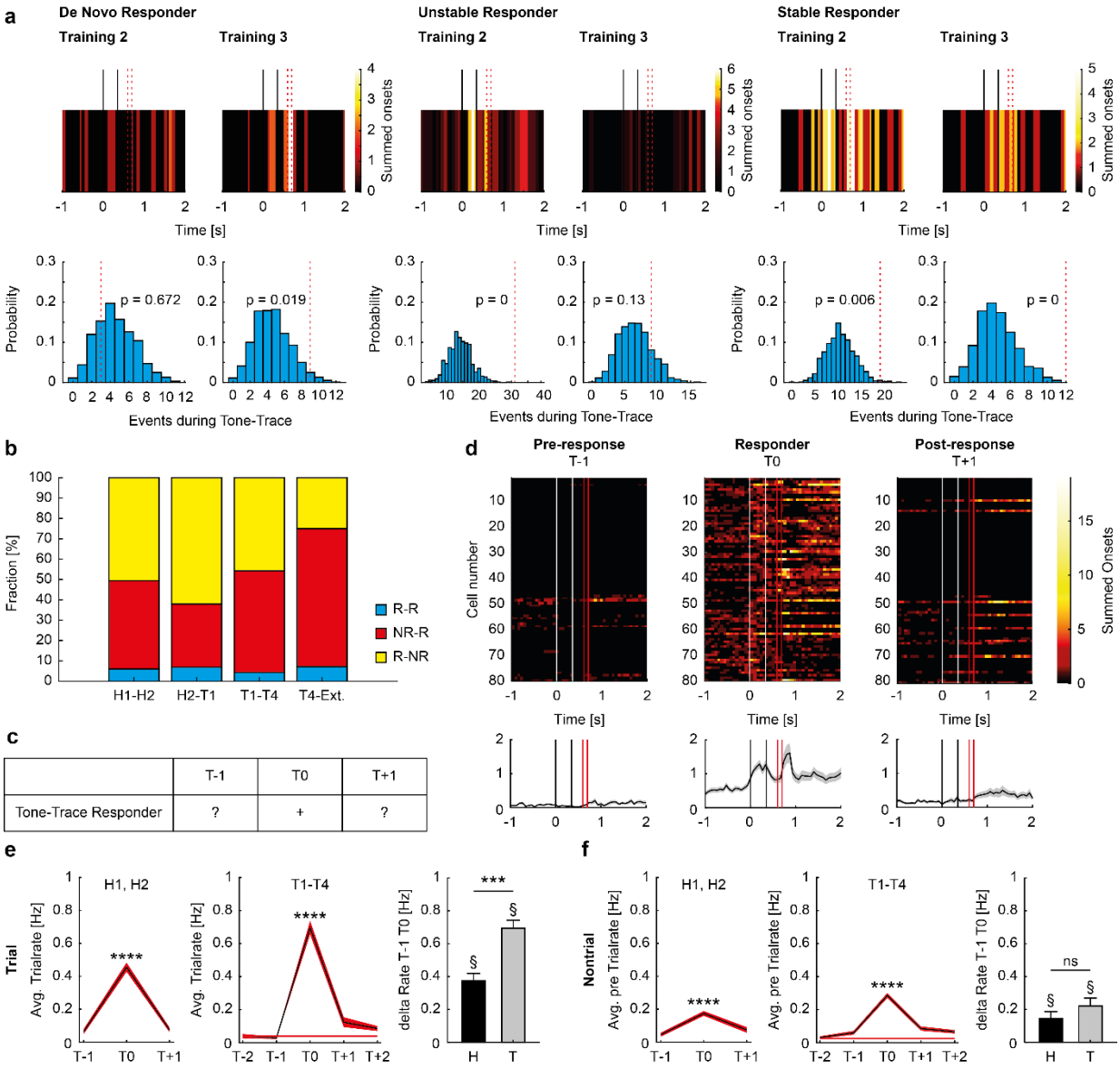

Fig. 3: Stability of tone-trace responses during learning. a, *Examples for nonresponders that convert to tone-trace responders (a, left), and conversely, tone-trace responders that convert to nonresponders (a, middle), or stable responders (a, right) in consecutive sessions.* ***b,*** *Tracking GCs over session pairs (indicated on the x-axis). Included are all GCs that were responders in any or both sessions. Fractions of nonresponders converting to responders (orange) and vice versa (yellow), as well as the fraction of stable responders (blue) during habituation (H1-H2), onset of training (H2-T1), and training (average of T1-T2, T2-T3, T3-T4), extinction (T4-Ext).* ***c,*** *Schematic of T-1, T0, and T+1 definition.* ***d****, Heatmaps of online responses of all GCs that were tone-trace responders on day T0. Only the four training days are depicted, so T0 is either Training day 2 or 3. Completely black rows result from silent cells.* ***e,*** *With the same filter logic as in d, the average trial rates are depicted for habituation responding and training responding cells. Dashed lines show the averages of these cells during H1 and H2. Barplot (right) difference between the rate on T-1 and T0. § indicates a statistically significant difference between Non-trial vs. Trial Habituation and Non-trial vs. Trial Training delta rates.* ***f,*** *Same as in E, but for the non-trial activity (20s before tone onset).*

3.4 Network events preferentially integrate trial-responsive granule cells into synchronous subensembles

Because task-responsive GCs seemed more generally active even in the intervals between trials, we scrutinized non-trial-related activity more closely. GCs show substantial offline activity when mice are immobile. In particular, they exhibit synchronized, sparse population events. We identified synchronized neuronal network events during tEBC sessions in all mice under

investigation, using a shuffling approach described previously (**Fig. 4a, b**, network events depicted in different colors, **Supplementary Fig. 5a**, Pofahl et al., 2021). Network events occurred predominantly during immobility outside of tEBC trial periods (83.4±3.4% (SEM over days), depending on the session, we detected a total of 447-773 network events per session pooled over four mice, **Supplementary Fig. 5b**). A significant fraction (87.8±3.4% (SEM over days) of network events occurred when mice were completely immobile.

We observed substantial learning-related changes in offline reactivation during network events. While the frequency of network events was not significantly altered during learning (**Fig. 4c**, One-way ANOVA, p=0.9674, n = 4 mice), we found a marked increase in the average size of network events compared to baseline conditions during both the non-probe and probe phases of each session (**Fig. 4d**, Kruskal-Wallis test, p<0.0001, Dunn's multiple comparisons test, Baseline vs. T1-Ext. p<0.0001, n = 4 mice, **Supplementary Fig. 5c**, Kruskal-Wallis test, p<0.0001, Dunn's multiple comparisons test, Baseline vs. T_1-Ext. p<0.0001, n=4 mice). The size of network events was increased both in terms of the fraction of active components in network events and in absolute cell numbers per network event (**Fig. 4d, Supplementary Fig. 5d**, Kruskal-Wallis test, p<0.0001, Dunn's multiple comparisons test, Baseline vs. T_1-Ext. p<0.0001, n=4 mice**)**.

We next examined if network events preferentially integrate GCs that respond during tEBC. We found that GCs that significantly respond during tEBC are integrated into NEs similarly during habituation and the first training sessions (T_1-T_2). However, subsequently, the tEBC responders were integrated into more of the NEs observed during late training sessions T_3 and T_4 (**Fig. 4e,** 2-way ANOVA, Interaction, Day and cell type p<0.0001, Holm-Šídák's multiple comparisons test, T3 and T4 Responder vs. Nonresponder p<0.0001, for other comparisons, see supplements, n=4 mice). Similar results were obtained when tracking cells over all seven sessions and plotting the NE participation rate (**Supplementary Fig. 6a**, 2-way ANOVA, Interaction, Day and Celltype p<0.0001, Holm-Šídák's multiple comparisons test, T_2, T_3, and T_4 Responder vs. Nonresponder p<0.0001, for other comparisons, see supplements n=4 mice).

We next asked if task-responsive GCs are more likely to be coactive within network events. We calculated population pairwise synchrony for both groups of GCs. We found that during learning, the correlations of responders strongly increased, with responders becoming significantly more correlated to other responders. This phenomenon was significantly more pronounced for responders than nonresponders in early learning. Nonresponder and responder correlations remained elevated during extinction compared to habituation trials. In addition, the activity of nonresponders vs. responders was comparatively uncorrelated in all phases of learning (**Fig. 4f**, Brown-Forsythe ANOVA test, p<0.0001, n = 4 mice). These effects were entirely neutralized

by using shuffling approaches of the activity vectors during network events (**Supplementary Fig. 6b**, Brown-Forsythe ANOVA test, p=0.8235, n=4 mice).

These data show that network events preferentially integrate task-related GCs during learning. They also reveal that task-responsive GCs are activated in an increasingly correlated fashion during learning.

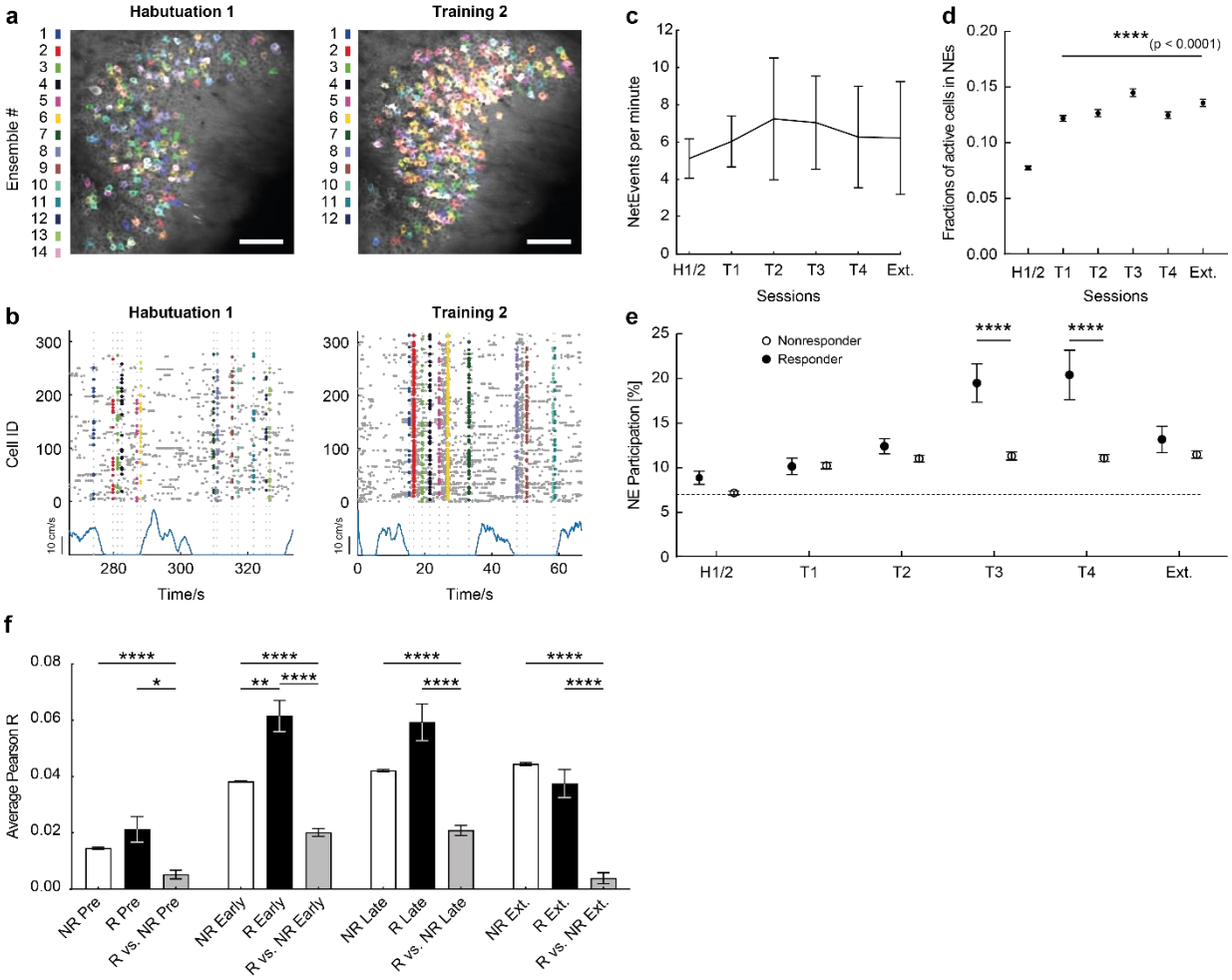

Fig. 4: Altered synchronized network events in the DG during tEBC. a, *Participation of GCs in synchronous network events. Representative FOV with highlighted simultaneously active GCs. Cells active during an individual network event are depicted in the same color. A subset of neurons is active in multiple network events, recognizable as white color. The upper panel depicts a habituation trial, lower panel a training trial (T_2) from the same mouse.* ***b,*** *Raster plot of network events. Dashed lines mark network events corresponding to the simultaneous activity of > four cells. Participating cells are highlighted according to the color scheme from panel A. Running speed is depicted (blue) to distinguish running and resting periods. The upper panel depicts a habituation trial, lower panel a training trial (T_2) from the same mouse.* ***c, d,*** *Network event frequency, and size, respectively. We first examined if these network events are modified during tEBC.* ***e,*** *Participation of tEBC responders and nonresponders in NEs across learning. Quantification shows average values across GCs for a fraction of NE events in which a GC is active.* ***f****, Pairwise linear correlation of different cell groups in network events (NR: Nonresponder correlated with nonresponder, R: Tone-Trace responder correlated with Tone-Trace responders, and R vs. NR: Tone-Trace responder with nonresponder.). Pre-Learning: Activity during H1 and H2. Early and late Learning: pooled results from sessions T1/T2 and T3/T4. Individual sessions are shown in* ***Supplementary Fig. 6b****.*

3.5 Stability of trial-responsive ensembles across sessions

Network events preferentially activate responder GCs in a correlated manner. We next examined how stable the integration of task-related ensembles of GCs into network events is across learning. To this end, we identified GCs that were task-responsive during a training session (termed T_0) and examined their incorporation into network events during T_0 and the two sessions before and after T_0 (T_{-2}, T_{-1}, T_{+1}, T_{+2}). We found that task-responsive cells in T_0 were more likely to participate in network events in the following session (T_{+1}) compared to baseline values (**Fig. 5a**, Kruskal-Wallis test, p<0.0001, Dunn's multiple comparisons test, Baseline vs. T_0 p<0.0001, Baseline vs. T_{+1} p=0.0124, n=3 mice). NE participation of habituation responders was not statistically different for T_{-1} and T_{+1} (**Supplementary Fig. 6c**, Kruskal-Wallis test, Dunn's multiple comparisons test, T_{-1} vs. T_{+1} p>0.9999, n=3 mice).

Tracking GCs over training also allowed us to assess how cells that were previously responders are correlated in subsequent sessions. As done previously, we calculated the pairwise Pearson's correlation for significantly responding GCs during an individual session (termed T_0). We found that correlations decreased over time but were still significantly elevated compared to shuffled data at T_{+2}. Interestingly, this was also true when we examined correlations between neurons that were responders at T_{+1} or T_{+2} with cells that were significant responders at T_0. This indicates that significant activity correlations emerge during network events integrating variable task-related GC ensembles over days (**Fig. 5b, c)**. Of note, this effect was not seen when correlating the activity of former responder GCs and current nonresponder GCs (**Fig. 5d**).

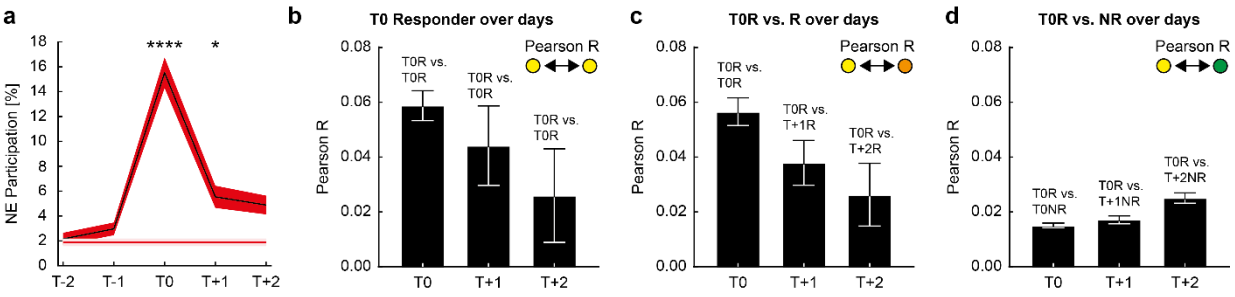

Fig. 5: Synchrony in network events over days. a, *NE integration of task responders across sessions (see extra info below).* ***b, c,d,*** *Correlation of magnitude data in NEs of T_0 responders within the same group vs. same-day responders and same-day nonresponders over days, respectively.*

This data show that task-responding GCs are more likely to participate in network events during successive sessions. Furthermore, they seem to form synchronized ensembles with other GCs that were responders in previous sessions.

3.6 Supplementary figures

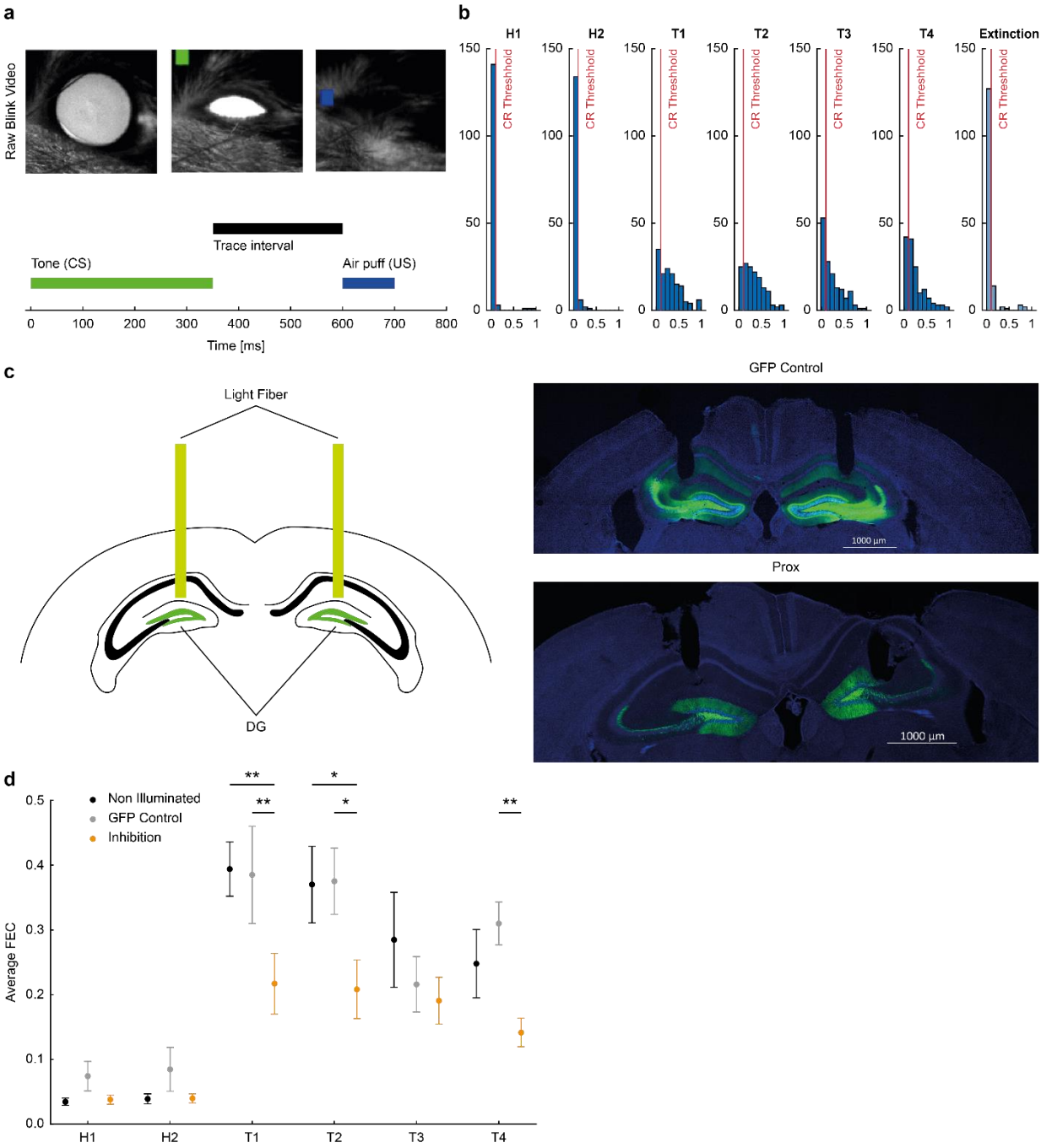

Supplementary Fig. 1: tEBC protocol and CR threshold. a, *Example of high-speed camera images during tEBC.* ***b,*** *Histogram of FEC values during training. The red line indicates the threshold for classification as a successful CR response.* ***c,*** *light fiber schematic and histological analysis of inhibition experiments.* ***d,*** *Average FEC values of non-illuminated control, illumination control, and inhibition group over days.*

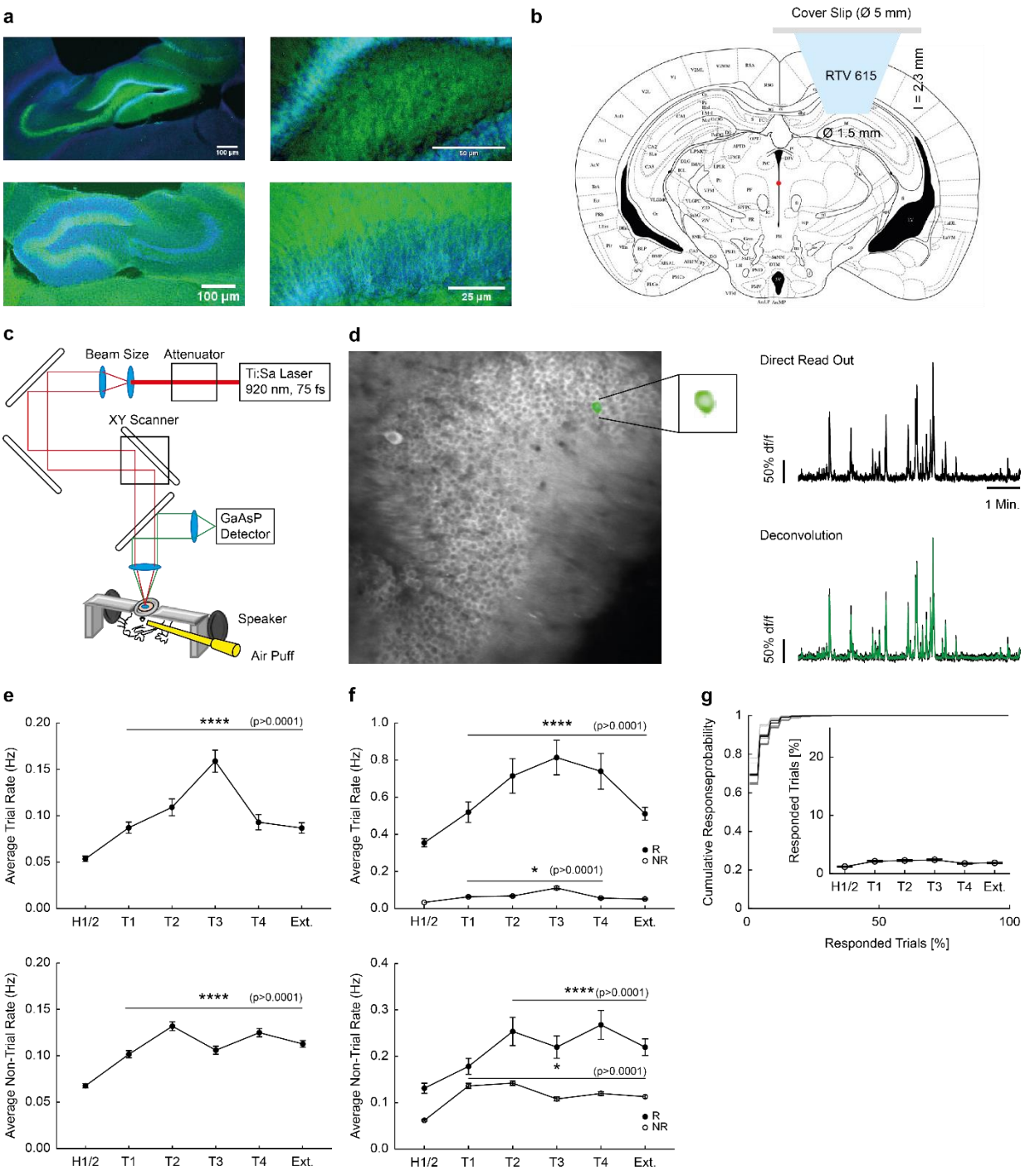

Supplementary Fig. 2: 2P imaging. a, *Expression of GCaMP,* ***b,*** *Dimensions of cranial window* ***c,*** *Experimental setup.* ***d,*** *Isolation of individual Ca^{2+} transients* ***e,*** *Characterization of Ca^{2+} transients with respect to their frequency within the trial period (top) and outside the trial period (bottom) average overall active cells. The trial period is defined as 1 second after tone onset and the non-trial period as the 20s before the tone onset.* ***f****, same as in* ***e****, but split into responder and nonresponder rates.* ***g****, the trial response rate of nonresponders.*

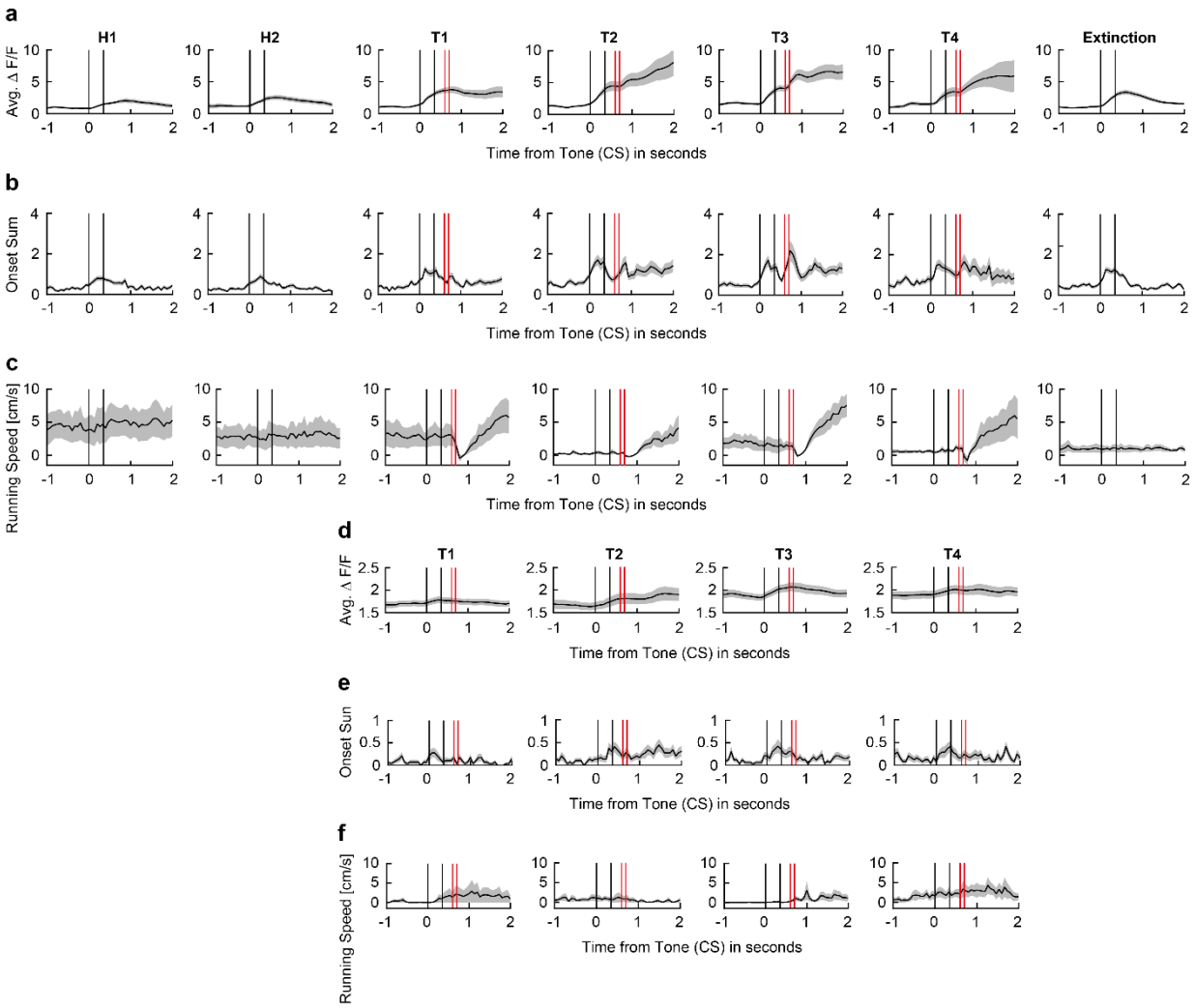

Supplementary Fig. 3: Tone-trace responder grand averages during probe trials. a,b, *average df/f and onset rate of responder cells over paired trials,* ***c,*** *average running speed over paired trials,* ***d-f,*** *same as a-c, but for probe trials only.*

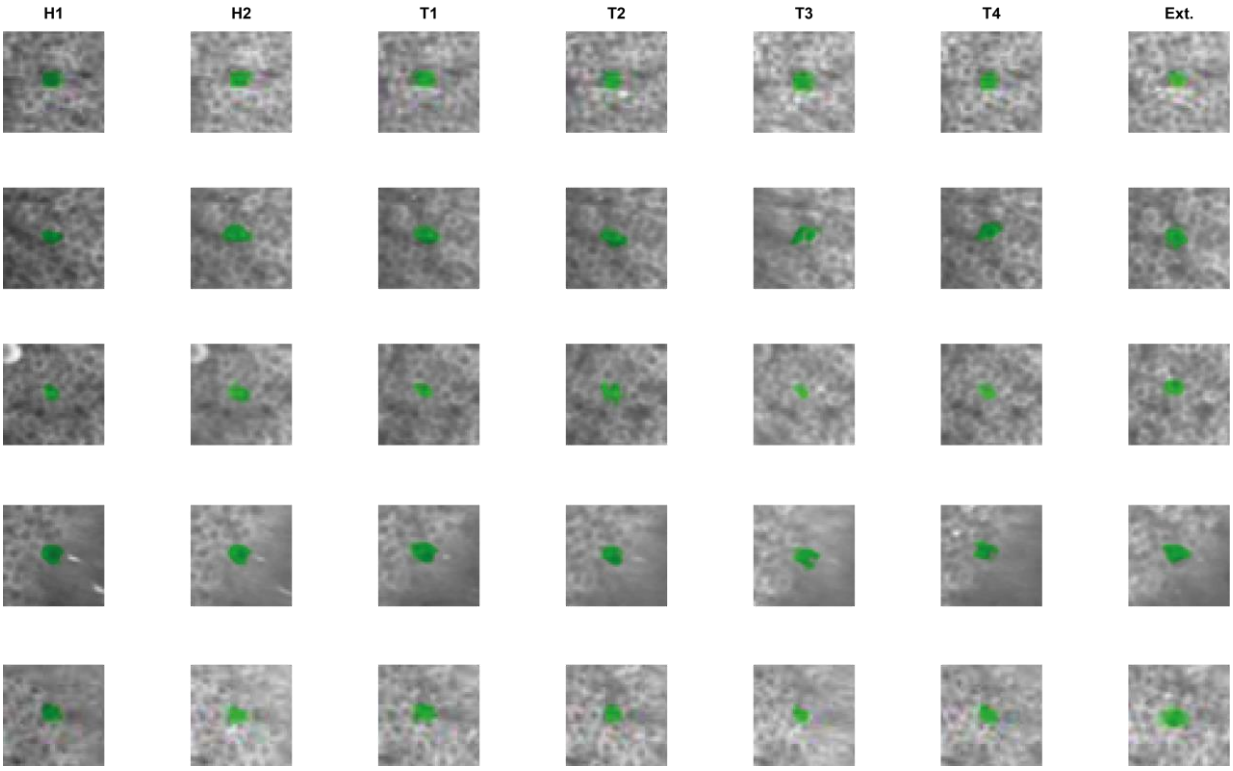

Supplementary Fig. 4: *7 session tracking examples.*

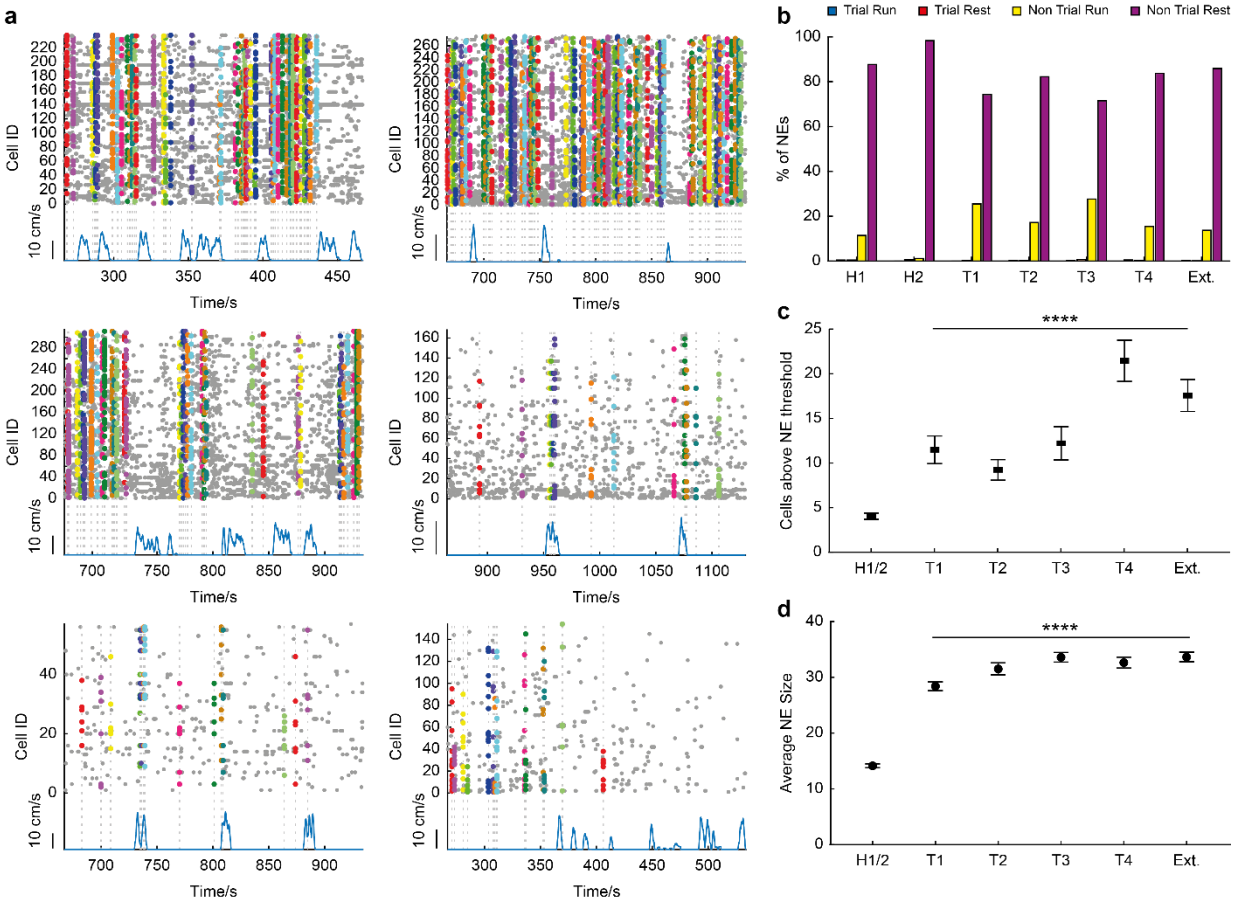

Supplementary Fig. 5: **Network event detection and shuffling. a,** NE Raster plot examples, **b**, NE distribution trial rest, trail run, nontribal rest, non-trial run, **c**, NE size during probe trials, **d**, average NE size during paired trials in absolute cell number per NE

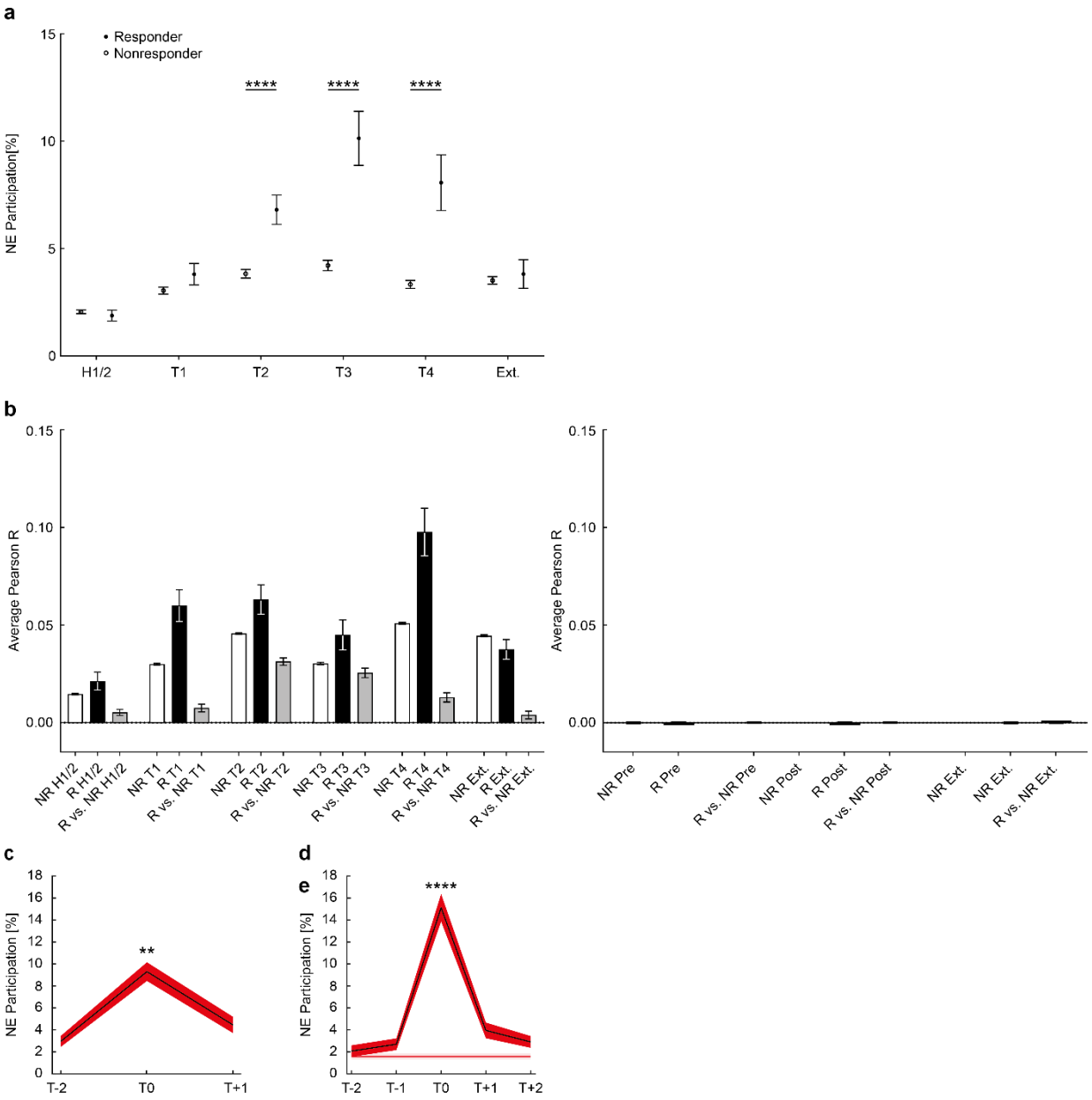

Supplementary Fig. 6: NE participation and synchrony in tracked data. a**, 7-day tracking of training responders and training nonresponder and their NE participation, **b**, pairwise correlations of NR-NR, R-R, NR-R over days and shuffle result of the same data (Results of the pairwise comparison are in supplements for readability sake), **c**, same as Figure 5a, but with baseline responders, **d**, figure 5a, but only with T_0 responders **(only ~1% of cells are responders on more than one consecutive day).

4 Discussion

In this study, we established a head-fixed tEBC task that allowed simultaneous calcium imaging of the DG GC population. tEBC is a form of simple associative learning that relies on an intact hippocampus (Moyer et al. 2015). Individual GC components could be tracked longitudinally to study activity changes over multiple days. In line with previous studies, we found specific stimuli responses in a subgroup of the imaged GC population that were higher than chance (Miller et al. 2022, 2019; Suter et al. 2018). The responder population in the DG was rather unstable. As reported in an earlier study, we found sizeable synchronous population activity of the dentate GCs, so-called network events (Pofahl et al. 2021). These network events grew in size by incorporating a higher fraction of the active cell population during training sessions than habituation sessions. Furthermore, the fraction of task-responding cells in network events was significantly higher than the nonresponder fraction during late learning. Responder cells were significantly more likely to participate in network events with other responder cells. This effect remained elevated after a cell stopped being a significant responder. Additionally, the requirement of the DG GCs during tEBC was scrutinized in a separate cohort.

4.1 Targeted inhibition of the dorsal dentate gyrus disrupts learning during trace eyeblink conditioning

Using lesion interventions, different brain areas have been associated with tEBC. For example, studies show that disrupting the cerebellum, hippocampus, medial prefrontal cortex, EC, perirhinal cortex, postrhinal cortex, visual cortex, caudate nucleus, and thalamus affects tEBC (Oswald et al. 2007; Powell and Churchwell 2002; Flores and Disterhoft 2009, 2013; Steinmetz et al. 2013; Suter et al. 2013; Ryou et al. 2001; Kronforst-Collins and Disterhoft 1998; Weible et al. 2000; McLaughlin et al. 2002; Lincoln et al. 1982; Tseng et al. 2004; Moyer et al. 2015). To probe whether the DG is needed for tEBC, we inhibited the dorsal DG GC population. As in previous studies, the disruption of the dentate GCs perturbed performance in tEBC (Madroñal et al. 2016; Miller et al. 2019). Madroñal et al. reported a loss of trace eyeblink memory when GCs were inhibited during training after mice reached the criterion. Miller et al. investigated how newborn GCs are involved explicitly in learning tEBC in mice. Our data adds to these studies by inhibiting mature GCs over the whole training process. These data demonstrate that the DG GC is relevant for learning tEBC in mice.

In our experiments, there was still residual acquisition of the CS-US association, even when GCs were inhibited. This phenomenon might be explained by some or a combination of the following. First, ding our experiments, we predominantly inhibit the dorsal DG **(Supplementary**

Fig. 1c, as in (Pofahl et al. 2021)**)**. Perhaps the dorsal GCs missed by our inhibition intervention are sufficient to allow for some learning.
Intradentate compensation mechanisms might allow for coding tEBC in the ventral DG once the dorsal DG is disrupted. One study reported a possible compensation mechanism between the ventral and dorsal hippocampus during two-way active avoidance (Wang et al. 2015). Another study demonstrated that the hippocampus and Amygdala can compensate for each other during fear conditioning (Yu et al. 2021). Evolutionarily, these compensation mechanisms might offer resilience against possible brain injuries. Generally, it is common to still see some trace learning in mice with disrupted hippocampal function (Miller et al. 2019; Tseng et al. 2004).

Both the average CR and FEC were significantly lower on T1, T2, and T4 in the inhibition group compared to the control. Interestingly, T3 did not show a significant difference **(Fig. 1f, g)**. However, the performance on T3 was generally lower across all cohorts compared to the other training days, which might explain why there was no significant difference between the control and inhibition groups on T3. The low performance on T3 might be explained by a slight habituation to the air puff over time, which is reflected in the lower FEC on T3 and T4 **(Fig. 1c)**. This might render the US less aversive, resulting in decreased relevance for the animal to associate it with the tone. Other studies that used an air puff as an US also reported a slight dip in CR performance on training days 3 and/or 4 (Miller et al. 2022; Suter et al. 2018). Another explanation for why the dentate inhibition seemed to have a more substantial effect during T1 and T2 is the idea that the hippocampal formation is more important during early learning of tEBC (Kim et al. 1995; Takehara et al. 2002; Takehara et al. 2003). Starting from T3, the DG might become less germane to code tEBC, as some relevant plasticity already occurred downstream in CA3 and CA1. However, these studies only investigated the time points of one day after learning and one month. If the DG is required for tEBC on a day or rather a week scale has not been investigated yet.

The inhibition group showed a significantly lower first tone FEC during training than the control **(Fig. 1g)**. We elaborate on two potential reasons for this in the following. The first explanation involves the disrupted encoding of tEBC. The inhibition group performs worse than the control group on almost all training days. This makes it more likely that an inhibited animal will also respond less frequently to the first tone on a given day. A different experimental design is needed to further scrutinize whether inhibition of the GCs affects encoding and/or recall of tEBC. One way to test this would be to have two cohorts, as in our dentate inhibition experiment. One group receives dentate inhibition during the paired portion of the session and no inhibition during the probe. This would test whether the DG is important for acquisition in tEBC. The second group would only be inhibited during the probe period to test if the recall is disrupted. Existing data suggest that the DG is unnecessary for recall in tEBC (Madroñal et al. 2016).

The second explanation for the observation lies in the disrupted recall of memory relevant for tEBC and is rather implausible. On the first day, the hippocampus undergoes some plasticity processes relevant for tEBC, despite inhibition of the dentate GC (see above how this might happen). The next day, the animal receives the first tone and must remember to blink to the stimulus. Since the DG gets inhibited during this moment, recall might be disrupted, making a sufficient conditioned response less likely. This explanation is rather unlikely since the DG is likely less relevant for the recall of tEBC than for encoding (Hainmueller and Bartos 2020; Rolls 2018; Lee and Kesner 2004; Madroñal et al. 2016).

4.2 A subpopulation of granule cells shows activity increases during the tone-trace interval and higher response probability.

Here we reported similar baseline calcium event rates of GCs as in a previous imaging study (Pofahl et al. 2021). However, there are some differences that we would like to address. Pilz et al. reported lower average event rates of GCs during an imaging study (Pilz et al. 2016). This study used an AAV-based GCaMP6s model compared to the transgenic Thy1-GCaMP6s mouse line we used in our experiments. Furthermore, different onset detection procedures were used, which likely makes a big difference.

Additionally, no tones were played, which might explain the higher event rates in our study as well. Similar differences in detected onset rates might be caused by using different calcium indicators other than GCaMP6s (Danielson et al. 2016). It has been shown that using different calcium indicators leads to variations in recorded cell activities (Dana et al. 2014). Furthermore, recent electrophysiological studies have reported a large variance in firing frequencies of GCs, depending on locomotion and the behavioral state of the animal (Zhang et al. 2020; Neunuebel and Knierim 2012; Senzai and Buzsáki 2017; Miller et al. 2022).

Using shuffling approaches, we found a tone-trace responder subpopulation of GCs. In our experiments, the fraction of these tone-trace responsive cells was constant across learning (6.74%±0.37). The fraction of tone-responsive GCs was similar (6.6%) to the reported fractions in another study (Woods et al. 2020). We showed that this constant fraction is associated with a constant turnover of an unstable responder population from session to session. While new GCs become responders, a similar number of cells stop being responders in every training session **(Fig. 3)**. As noted before, the responder population expressed higher firing frequencies during and outside stimulus presentations **(Supplementary Fig. 2e, f)**. Seemingly, responder GCs switch into a high-activity state on the day of being a responder and return to a low-activity state after that **(Fig. 3).**

We found learning-related increases in trial response rate in GCs. This aligns with previous reports (Miller et al. 2022; Buzsáki and Draguhn 2004; Suter et al. 2018). Additionally, we observed that the likelihood of responder cells responding to any given trial increased with training. However, the response pattern in the DG was still very sparse and unreliable. This raises the question of how the DG can facilitate the encoding of tEBC. Maybe plasticity related to associative learning happens outside the dentate in downstream regions like CA3 and CA1 (Gruart et al. 2006). The DG might be required to entrain downstream areas and facilitate proper encoding (Scharfman 2007a, p. 567, 2007a, p. 572; Hainmueller and Bartos 2020). We detected lasting increases in calcium signal and onset rate after the air puff emerging from T2 onwards **(Supplementary Fig. 3a,b)**. This was not reported in electrophysiological recordings of GCs during tEBC (Miller et al. 2022; Suter et al. 2018). The explanation for this might lie in the different temporal dynamics in calcium imaging data compared to, e.g., tetrode recordings (Huang et al. 2021). One physiological cause might be that we observed that animals would, on average, stop when the air puff was given and start running shortly after. This running onset seems to happen at a similar time as the post-air puff rise in the signal. The phenomenon might be driven by speed-modulated GCs (Pofahl et al. 2021). Another reason for this could be a longer-lasting air puff response since the effect is not present in the probe trials **(Supplementary Fig. 3c-f).** In our experiments, it is impossible to say whether the effect is driven by locomotion or the air puff since the two are intermingled in our data set. Interestingly, the learning-related increase in GC activity did not return to habituation levels during extinction. This might indicate plasticity changes in the dentate GC population, which were not reversed by one extinction session.

4.3 The tone-trace responder population in the dentate gyrus is unstable

The fraction of GCs that responded to the tone-trace interval in two consecutive sessions was meager (6.04%±0.69 of all cells that were responders in either of the two sessions). Interestingly, the number of de novo responders in the T4-Ext. was significantly higher than during habituation, and the unstable responders were lower. This raises the question of whether a different set of GCs gets activated during extinction compared to the encoding sessions. A similar effect was reported in CA1 pyramidal cells during tEBC (Mount and Sridhar 2021). This rise in new responder cells possibly reflects the DG detecting the novel aspect of the situation. The relation of the tone in the context of the experimental setting has changed and does not predict the air puff anymore. There have been reports of the hippocampus being essential for the extinction of tEBC (Moyer et al. 1990; Schmaltz and Theios 1972). This goes in line with the notion of extinction being a form of learning a new association and not just forgetting an existing one (Kandel et al. 2000). Furthermore, it makes sense that there is a mechanism in the brain

that detects when a stimulus is no longer associated with an event or another stimulus. This mechanism induces the adaption of behavior and response patterns to a new situation. Changes in context and stimulus contingency can change in subtle or more obvious ways. This poses the need for a pattern separator that can detect nuanced environmental differences. The dentate has been shown to be involved in tasks like this (Pofahl et al. 2021; Leutgeb et al. 2007). The constant change of the GC responder population in tEBC raises the question of how stable presentations of aversive memories can be formed in the hippocampus. Furthermore, it is striking how the responder population varies daily, but the tone-trace rate seems to increase from T1-T3 (Fig. 2g). It is unclear which plasticity mechanism would facilitate such activity patterns. Two systems that could accommodate this mechanism are neuromodulatory inputs into the DG and/or stable responder cells or recurring responder cells that increase the average tone-trace rate (Kesner 2013a; Kaneko and Thompson 1997; Solomon et al. 1993). Responder cells fire at higher rates during the session they are responder cells **(Fig. 3e, f)**. It is unclear if this process is random or specific to tEBC. Potentially, a constant pool of higher activity cells in the DG can code task-relevant information. Which cells get into this state might be predominantly random, serving the role of the DG as a randomizer (Rolls 2013a). These sparse competitive network properties support encoding of overlapping attractor ensembles in CA3 (Rolls 2013a). CA3 and/or CA1 might be where tEBC correlates are more stable than in the DG (Gruart et al. 2006).

The low stability of tone-trace responders was in contrast to reports of stable spatial representations in the DG (Hainmueller and Bartos 2018). However, the response stability of odors was also unreliable in the dentate GC population. The authors argued that the MEC-DG pathway might underlie different stability than the LEC-DG inputs (Woods et al. 2020). It seems that information conveyed by LEC, like tones and odors, has lower stability in the DG than metric information coming in via the MEC (e.g., spatial information).

4.4 Large synchronous population events increase in size

As reported, we found large population events of dentate GCs, called network events (Pofahl et al. 2021). These population events have not been reported in other *in vivo* imaging studies of the DG. One *in vitro* study reported wave-like population events in the GC population (Seki et al. 2012). The recorded waves were limited to the first postnatal week, though. In our study, training the mice in tEBC significantly increased network events' size. During extinction, network events remained larger than during habituation. This means the average network event size remained elevated after learning compared to pre-learning conditions. The increase in network event size seems to correlate with the overall increase in GC activity **(Fig. 4d, Supplementary Fig. 2e, f)**. Network event size was also increased by adding spatial cues to a previously empty belt (Pofahl et al. 2021). During this study, the increase in network event size was more

prominent. As in Pofahl et al., the fraction of feature-coding cells in network events increased with training (Pofahl et al. 2021). In the current study, this effect was confined to training days T3 and T4 **(Fig. 4e)**. This was the case even though the fraction of active cells in network events increased before that, and network event frequency was not altered.

This raises the question of which mechanism affects the enlargement of network events and the preferential recruitment of task-responding cells into them. For example, perforant path inputs might drive the size increase of network events. It has been shown that dentate network events correlate with inputs of the MPP (Pofahl et al. 2021). Furthermore, learning-related activity in the EC co-occurs with increased DG activity during tEBC (Suter et al. 2018). Septal cholinergic inputs to the dentate GCs might also modulate the network event size during tEBC (Mosko et al. 1973; Amaral and Kurz 1985; Swanson 1977). In addition, it has been shown that cholinergic activity is crucial for learning tEBC (Kaneko and Thompson 1997; Solomon et al. 1993).

The CA3-DG back-projection could additionally drive the effect of larger network events that incorporate more task responders. The higher trial activity of tone-trace responders leads to plasticity changes in CA3, forming overlapping responder-driven ensembles (Neubrandt et al. 2018; O'Reilly and McClelland 1994). During network events, these CA3 ensembles might get activated, increasing the propensity to reactivate responder cells in the DG via CA3-DG back-projections. This hypothesis gets strengthened by the observation that responder cells seem to preferentially co-participate in the same network events compared to nonresponders **(Fig. 4f)**. The cellular mechanism might work as described in the following. The CA3-DG back-projection can affect the dentate GC population via disynaptic connections (CA3PC-MC-GC, or CA3PC-dentate IN-GC (Sun et al. 2017; Kneisler and Dingledine 1995a; Hashimotodani et al. 2017)). There is also evidence for direct inputs from CA3 to the DG GC (Sun et al. 2017). Reactivation of CA3 ensembles during sharp-wave ripples can increase mossy cell activity, which can increase GC activity (Swaminathan et al. 2018). Interestingly, when looking at the general effect of CA3 activation *in vitro* on GC activity, CA3 seemed to mainly inhibit GCs (Kneisler and Dingledine 1995a). This raises the question of whether activation of the dentate GCs via the CA3-DG back-projection is confined to sharp-wave ripple events in CA3. This leads to a gradual formation of tEBC relevant ensembles in CA3 and the dentate GC population.

4.4.1 Are network events dentate spikes and/or dentate sharp waves?

Two reported population events in the DG are DSs and dentate sharp waves (Bragin et al. 1995; Dvorak et al. 2021; Meier et al. 2020). There are two types of DSs. DS type 1 is evoked by the LPP, whereas DS type 2 is caused by MPP activity (Bragin et al. 1995; Dvorak et al. 2021). DSs modulate how inputs from the perforant path can excite GCs. GCs are more excitable by the

perforant path during DSs (Lehtonen et al. 2022; Bramham 1998). Additionally, DSs are important for learning tEBC (Nokia et al. 2017).
It is currently unclear which net effect DSs have on CA3/CA1 activity. Initially, DSs were reported to suppress sharp-wave ripples (Bragin et al. 1995; Penttonen et al. 1997). However, one study found no effect of DSs on CA3/1 activity (Lehtonen et al. 2022). Another study reported that DSs type 2 can change firing patterns in CA3/1, while DSs type 1 cannot (Dvorak et al. 2021). These differences in findings might result from the fact that DSs should always be separated into type 1 and type 2 since they seem to have different effects (Dvorak et al. 2021). Contrary to this, reward-related CA3 sharp-wave activity depended on the DG during a working memory task. However, the authors did not look at DSs (Sasaki et al. 2018).

The phenomenon of network events in the DG begs the question of how these population events relate to DSs and dentate sharp waves. Unfortunately, in this study, we did not record local field potentials or other electrophysiological data, making it impossible to detect such events reliably. However, we can analyze similarities between the reported properties of DSs and dentate sharp waves and our network event data.
During habituation, we measured network event rates of 4.2±1.6 events per minute. Reported rates of DSs vary depending on the study. The first study introducing DSs reported rates of about 15 events/minute during quiet wakefulness in rats (Bragin et al. 1995). Other reports range from 12 (Headley et al. 2017) to over 60 DSs/minute in awake resting rats (Dvorak et al. 2021). The reason for this discrepancy might be variations in spike detection methods, low n number, and differences in DS1 and DS2 rates (Dvorak et al. 2021). A similarity between DSs and network events is that they predominantly occur during rest and not locomotion (Bragin et al. 1995; Headley et al. 2017). However, one study reported more DS2 during higher running speeds than rest (Dvorak et al. 2021). The presented studies were done in rats. It could be that the DS rates in mice are different or that we could not measure the actual network event rate with our imaging approach. Possibly, some network events are DSs.

The dentate sharp-wave data is currently limited to one study (Meier et al. 2020). Dentate sharp waves occur independently or during CA1 sharp waves at rates of 12-30 events/minute. They are defined as large amplitude events with a current sink in the inner molecular layer and a current source in the outer molecular and granule cell layers. Because of their overlap with sharp-wave ripples, dentate sharp waves might be triggered by CA3-DG back-projections. The rate of dentate sharp waves increased after hippocampus-dependent learning (Meier et al. 2020). All in all, the evidence is inconclusive regarding whether network events are DSs or dentate sharp waves. However, there is no clear evidence that some network events might overlap with DSs or dentate sharp waves. Further experiments using imaging interventions paired with electrophysiological recordings are needed.

4.5 The task-responsive granule cell population becomes more synchronous in network events

After we observed a higher participation rate of task-responsive GCs during late learning, we investigated how network event participation behaves before and after a cell became a responder cell **(Fig. 5)**. We found that once a cell was a tone-trace responder, it participated more often in network event in subsequent sessions. This may reflect learning-related plastic changes in the task-responsive population.

This mechanism might be necessary for a more stable neuronal representation during tEBC in the hippocampus. While the task activity and responder population are unstable from session to session, more stability is reflected in the network event activity. This is evident from comparing the T_{+1} trial activity of task-responsive cells with their network participation probability. The T_{+1} trail activity of task responders returned to baseline conditions, while the network participation remained elevated **(Fig. 3e, Fig. 5a)**.

This is consistent with our finding of increased synchrony in network events **(Fig. 5b-d)**. After a cell was task-responsive, it showed an increased propensity to participate in network events with other former or current responders. This was not the case for nonresponders, and the effect was completely abolished by shuffling network event activity.

Based on these data, sparse, correlated, and relatively stable ensembles of task responders in the DG may be generated during quiet immobility. This coordinated activity was not present during habituation trials, which suggests that it was related to learning during tEBC **(Supplementary Fig. 6b, c)**.

A similar process has been reported for CA3/1. Neurons that conveyed task-relevant information from CA3 to CA1 were preferentially reactivated in sharp-wave ripples. Cells that did code for information that was not important for the task, on the other hand, were inhibited (Terada et al. 2022). This underlines that resting activity in the hippocampus is important to strengthen task-relevant neuronal connections.

4.6 Conclusion - The proposed role of the dentate gyrus during trace eyeblink conditioning

Together with the existing evidence of computation in the DG, we can formulate a tentative mechanism of how the DG facilitates learning during tEBC. During every training session, a changing population of highly active responder cells emerges from the pool of GCs. However, whether this subpopulation gets recruited randomly or causally by presenting the tone and air puff remains unclear.

4.6.1 What drives the increased activity of task-responsive granule cells?

Training the mice in tEBC led to increased activity and reliability of task-responsive cells. Three different afferent inputs might drive this effect to the DG. First, the perforant path is the primary input to the DG (Amaral et al. 2007). It has been reported that the EC shows learning-related activity changes during tEBC and is necessary for learning the task (Suter et al. 2018; Ryou et al. 2001). This increased EC activity can likely cause plastic changes at the perforant path-GC synapse (Bliss and Lømo 1973). Additionally, DG network events correlate with MPP activity (Pofahl et al. 2021).

Another relevant input are septal cholinergic inputs to the DG (Mosko et al. 1973; Amaral and Kurz 1985; Swanson 1977). Cholinergic activity is needed for tEBC (Kaneko and Thompson 1997; Solomon et al. 1993). These cholinergic inputs might also alter the cellular activity of the DG.

Lastly, the CA3-DG back-projection can change the cellular activity of dentate GCs. This can happen via a connection between CA3-MC-GC, CA3-IN-GC, or possibly direct inputs from CA3 pyramidal cells to the GCs (Swaminathan et al. 2018; Sun et al. 2017; Kneisler and Dingledine 1995a).

4.6.2 Dentate gyrus activity possibly drives CA3 plasticity during trace eyeblink conditioning

The increased task-responder activity during tEBC might increase the likelihood of CA3 activation (Henze et al. 2002). It could be that the different task-responsive GCs activate the same CA3 pyramidal cell. It has been shown that one CA3 pyramidal cell gets input from up to 70 dentate GCs (Andersen 2007). However, is still crucial that GC activity is sparse so that the engrams in CA3 are as distinct as possible to avoid storage and recall problems (Rolls 2013a). CA3 has been proposed to serve as an attractor network. An attractor network is a neural network that can spontaneously generate and maintain stable activity patterns, even without external input (Kesner 2013a). Given that stability in the DG is low during tEBC, CA3 is a potential candidate to enable a more stable neural correlate for tEBC. This is possible because of the strong recurrent associative network of CA3 (Le Duigou et al. 2014).

These more stable representations in CA3 might then enable learning-related changes at the CA3-CA1 synapse. Plastic changes in the CA3-CA1 synapse are important for trace learning (Gruart and Delgado-Garcia 2007; Gruart et al. 2006).

Another role for CA3 in learning tEBC might be that it can potentially provide a neuronal basis for temporal learning. This is important to link the relevant stimuli together during tEBC (Kesner 2013a). This idea gets strengthened by the fact that bridging activity between stimuli has been described for CA1, but not for dentate granule and mossy cells during tEBC (Modi et al. 2014;

Miller et al. 2022). Since CA1 is the downstream region of CA3, this makes it likely that temporal processing either happens in CA3 and/or CA1.

4.6.3 Why dentate network events get larger and integrate more task-responder in a synchronous manner

Our shuffling approach shows the increase in network event size is not merely a function of increased cellular activity. Instead, there has to be a more directed mechanism that recruits more task-responsive cells into the network events and increases synchrony in the current and former task-responder population. As described above, the increase in size might be attributed to perforant path inputs, cholinergic activity, or the CA3-DG back-projection. Furthermore, the perforant path is correlated with network events in the DG and might drive synchrony in these (Pofahl et al. 2021).

The CA3-DG back-projection may allow for preferential recruitment of task responders into network events (Swaminathan et al. 2018; Sun et al. 2017; Kneisler and Dingledine 1995a). We already established that task-responder activity likely drives the formation of stable attractor-like ensembles in CA3 (see above). Reactivating these CA3 ensembles will increase the propensity for task responders to participate in network events synchronously (Swaminathan et al. 2018). Moreover, task-relevant cells have a higher chance of being reactivated in replay events in CA3 (Terada et al. 2022).

One can speculate that both the perforant path and the CA3 back-projection are important for offline coordination in the DG, but their functions differ. For example, the perforant path might be more important to drive the activity of current responders and recruit them into network events. The CA3 back-projection, on the other hand, might reactivate former and recurrent task-responsive cells, recruiting them together into network events. This is possible because multiple GCs are associated with the same attractor network in CA3 (Andersen 2007).

Taken together, the role of the DG during tEBC seems to involve several aspects. First, an unstable population of stimulus-responsive GCs emerges during tEBC. Second, activity in network events is more stable and synchronous. This could happen via a drive from the perforant path, the CA3 back-projection, and/or modulatory inputs. Third, the sparse activity of this responder population allows for optimal storage of more stable attractor ensembles in CA3. A better understanding of the dentate network events could be an essential puzzle piece in understanding how the population code in the DG facilitates associative learning.

4.7 Limitations of the study

As with most studies, this study has limitations. Two of the most significant limitations are the electrophysiological identity of network events and how these population events are affected by

CA3 activity. Imaging the DG during a learning paradigm is challenging, and adding implanted probes for simultaneous electrophysiological recordings can be even more difficult. Since DSs seem not to be synchronized between hemispheres, it will be necessary to image and record electrophysiological signals from the same region of interest (Lehtonen et al. 2022). New approaches show promising applications to link network events with electrophysiological events in the DG (Liu et al. 2022).

Scrutinizing the effect of CA3 activity on dentate network events is currently hard to do. One would have to alter CA3 activity in the same experiment to see how this affects dentate network events. Currently, available hardware solutions make the implantation of this many measurement probes into the skull of a mouse unfeasible.

Another point is the reported contribution of newborn GCs in tEBC (Miller et al. 2019; Takehara-Nishiuchi 2018; Hofer et al. 2015). However, with our imaging approach, we will not record calcium activity from newborn but mainly from mature GCs. This is because the used Thy1-GCaMP mouse line expresses GCaMP, preferably in matured GCs (Hofer et al. 2015; Radic et al. 2015). Therefore, it would be interesting to study how the population activity of newborn and matured GCs differs in tEBC.

Other experiments of interest would include large scale recordings of CA3 and CA1 activity over multiple days during tEBC. The existing imaging data of CA1 during tEBC is either limited to one session or did not track individual components over days (Modi et al. 2014; Mount and Sridhar 2021).

Despite the limitations, this study is the first to image a large number of dentate GCs during tEBC over multiple days. These data add new insight to better understand associative learning in the DG.

5 List of abbreviations

CA1-3:	Cornu ammonis 1-3
DG:	Dentate gyrus
DSs:	Dentate spikes
EC:	Entorhinal cortex
MEC/LEC:	Medial entorhinal cortex, Lateral entorhinal cortex
MPP/LPP:	Medial perforant path, Lateral perforant path
FOV:	Field of view
GABA:	Gamma-aminobutyric acid
GC:	Granule cell
tEBC:	Trace eyeblink conditioning
CS:	Conditioned stimulus (tone)
US:	Unconditioned stimulus (air puff)

6 Statement

I hereby certify that the work presented here was accomplished by myself and without the use of illegitimate means or support, and that no sources and tools were used other than those cited.

Cologne, June 18 2023

7 Addendum

7.1 Tabular overview of statistical results

Fig 1c:

Friedman test	
P value	0.0004
Exact or approximate P value?	Approximate
P value summary	***
Are means signif. different? (P < 0.05)	Yes
Number of groups	6
Friedman statistic	22.38
Data summary	
Number of treatments (columns)	6
Number of subjects (rows)	6

Number of families	1					
Number of comparisons per family	5					
Alpha	0.05					
Dunn's multiple comparisons test	**Rank sum diff.**	**Significant ?**	**Summary**	**Adjusted P Value**	**A-?**	
H1+2avg vs. T1	-20.00	Yes	*	0.0101	B	T1
H1+2avg vs. T2	-26.00	Yes	***	0.0003	C	T2
H1+2avg vs. T3	-16.00	No	ns	0.0678	D	T3
H1+2avg vs. T4	-17.00	Yes	*	0.0436	E	T4
H1+2avg vs. Ext	-5.000	No	ns	>0.9999	F	Ext
Test details	Rank sum 1	Rank sum 2	Rank sum diff.	n1	n2	Z
H1+2avg vs. T1	7.000	27.00	-20.00	6	6	3.086
H1+2avg vs. T2	7.000	33.00	-26.00	6	6	4.012
H1+2avg vs. T3	7.000	23.00	-16.00	6	6	2.469
H1+2avg vs. T4	7.000	24.00	-17.00	6	6	2.623
H1+2avg vs. Ext	7.000	12.00	-5.000	6	6	0.7715

Fig 1d:

Friedman test	
P value	0.0005
Exact or approximate P value?	Approximate
P value summary	***
Are means signif. different? (P < 0.05)	Yes
Number of groups	6
Friedman statistic	22.31
Data summary	
Number of treatments (columns)	6
Number of subjects (rows)	6

Number of families	1					
Number of comparisons per family	5					

Alpha	0.05					
Dunn's multiple comparisons test	**Rank sum diff.**	**Significant?**	**Summary**	**Adjusted P Value**	**A-?**	
H1+2avg vs. T1	-20.00	Yes	*	0.0101	B	T1
H1+2avg vs. T2	-23.00	Yes	**	0.0019	C	T2
H1+2avg vs. T3	-17.00	Yes	*	0.0436	D	T3
H1+2avg vs. T4	-16.00	No	ns	0.0678	E	T4
H1+2avg vs. Ext	-2.000	No	ns	>0.9999	F	Ext
Test details	Rank sum 1	Rank sum 2	Rank sum diff.	n1	n2	Z
H1+2avg vs. T1	8.000	28.00	-20.00	6	6	3.086
H1+2avg vs. T2	8.000	31.00	-23.00	6	6	3.549
H1+2avg vs. T3	8.000	25.00	-17.00	6	6	2.623
H1+2avg vs. T4	8.000	24.00	-16.00	6	6	2.469
H1+2avg vs. Ext	8.000	10.00	-2.000	6	6	0.3086

Fig 1e:

Column B	Post
vs.	vs,
Column A	H1-2
Mann-Whitney test	
P value	0,0057
Exact or approximate P value?	Exact
P value summary	**
Significantly different (P < 0.05)?	Yes
One- or two-tailed P value?	Two-tailed
Sum of ranks in column A,B	295 , 930
Mann-Whitney U	142
Difference between medians	
Median of column A	0,01455, n=17
Median of column B	0,04252, n=32
Difference: Actual	0,02797
Difference: Hodges-Lehmann	0,03019

Fig 1f:
FEC data:

Two-way ANOVA	**Ordinary**				
Alpha	0,05				
Source of Variation	% of total variation	P value	P value summary	Significant?	
Interaction	3,166	0,0619	ns	No	
Day	32,13	<0,0001	****	Yes	
Group	6,926	<0,0001	****	Yes	
ANOVA table	SS (Type III)	DF	MS	F (DFn, DFd)	P value
Interaction	0,1833	5	0,03666	F (5, 173) = 2,149	P=0,0619
Day	1,860	5	0,3720	F (5, 173) = 21,81	P<0,0001
Group	0,4009	1	0,4009	F (1, 173) = 23,51	P<0,0001
Residual	2,951	173	0,01706		
Difference between column means					
Predicted (LS) mean of Control	0,2349				

Predicted (LS) mean of Inhibition	0,1392				
Difference between predicted means	0,09576				
SE of difference	0,01975				
95% CI of difference	0,05677 to 0,1347				
Data summary					
Number of columns (Group)	2				
Number of rows (Day)	6				
Number of values	185				

Number of families	1							
Number of comparisons per family	6							
Alpha	0,05							
Holm-Šídák's multiple comparisons test	**Predicted (LS) mean diff,**	**Below threshold?**	**Summary**	**Adjusted P Value**				
Control - Inhibition								
H1	0,01764	No	ns	0,8629				
H2	0,02326	No	ns	0,8629				
T1	0,1723	Yes	**	0,0038				
T2	0,1644	Yes	**	0,0040				
T3	0,05793	No	ns	0,5446				
T4	0,1390	Yes	*	0,0175				
Test details	Predicted (LS) mean 1	Predicted (LS) mean 2	Predicted (LS) mean diff,	SE of diff,	N1	N2	t	DF
Control - Inhibition								
H1	0,05546	0,03782	0,01764	0,04816	19	12	0,3663	173,0
H2	0,06304	0,03979	0,02326	0,04816	19	12	0,4829	173,0
T1	0,3893	0,2170	0,1723	0,04948	19	11	3,483	173,0
T2	0,3728	0,2084	0,1644	0,04816	19	12	3,414	173,0
T3	0,2486	0,1906	0,05793	0,04816	19	12	1,203	173,0
T4	0,2805	0,1416	0,1390	0,04816	19	12	2,886	173,0

CR data:

Two-way ANOVA	**Ordinary**				
Alpha	0,05				
Source of Variation	% of total variation	P value	P value summary	Significant?	
Interaction	2,281	0,0402	*	Yes	
Day	51,19	<0,0001	****	Yes	
Group	5,264	<0,0001	****	Yes	
ANOVA table	SS (Type III)	DF	MS	F (DFn, DFd)	P value
Interaction	5347	5	1069	F (5, 173) = 2,385	P=0,0402
Day	119991	5	23998	F (5, 173) = 53,51	P<0,0001
Group	12341	1	12341	F (1, 173) = 27,52	P<0,0001
Residual	77590	173	448,5		

Difference between column means					
Predicted (LS) mean of Control	50,80				
Predicted (LS) mean of Inhibition	34,00				
Difference between predicted means	16,80				
SE of difference	3,203				
95% CI of difference	10,48 to 23,12				
Data summary					
Number of columns (Group)	2				
Number of rows (Day)	6				
Number of values	185				

Number of families	1							
Number of comparisons per family	6							
Alpha	0,05							
Holm-Šídák's multiple comparisons test	**Predicted (LS) mean diff,**	**Below threshold?**	**Summary**	**Adjusted P Value**				
Control - Inhibition								
H1	5,994	No	ns	0,6906				
H2	2,412	No	ns	0,7578				
T1	32,11	Yes	***	0,0006				
T2	28,39	Yes	**	0,0018				
T3	11,18	No	ns	0,3949				
T4	20,72	Yes	*	0,0344				
Test details	Predicted (LS) mean 1	Predicted (LS) mean 2	Predicted (LS) mean diff,	SE of diff,	N1	N2	t	DF
Control - Inhibition								
H1	8,772	2,778	5,994	7,809	19	12	0,7676	173,0
H2	8,246	5,833	2,412	7,809	19	12	0,3089	173,0
T1	84,84	52,73	32,11	8,024	19	11	4,003	173,0
T2	81,05	52,67	28,39	7,809	19	12	3,635	173,0
T3	56,84	45,67	11,18	7,809	19	12	1,431	173,0
T4	65,05	44,33	20,72	7,809	19	12	2,653	173,0

Fig 1 g:

Two-way ANOVA	**Ordinary**				
Alpha	0,05				
Source of Variation	% of total variation	P value	P value summary	Significant?	
Interaction	1,803	0,0727	ns	No	
Day	18,97	<0,0001	****	Yes	
Group	2,076	0,0543	ns	No	
ANOVA table	SS (Type III)	DF	MS	F (DFn, DFd)	P value
Interaction	0,1900	1	0,1900	F (1, 132) = 3,273	P=0,0727
Day	1,999	1	1,999	F (1, 132) = 34,44	P<0,0001

Group	0,2187	1	0,2187	F (1, 132) = 3,769	P=0,0543
Residual	7,660	132	0,05803		
Difference between column means					
Predicted (LS) mean of Control(GFP+nonIlluminated)	0,1938				
Predicted (LS) mean of Inhibition	0,1110				
Difference between predicted means	0,08275				
SE of difference	0,04262				
95% CI of difference	-0,001560 to 0,1671				
Difference between row means					
Predicted (LS) mean of H1-H2	0,02731				
Predicted (LS) mean of T2-Ext.	0,2774				
Difference between predicted means	-0,2501				
SE of difference	0,04262				
95% CI of difference	-0,3344 to -0,1658				
Interaction CI					
Mean diff, A1 - B1	0,005636				
Mean diff, A2 - B2	0,1599				
(A1 -B1) - (A2 - B2)	-0,1542				
95% CI of difference	-0,3228 to 0,01439				
(B1 - A1) - (B2 - A2)	0,1542				
95% CI of difference	-0,01439 to 0,3228				
Data summary					
Number of columns (Group)	2				
Number of rows (Day)	2				
Number of values	136				

Number of families	1							
Number of comparisons per family	2							
Alpha	0,05							
Holm-Šídák's multiple comparisons test	**Predicted (LS) mean diff,**	**Below threshold?**	**Summary**	**Adjusted P Value**				
Control(GFP+nonIlluminated) - Inhibition								
H1-H2	0,005636	No	ns	0,9294				
T2-Ext.	0,1599	Yes	*	0,0114				
Test details	Predicted (LS) mean 1	Predicted (LS) mean 2	Predicted (LS) mean diff,	SE of diff,	N1	N2	t	DF
Control(GFP+nonIlluminated) - Inhibition								
H1-H2	0,03013	0,02450	0,005636	0,06348	36	24	0,08878	132,0
T2-Ext.	0,3574	0,1975	0,1599	0,05688	47	29	2,810	132,0

Fig 2e:

P value and statistical significance	
Test	**Chi-square**
Chi-square. df	6.092. 5
P value	0.2973
P value summary	ns
One- or two-sided	NA
Statistically significant (P < 0.05)?	No
Data analyzed	
Number of rows	6
Number of columns	2

Fig 2g:

Two-way ANOVA	**Ordinary**				
Alpha	0.05				
Source of Variation	% of total variation	P value	P value summary	Significant?	
Interaction	2.416	<0.0001	****	Yes	
Day	3.998	<0.0001	****	Yes	
Cell Goup	30.01	<0.0001	****	Yes	
ANOVA table	SS (Type III)	DF	MS	F (DFn. DFd)	P value
Interaction	8.828	5	1.766	F (5. 6528) = 46.92	P<0.0001
Day	14.61	5	2.922	F (5. 6528) = 77.64	P<0.0001
Cell Goup	109.6	1	109.6	F (1. 6528) = 2914	P<0.0001
Residual	245.6	6528	0.03763		
Difference between column means					
Predicted (LS) mean of Nonresponder	0.06386				
Predicted (LS) mean of Responder	0.6088				
Difference between predicted means	-0.5450				
SE of difference	0.01010				
95% CI of difference	-0.5647 to -0.5252				
Data summary					
Number of columns (Cell Goup)	2				
Number of rows (Day)	6				
Number of values	6540				

Compare cell means regardless of rows and columns								
Number of families	1							
Number of comparisons per family	66							
Alpha	0.05							

Holm-Šídák's multiple comparisons test	Predicted (LS) mean diff.	Below threshold?	Summary	Adjusted P Value				
H1+2avg:Nonresponder vs. H1+2avg:Responder	-0.3217	Yes	****	<0.0001				
H1+2avg:Nonresponder vs. T1:Nonresponder	-0.03044	Yes	**	0.0016				
H1+2avg:Nonresponder vs. T1:Responder	-0.4863	Yes	****	<0.0001				
H1+2avg:Nonresponder vs. T2:Nonresponder	-0.03463	Yes	***	0.0003				
H1+2avg:Nonresponder vs. T2:Responder	-0.6816	Yes	****	<0.0001				
H1+2avg:Nonresponder vs. T3:Nonresponder	-0.07807	Yes	****	<0.0001				
H1+2avg:Nonresponder vs. T3:Responder	-0.7809	Yes	****	<0.0001				
H1+2avg:Nonresponder vs. T4:Nonresponder	-0.02349	Yes	*	0.0483				
H1+2avg:Nonresponder vs. T4:Responder	-0.7066	Yes	****	<0.0001				
H1+2avg:Nonresponder vs. Ext:Nonresponder	-0.01834	No	ns	0.1983				
H1+2avg:Nonresponder vs. Ext:Responder	-0.4778	Yes	****	<0.0001				
H1+2avg:Responder vs. T1:Nonresponder	0.2912	Yes	****	<0.0001				
H1+2avg:Responder vs. T1:Responder	-0.1646	Yes	****	<0.0001				
H1+2avg:Responder vs. T2:Nonresponder	0.2870	Yes	****	<0.0001				
H1+2avg:Responder vs. T2:Responder	-0.3599	Yes	****	<0.0001				
H1+2avg:Responder vs. T3:Nonresponder	0.2436	Yes	****	<0.0001				
H1+2avg:Responder vs. T3:Responder	-0.4592	Yes	****	<0.0001				
H1+2avg:Responder vs. T4:Nonresponder	0.2982	Yes	****	<0.0001				
H1+2avg:Responder vs. T4:Responder	-0.3849	Yes	****	<0.0001				
H1+2avg:Responder vs. Ext:Nonresponder	0.3033	Yes	****	<0.0001				
H1+2avg:Responder vs. Ext:Responder	-0.1561	Yes	****	<0.0001				
T1:Nonresponder vs. T1:Responder	-0.4558	Yes	****	<0.0001				
T1:Nonresponder vs. T2:Nonresponder	-0.004190	No	ns	0.9473				

T1:Nonresponder vs. T2:Responder	-0.6511	Yes	****	<0.0001					
T1:Nonresponder vs. T3:Nonresponder	-0.04763	Yes	****	<0.0001					
T1:Nonresponder vs. T3:Responder	-0.7504	Yes	****	<0.0001					
T1:Nonresponder vs. T4:Nonresponder	0.006950	No	ns	0.9473					
T1:Nonresponder vs. T4:Responder	-0.6761	Yes	****	<0.0001					
T1:Nonresponder vs. Ext:Nonresponder	0.01210	No	ns	0.7409					
T1:Nonresponder vs. Ext:Responder	-0.4473	Yes	****	<0.0001					
T1:Responder vs. T2:Nonresponder	0.4516	Yes	****	<0.0001					
T1:Responder vs. T2:Responder	-0.1953	Yes	****	<0.0001					
T1:Responder vs. T3:Nonresponder	0.4082	Yes	****	<0.0001					
T1:Responder vs. T3:Responder	-0.2946	Yes	****	<0.0001					
T1:Responder vs. T4:Nonresponder	0.4628	Yes	****	<0.0001					
T1:Responder vs. T4:Responder	-0.2203	Yes	****	<0.0001					
T1:Responder vs. Ext:Nonresponder	0.4679	Yes	****	<0.0001					
T1:Responder vs. Ext:Responder	0.008500	No	ns	0.9473					
T2:Nonresponder vs. T2:Responder	-0.6469	Yes	****	<0.0001					
T2:Nonresponder vs. T3:Nonresponder	-0.04344	Yes	****	<0.0001					
T2:Nonresponder vs. T3:Responder	-0.7462	Yes	****	<0.0001					
T2:Nonresponder vs. T4:Nonresponder	0.01114	No	ns	0.7957					
T2:Nonresponder vs. T4:Responder	-0.6719	Yes	****	<0.0001					
T2:Nonresponder vs. Ext:Nonresponder	0.01629	No	ns	0.4668					
T2:Nonresponder vs. Ext:Responder	-0.4431	Yes	****	<0.0001					
T2:Responder vs. T3:Nonresponder	0.6035	Yes	****	<0.0001					
T2:Responder vs. T3:Responder	-0.09930	Yes	*	0.0483					
T2:Responder vs. T4:Nonresponder	0.6581	Yes	****	<0.0001					
T2:Responder vs. T4:Responder	-0.02500	No	ns	0.9473					
T2:Responder vs. Ext:Nonresponder	0.6632	Yes	****	<0.0001					
T2:Responder vs. Ext:Responder	0.2038	Yes	****	<0.0001					
T3:Nonresponder vs. T3:Responder	-0.7028	Yes	****	<0.0001					

T3:Nonresponder vs. T4:Nonresponder	0.05458	Yes	****	<0.0001				
T3:Nonresponder vs. T4:Responder	-0.6285	Yes	****	<0.0001				
T3:Nonresponder vs. Ext:Nonresponder	0.05973	Yes	****	<0.0001				
T3:Nonresponder vs. Ext:Responder	-0.3997	Yes	****	<0.0001				
T3:Responder vs. T4:Nonresponder	0.7574	Yes	****	<0.0001				
T3:Responder vs. T4:Responder	0.07430	No	ns	0.3221				
T3:Responder vs. Ext:Nonresponder	0.7625	Yes	****	<0.0001				
T3:Responder vs. Ext:Responder	0.3031	Yes	****	<0.0001				
T4:Nonresponder vs. T4:Responder	-0.6831	Yes	****	<0.0001				
T4:Nonresponder vs. Ext:Nonresponder	0.005150	No	ns	0.9473				
T4:Nonresponder vs. Ext:Responder	-0.4543	Yes	****	<0.0001				
T4:Responder vs. Ext:Nonresponder	0.6882	Yes	****	<0.0001				
T4:Responder vs. Ext:Responder	0.2288	Yes	****	<0.0001				
Ext:Nonresponder vs. Ext:Responder	-0.4594	Yes	****	<0.0001				

Test details	Predicted (LS) mean 1	Predicted (LS) mean 2	Predicted (LS) mean diff.	SE of diff.	N1	N2	t	DF
H1+2avg:Nonresponder vs. H1+2avg:Responder	0.03303	0.3547	-0.3217	0.01881	1596	114	17.10	6528
H1+2avg:Nonresponder vs. T1:Nonresponder	0.03303	0.06347	-0.03044	0.007933	1596	956	3.837	6528
H1+2avg:Nonresponder vs. T1:Responder	0.03303	0.5193	-0.4863	0.02593	1596	58	18.75	6528
H1+2avg:Nonresponder vs. T2:Nonresponder	0.03303	0.06766	-0.03463	0.008199	1596	862	4.223	6528
H1+2avg:Nonresponder vs. T2:Responder	0.03303	0.7146	-0.6816	0.02572	1596	59	26.50	6528
H1+2avg:Nonresponder vs. T3:Nonresponder	0.03303	0.1111	-0.07807	0.008078	1596	903	9.665	6528
H1+2avg:Nonresponder vs. T3:Responder	0.03303	0.8139	-0.7809	0.02437	1596	66	32.05	6528
H1+2avg:Nonresponder vs. T4:Nonresponder	0.03303	0.05652	-0.02349	0.008184	1596	867	2.870	6528
H1+2avg:Nonresponder vs. T4:Responder	0.03303	0.7396	-0.7066	0.02813	1596	49	25.11	6528

H1+2avg:Nonresponder vs. Ext:Nonresponder	0.03303	0.05137	-0.01834	0.007997	1596	932	2.293	6528
H1+2avg:Nonresponder vs. Ext:Responder	0.03303	0.5108	-0.4778	0.02249	1596	78	21.24	6528
H1+2avg:Responder vs. T1:Nonresponder	0.3547	0.06347	0.2912	0.01922	114	956	15.15	6528
H1+2avg:Responder vs. T1:Responder	0.3547	0.5193	-0.1646	0.03129	114	58	5.261	6528
H1+2avg:Responder vs. T2:Nonresponder	0.3547	0.06766	0.2870	0.01933	114	862	14.85	6528
H1+2avg:Responder vs. T2:Responder	0.3547	0.7146	-0.3599	0.03111	114	59	11.57	6528
H1+2avg:Responder vs. T3:Nonresponder	0.3547	0.1111	0.2436	0.01928	114	903	12.63	6528
H1+2avg:Responder vs. T3:Responder	0.3547	0.8139	-0.4592	0.03000	114	66	15.30	6528
H1+2avg:Responder vs. T4:Nonresponder	0.3547	0.05652	0.2982	0.01933	114	867	15.43	6528
H1+2avg:Responder vs. T4:Responder	0.3547	0.7396	-0.3849	0.03314	114	49	11.62	6528
H1+2avg:Responder vs. Ext:Nonresponder	0.3547	0.05137	0.3033	0.01925	114	932	15.76	6528
H1+2avg:Responder vs. Ext:Responder	0.3547	0.5108	-0.1561	0.02850	114	78	5.476	6528
T1:Nonresponder vs. T1:Responder	0.06347	0.5193	-0.4558	0.02623	956	58	17.38	6528
T1:Nonresponder vs. T2:Nonresponder	0.06347	0.06766	-0.004190	0.009111	956	862	0.4599	6528
T1:Nonresponder vs. T2:Responder	0.06347	0.7146	-0.6511	0.02602	956	59	25.02	6528
T1:Nonresponder vs. T3:Nonresponder	0.06347	0.1111	-0.04763	0.009002	956	903	5.291	6528
T1:Nonresponder vs. T3:Responder	0.06347	0.8139	-0.7504	0.02469	956	66	30.40	6528
T1:Nonresponder vs. T4:Nonresponder	0.06347	0.05652	0.006950	0.009097	956	867	0.7639	6528
T1:Nonresponder vs. T4:Responder	0.06347	0.7396	-0.6761	0.02841	956	49	23.80	6528
T1:Nonresponder vs. Ext:Nonresponder	0.06347	0.05137	0.01210	0.008930	956	932	1.355	6528
T1:Nonresponder vs. Ext:Responder	0.06347	0.5108	-0.4473	0.02284	956	78	19.58	6528
T1:Responder vs. T2:Nonresponder	0.5193	0.06766	0.4516	0.02631	58	862	17.16	6528
T1:Responder vs. T2:Responder	0.5193	0.7146	-0.1953	0.03587	58	59	5.445	6528
T1:Responder vs. T3:Nonresponder	0.5193	0.1111	0.4082	0.02628	58	903	15.53	6528
T1:Responder vs. T3:Responder	0.5193	0.8139	-0.2946	0.03491	58	66	8.438	6528
T1:Responder vs. T4:Nonresponder	0.5193	0.05652	0.4628	0.02631	58	867	17.59	6528
T1:Responder vs. T4:Responder	0.5193	0.7396	-0.2203	0.03764	58	49	5.853	6528
T1:Responder vs. Ext:Nonresponder	0.5193	0.05137	0.4679	0.02625	58	932	17.82	6528

T1:Responder vs. Ext:Responder	0.5193	0.5108	0.008500	0.03363	58	78	0.2527	6528
T2:Nonresponder vs. T2:Responder	0.06766	0.7146	-0.6469	0.02610	862	59	24.78	6528
T2:Nonresponder vs. T3:Nonresponder	0.06766	0.1111	-0.04344	0.009237	862	903	4.703	6528
T2:Nonresponder vs. T3:Responder	0.06766	0.8139	-0.7462	0.02478	862	66	30.12	6528
T2:Nonresponder vs. T4:Nonresponder	0.06766	0.05652	0.01114	0.009330	862	867	1.194	6528
T2:Nonresponder vs. T4:Responder	0.06766	0.7396	-0.6719	0.02849	862	49	23.59	6528
T2:Nonresponder vs. Ext:Nonresponder	0.06766	0.05137	0.01629	0.009167	862	932	1.777	6528
T2:Nonresponder vs. Ext:Responder	0.06766	0.5108	-0.4431	0.02294	862	78	19.32	6528
T2:Responder vs. T3:Nonresponder	0.7146	0.1111	0.6035	0.02607	59	903	23.15	6528
T2:Responder vs. T3:Responder	0.7146	0.8139	-0.09930	0.03476	59	66	2.857	6528
T2:Responder vs. T4:Nonresponder	0.7146	0.05652	0.6581	0.02610	59	867	25.21	6528
T2:Responder vs. T4:Responder	0.7146	0.7396	-0.02500	0.03749	59	49	0.6668	6528
T2:Responder vs. Ext:Nonresponder	0.7146	0.05137	0.6632	0.02604	59	932	25.47	6528
T2:Responder vs. Ext:Responder	0.7146	0.5108	0.2038	0.03347	59	78	6.089	6528
T3:Nonresponder vs. T3:Responder	0.1111	0.8139	-0.7028	0.02474	903	66	28.41	6528
T3:Nonresponder vs. T4:Nonresponder	0.1111	0.05652	0.05458	0.009224	903	867	5.917	6528
T3:Nonresponder vs. T4:Responder	0.1111	0.7396	-0.6285	0.02845	903	49	22.09	6528
T3:Nonresponder vs. Ext:Nonresponder	0.1111	0.05137	0.05973	0.009058	903	932	6.594	6528
T3:Nonresponder vs. Ext:Responder	0.1111	0.5108	-0.3997	0.02289	903	78	17.46	6528
T3:Responder vs. T4:Nonresponder	0.8139	0.05652	0.7574	0.02477	66	867	30.58	6528
T3:Responder vs. T4:Responder	0.8139	0.7396	0.07430	0.03658	66	49	2.031	6528
T3:Responder vs. Ext:Nonresponder	0.8139	0.05137	0.7625	0.02471	66	932	30.86	6528
T3:Responder vs. Ext:Responder	0.8139	0.5108	0.3031	0.03244	66	78	9.342	6528
T4:Nonresponder vs. T4:Responder	0.05652	0.7396	-0.6831	0.02848	867	49	23.98	6528
T4:Nonresponder vs. Ext:Nonresponder	0.05652	0.05137	0.005150	0.009153	867	932	0.5627	6528
T4:Nonresponder vs. Ext:Responder	0.05652	0.5108	-0.4543	0.02293	867	78	19.81	6528
T4:Responder vs. Ext:Nonresponder	0.7396	0.05137	0.6882	0.02843	49	932	24.21	6528
T4:Responder vs. Ext:Responder	0.7396	0.5108	0.2288	0.03536	49	78	6.470	6528
Ext:Nonresponder vs. Ext:Responder	0.05137	0.5108	-0.4594	0.02287	932	78	20.09	6528

Fig 2h:

Kruskal-Wallis test	
P value	<0.0001
Exact or approximate P value?	Approximate
P value summary	****
Do the medians vary signif. (P < 0.05)?	Yes
Number of groups	6
Kruskal-Wallis statistic	50.93

Dunn's multiple comparisons test	**Mean rank diff.**	**Significant?**	**Summary**	**Adjusted P Value**	**A-?**	
H1+H2 vs. T1	-46.36	No	ns	0.0869	B	T1
H1+H2 vs. T2	-99.63	Yes	****	<0.0001	C	T2
H1+H2 vs. T3	-108.2	Yes	****	<0.0001	D	T3
H1+H2 vs. T4	-87.89	Yes	***	0.0001	E	T4
H1+H2 vs. Ext	-82.96	Yes	****	<0.0001	F	Ext
Test details	Mean rank 1	Mean rank 2	Mean rank diff.	n1	n2	Z
H1+H2 vs. T1	150	196.4	-46.36	114	58	2.379
H1+H2 vs. T2	150	249.7	-99.63	114	59	5.141
H1+H2 vs. T3	150	258.2	-108.2	114	66	5.788
H1+H2 vs. T4	150	237.9	-87.89	114	49	4.258
H1+H2 vs. Ext	150	233	-82.96	114	78	4.672

Fig 3b. Fractions Barplot

A Chi- square was done with the entire contingency table. After that every time interval for the different transition groups (R-R. NR-R. R-NR) was compared to baseline in separate Fishers-exact tests. The resulting nine p values were analyzed using a Holm-Šídák post-test with a family alpha of 0.05.

Chi-square results of entire contingency table.

P value and statistical significance	
Test	**Chi-square**
Chi-square. df	23.95. 6
P value	0.0005

P value summary	***
One- or two-sided	NA
Statistically significant (P < 0.05)?	Yes
Data analyzed	
Number of rows	4
Number of columns	3

Table Analyzed	R-R H2-T1
P value and statistical significance	
Test	**Fisher's exact test**
P value	>0.9999
P value summary	ns
One- or two-sided	Two-sided
Statistically significant (P < 0.05)?	No

Table Analyzed	R-R T1-T4
P value and statistical significance	
Test	**Fisher's exact test**
P value	0.5455
P value summary	ns
One- or two-sided	Two-sided
Statistically significant (P < 0.05)?	No

Table Analyzed	R-R T4-Ext
P value and statistical significance	
Test	**Fisher's exact test**
P value	>0.9999
P value summary	ns
One- or two-sided	Two-sided
Statistically significant (P < 0.05)?	No

Table Analyzed	NR-R H2-T1
P value and statistical significance	
Test	**Fisher's exact test**
P value	0.161
P value summary	ns
One- or two-sided	Two-sided
Statistically significant (P < 0.05)?	No

Table Analyzed	NR-R T1-T4
P value and statistical significance	
Test	**Fisher's exact test**
P value	0.451
P value summary	ns
One- or two-sided	Two-sided
Statistically significant (P < 0.05)?	No

Table Analyzed	NR-R T4-Ext
P value and statistical significance	
Test	**Fisher's exact test**
P value	0.0018
P value summary	**
One- or two-sided	Two-sided
Statistically significant (P < 0.05)?	Yes

Table Analyzed	R-NR H2-T1
P value and statistical significance	
Test	**Fisher's exact test**
P value	0.2284

Table Analyzed	R-NR T1-T4
P value and statistical significance	
Test	**Fisher's exact test**
P value	0.6167

Table Analyzed	R-NR T4-Ext
P value and statistical significance	
Test	**Fisher's exact test**
P value	0.0008

P value summary	ns
One- or two-sided	Two-sided
Statistically significant (P < 0.05)?	No

P value summary	ns
One- or two-sided	Two-sided
Statistically significant (P < 0.05)?	No

P value summary	***
One- or two-sided	Two-sided
Statistically significant (P < 0.05)?	Yes

Holm-Šídák post-test

Group	Comparism vs. Baseline (H1-H2)	P value	Adjusted P Value
R-R	H2-T1	0.9999	1
R-R	T1-T4	0.5455	0.9573
R-R	T4-Ext.	0.9999	1
NR-R	H2-T1	0.161	0.7074
NR-R	T1-T4	0.451	0.9501
NR-R	T4-Ext.	0.0018	0.0143
R-NR	H2-T1	0.2284	0.789
R-NR	T1-T4	0.6167	0.9573
R-NR	T4-Ext.	0.0008	0.0072

Fig 3e:

Trial activity Baseline:

Kruskal-Wallis test	
P value	<0,0001
Exact or approximate P value?	Approximate
P value summary	****
Do the medians vary signif. (P < 0.05)?	Yes
Number of groups	3
Kruskal-Wallis statistic	93,67
Data summary	
Number of treatments (columns)	3
Number of values (total)	154

Number of families	1					
Number of comparisons per family	3					
Alpha	0,05					
Dunn's multiple comparisons test	**Mean rank diff,**	**Significant ?**	**Summary**	**Adjusted P Value**		
T-1 vs. T0	-69,49	Yes	****	<0,0001	A-B	
T-1 vs. T+1	-2,709	No	ns	>0,9999	A-C	

T0 vs. T+1	66,78	Yes	****	<0,0001	B-C	
Test details	Mean rank 1	Mean rank 2	Mean rank diff,	n1	n2	Z
T-1 vs. T0	42,00	111,5	-69,49	34	77	7,741
T-1 vs. T+1	42,00	44,71	-2,709	34	43	0,2708
T0 vs. T+1	111,5	44,71	66,78	77	43	8,046

Trial activity training:

Kruskal-Wallis test	
P value	<0,0001
Exact or approximate P value?	Approximate
P value summary	****
Do the medians vary signif. (P < 0.05)?	Yes
Number of groups	6
Kruskal-Wallis statistic	337,0
Data summary	
Number of treatments (columns)	6
Number of values (total)	574

Number of families	1					
Number of comparisons per family	5					
Alpha	0,05					
Dunn's multiple comparisons test	**Mean rank diff,**	**Significant ?**	**Summary**	**Adjusted P Value**	**A-?**	
Baseline vs. T-2	13,49	No	ns	>0,9999	B	T-2
Baseline vs. T-1	9,098	No	ns	>0,9999	C	T-1
Baseline vs. T0	-272,4	Yes	****	<0,0001	D	T0
Baseline vs. T+1	-20,54	No	ns	>0,9999	E	T+1
Baseline vs. T+2	-24,44	No	ns	>0,9999	F	T+2
Test details	Mean rank 1	Mean rank 2	Mean rank diff,	n1	n2	Z
Baseline vs. T-2	226,0	212,6	13,49	123	63	0,6017
Baseline vs. T-1	226,0	216,9	9,098	123	103	0,4708
Baseline vs. T0	226,0	498,4	-272,4	123	123	14,76
Baseline vs. T+1	226,0	246,6	-20,54	123	102	1,060
Baseline vs. T+2	226,0	250,5	-24,44	123	60	1,073

Stats for delta rates are below 3f stats.

Fig 3f:

Non- Trial activity baseline:

Kruskal-Wallis test	
P value	<0,0001
Exact or approximate P value?	Approximate

P value summary	****
Do the medians vary signif. (P < 0.05)?	Yes
Number of groups	3
Kruskal-Wallis statistic	60,69
Data summary	
Number of treatments (columns)	3
Number of values (total)	154

Number of families	1					
Number of comparisons per family	3					
Alpha	0,05					
Dunn's multiple comparisons test	**Mean rank diff,**	**Significant ?**	**Summary**	**Adjusted P Value**		
T-1 vs. T0	-60,31	Yes	****	<0,0001	A-B	
T-1 vs. T+1	-9,556	No	ns	>0,9999	A-C	
T0 vs. T+1	50,75	Yes	****	<0,0001	B-C	
Test details	Mean rank 1	Mean rank 2	Mean rank diff,	n1	n2	Z
T-1 vs. T0	44,68	105,0	-60,31	34	77	6,640
T-1 vs. T+1	44,68	54,23	-9,556	34	43	0,9440
T0 vs. T+1	105,0	54,23	50,75	77	43	6,044

Non- Trial activity training:

Kruskal-Wallis test	
P value	<0,0001
Exact or approximate P value?	Approximate
P value summary	****
Do the medians vary signif. (P < 0.05)?	Yes
Number of groups	6
Kruskal-Wallis statistic	233,9
Data summary	
Number of treatments (columns)	6
Number of values (total)	574

Number of families	1					
Number of comparisons per family	5					
Alpha	0,05					
Dunn's multiple comparisons test	**Mean rank diff,**	**Significant ?**	**Summary**	**Adjusted P Value**	**A-?**	
Baseline vs. T-2	23,65	No	ns	>0,9999	B	T-2
Baseline vs. T-1	-6,918	No	ns	>0,9999	C	T-1
Baseline vs. T0	-246,2	Yes	****	<0,0001	D	T0
Baseline vs. T+1	-37,14	No	ns	0,3581	E	T+1
Baseline vs. T+2	-31,25	No	ns	0,9868	F	T+2
Test details	Mean rank 1	Mean rank 2	Mean rank diff,	n1	n2	Z
Baseline vs. T-2	226,2	202,6	23,65	123	63	0,9916
Baseline vs. T-1	226,2	233,1	-6,918	123	103	0,3365

Baseline vs. T0	226,2	472,4	-246,2	123	123	12,54
Baseline vs. T+1	226,2	263,4	-37,14	123	102	1,801
Baseline vs. T+2	226,2	257,5	-31,25	123	60	1,289

Fig 3ef:

Delta rates.

Kruskal-Wallis test	
P value	<0,0001
Exact or approximate P value?	Approximate
P value summary	****
Do the medians vary signif. (P < 0.05)?	Yes
Number of groups	4
Kruskal-Wallis statistic	126,6
Data summary	
Number of treatments (columns)	4
Number of values (total)	274

Number of families	1					
Number of comparisons per family	4					
Alpha	0,05					
Dunn's multiple comparisons test	**Mean rank diff,**	**Significant?**	**Summary**	**Adjusted P Value**		
Trial Baseline vs. Trial Training	-59,01	Yes	***	0,0007	A-B	
Pretrial Baseline vs. Pretrial Training	-28,52	No	ns	0,2748	C-D	
Trial Training vs. Pretrial Training	107,6	Yes	****	<0,0001	B-D	
Trial Baseline vs. Pretrial Baseline	77,07	Yes	***	0,0002	A-C	
Test details	Mean rank 1	Mean rank 2	Mean rank diff,	n1	n2	Z
Trial Baseline vs. Trial Training	143,1	202,1	-59,01	34	103	3,766
Pretrial Baseline vs. Pretrial Training	66,06	94,58	-28,52	34	103	1,820
Trial Training vs. Pretrial Training	202,1	94,58	107,6	103	103	9,743
Trial Baseline vs. Pretrial Baseline	143,1	66,06	77,07	34	34	4,011

Fig 4c:

Paired Trials:

ANOVA summary	
F	0.2192
P value	0.9674
P value summary	ns
Significant diff. among means (P < 0.05)?	No
R squared	0.04487
Bartlett's test	

Bartlett's statistic (corrected)	4.496
P value	0.6098
P value summary	ns
Are SDs significantly different (P < 0.05)?	No

ANOVA table	SS	DF	MS	F (DFn. DFd)	P value
Treatment (between columns)	46.69	6	7.781	F (6. 28) = 0.2192	P=0.9674
Residual (within columns)	993.9	28	35.5		
Total	1041	34			

Šídák's multiple comparisons test	**Mean Diff.**	**95.00% CI of diff.**	**Below threshold?**	**Summary**	**Adjusted P Value**			
H1 vs. H2	-1.823	-13.41 to 9.767	No	ns	>0.9999	A-B		
H1 vs. T1	-3.032	-14.62 to 8.558	No	ns	0.9978	A-C		
H1 vs. T2	-2.833	-14.42 to 8.757	No	ns	0.9988	A-D		
H1 vs. T3	-2.061	-13.65 to 9.529	No	ns	>0.9999	A-E		
H1 vs. T4	-2.009	-13.60 to 9.581	No	ns	>0.9999	A-F		
H1 vs. Extinction	-3.996	-15.59 to 7.594	No	ns	0.9796	A-G		
H2 vs. T1	-1.21	-12.80 to 10.38	No	ns	>0.9999	B-C		
H2 vs. T2	-1.01	-12.60 to 10.58	No	ns	>0.9999	B-D		
H2 vs. T3	-0.2388	-11.83 to 11.35	No	ns	>0.9999	B-E		
H2 vs. T4	-0.1869	-11.78 to 11.40	No	ns	>0.9999	B-F		
H2 vs. Extinction	-2.173	-13.76 to 9.417	No	ns	>0.9999	B-G		
Test details	Mean 1	Mean 2	Mean Diff.	SE of diff.	n1	n2	t	DF
H1 vs. H2	4.213	6.036	-1.823	3.768	5	5	0.4837	28
H1 vs. T1	4.213	7.246	-3.032	3.768	5	5	0.8047	28
H1 vs. T2	4.213	7.046	-2.833	3.768	5	5	0.7518	28
H1 vs. T3	4.213	6.275	-2.061	3.768	5	5	0.5471	28
H1 vs. T4	4.213	6.223	-2.009	3.768	5	5	0.5333	28
H1 vs. Extinction	4.213	8.209	-3.996	3.768	5	5	1.06	28
H2 vs. T1	6.036	7.246	-1.21	3.768	5	5	0.321	28
H2 vs. T2	6.036	7.046	-1.01	3.768	5	5	0.2681	28
H2 vs. T3	6.036	6.275	-0.2388	3.768	5	5	0.06337	28
H2 vs. T4	6.036	6.223	-0.1869	3.768	5	5	0.04959	28
H2 vs. Extinction	6.036	8.209	-2.173	3.768	5	5	0.5767	28

Probe Trials:

ANOVA summary	
F	0.2032
P value	0.9729
P value summary	ns
Significant diff. among means (P < 0.05)?	No
R squared	0.04173
Bartlett's test	
Bartlett's statistic (corrected)	5.89
P value	0.4356
P value summary	ns
Are SDs significantly different (P < 0.05)?	No

ANOVA table	SS	DF	MS	F (DFn. DFd)	P value
Treatment (between columns)	25.4	6	4.234	F (6. 28) = 0.2032	P=0.9729
Residual (within columns)	583.4	28	20.83		
Total	608.8	34			

Šídák's multiple comparisons test	**Mean Diff.**	**95.00% CI of diff.**	**Below threshold?**	**Summary**	**Adjusted P Value**			
H1 vs. H2	1.585	-7.295 to 10.46	No	ns	>0.9999	A-B		
H1 vs. T1	-0.2018	-9.081 to 8.678	No	ns	>0.9999	A-C		
H1 vs. T2	-0.626	-9.505 to 8.253	No	ns	>0.9999	A-D		
H1 vs. T3	1.179	-7.700 to 10.06	No	ns	>0.9999	A-E		
H1 vs. T4	-0.9274	-9.807 to 7.952	No	ns	>0.9999	A-F		
H1 vs. Extinction	0.4203	-8.459 to 9.300	No	ns	>0.9999	A-G		
H2 vs. T1	-1.787	-10.67 to 7.093	No	ns	0.9998	B-C		
H2 vs. T2	-2.211	-11.09 to 6.669	No	ns	0.9986	B-D		
H2 vs. T3	-0.4055	-9.285 to 8.474	No	ns	>0.9999	B-E		
H2 vs. T4	-2.512	-11.39 to 6.367	No	ns	0.9958	B-F		
H2 vs. Extinction	-1.165	-10.04 to 7.715	No	ns	>0.9999	B-G		
Test details	Mean 1	Mean 2	Mean Diff.	SE of diff.	n1	n2	t	DF
H1 vs. H2	4.86	3.275	1.585	2.887	5	5	0.549	28
H1 vs. T1	4.86	5.062	-0.2018	2.887	5	5	0.06989	28

H1 vs. T2	4.86	5.486	-0.626	2.887	5	5	0.2168	28
H1 vs. T3	4.86	3.681	1.179	2.887	5	5	0.4085	28
H1 vs. T4	4.86	5.788	-0.9274	2.887	5	5	0.3212	28
H1 vs. Extinction	4.86	4.44	0.4203	2.887	5	5	0.1456	28
H2 vs. T1	3.275	5.062	-1.787	2.887	5	5	0.6189	28
H2 vs. T2	3.275	5.486	-2.211	2.887	5	5	0.7659	28
H2 vs. T3	3.275	3.681	-0.4055	2.887	5	5	0.1405	28
H2 vs. T4	3.275	5.788	-2.512	2.887	5	5	0.8703	28
H2 vs. Extinction	3.275	4.44	-1.165	2.887	5	5	0.4034	28

Fig 4d:

Kruskal-Wallis test	
P value	<0,0001
Exact or approximate P value?	Approximate
P value summary	****
Do the medians vary signif. (P < 0.05)?	Yes
Number of groups	6
Kruskal-Wallis statistic	572,3
Data summary	
Number of treatments (columns)	6
Number of values (total)	3857

Number of families	1					
Number of comparisons per family	5					
Alpha	0,05					
Dunn's multiple comparisons test	**Mean rank diff,**	**Significant ?**	**Summary**	**Adjusted P Value**	**A-?**	
Baseline vs. T1	-957,1	Yes	****	<0,0001	B	T1
Baseline vs. T2	-941,8	Yes	****	<0,0001	C	T2
Baseline vs. T3	-1229	Yes	****	<0,0001	D	T3
Baseline vs. T4	-975,9	Yes	****	<0,0001	E	T4
Baseline vs. Ext.	-1025	Yes	****	<0,0001	F	Ext,
Test details	Mean rank 1	Mean rank 2	Mean rank diff,	n1	n2	Z
Baseline vs. T1	1128	2085	-957,1	830	645	16,37
Baseline vs. T2	1128	2070	-941,8	830	613	15,88
Baseline vs. T3	1128	2357	-1229	830	537	19,93
Baseline vs. T4	1128	2104	-975,9	830	547	15,91
Baseline vs. Ext.	1128	2152	-1025	830	685	17,82

Fig 4e:

Two-way ANOVA	**Ordinary**				
Alpha	0,05				
Source of Variation	% of total variation	P value	P value summary	Significant?	

Interaction	0,6459	<0,0001	****	Yes	
Day	1,799	<0,0001	****	Yes	
Celltype	0,7434	<0,0001	****	Yes	
ANOVA table	SS (Type III)	DF	MS	F (DFn, DFd)	P value
Interaction	3715	5	743,0	F (5, 5279) = 7,122	P<0,0001
Day	10348	5	2070	F (5, 5279) = 19,84	P<0,0001
Celltype	4276	1	4276	F (1, 5279) = 40,98	P<0,0001
Residual	550789	5279	104,3		
Difference between column means					
Predicted (LS) mean of Nonresponder	10,39				
Predicted (LS) mean of Responder	14,09				
Difference between predicted means	-3,697				
SE of difference	0,5775				
95% CI of difference	-4,829 to -2,565				
Data summary					
Number of columns (Celltype)	2				
Number of rows (Day)	6				
Number of values	5291				

Number of families	1							
Number of comparisons per family	6							
Alpha	0,05							
Šídák's multiple comparisons test	**Predicted (LS) mean diff,**	**95,00% CI of diff,**	**Below threshold ?**	**Summary**	**Adjusted P Value**			
Nonresponder - Responder								
Habituation	-1,701	-4,653 to 1,251	No	ns	0,5647			
T1	0,08000	-4,003 to 4,163	No	ns	>0,9999			
T2	-1,390	-5,209 to 2,429	No	ns	0,9159			
T3	-8,170	-11,96 to -4,377	Yes	****	<0,0001			
T4	-9,310	-13,53 to -5,089	Yes	****	<0,0001			
Extinction	-1,690	-5,005 to 1,625	No	ns	0,6955			
Test details	Predicted (LS) mean 1	Predicted (LS) mean 2	Predicted (LS) mean diff,	SE of diff,	N1	N2	t	DF
Nonresponder - Responder								
Habituation	7,188	8,889	-1,701	1,122	1218	89	1,517	5279
T1	10,24	10,16	0,08000	1,551	754	46	0,05157	5279
T2	11,02	12,41	-1,390	1,451	766	53	0,9581	5279
T3	11,32	19,49	-8,170	1,441	723	54	5,670	5279
T4	11,09	20,40	-9,310	1,604	715	43	5,805	5279
Extinction	11,48	13,17	-1,690	1,260	758	72	1,342	5279

Fig 4f:

Brown-Forsythe ANOVA test	
F* (DFn, DFd)	307,5 (11,00, 10799)
P value	<0,0001
P value summary	****
Significant diff. among means (P < 0.05)?	Yes
Welch's ANOVA test	
W (DFn, DFd)	426,8 (11,00, 7656)
P value	<0,0001
P value summary	****
Significant diff. among means (P < 0.05)?	Yes
Data summary	
Number of treatments (columns)	12
Number of values (total)	392443

Number of families	1							
Number of comparisons per family	21							
Alpha	0,05							
Games-Howell's multiple comparisons test	**Mean Diff,**	**95,00% CI of diff,**	**Below threshold ?**	**Summary**	**Adjusted P Value**			
NR Pre vs. R Pre	-0,006707	-0,02175 to 0,008333	No	ns	0,9499	A-B		
NR Pre vs. R vs. NR Pre	0,009352	0,004176 to 0,01453	Yes	****	<0,0001	A-C		
R Pre vs. R vs. NR Pre	0,01606	0,000242 9 to 0,03187	Yes	*	0,0428	B-C		
NR Early vs. R Early	-0,02327	-0,04138 to -0,005159	Yes	**	0,0017	D-E		
NR Early vs. R vs. NR Early	0,01810	0,01346 to 0,02274	Yes	****	<0,0001	D-F		
R Early vs. R vs. NR Early	0,04137	0,02274 to 0,06001	Yes	****	<0,0001	E-F		
NR Extinction vs. R Extinction	0,006950	-0,009531 to 0,02343	No	ns	0,9666	J-K		
NR Extinction vs. R vs. NR Extinction	0,04054	0,03398 to 0,04711	Yes	****	<0,0001	J-L		
R Extinction vs. R vs. NR Extinction	0,03359	0,01602 to 0,05117	Yes	****	<0,0001	K-L		
NR Pre vs. NR Early	-0,02368	-0,02523 to -0,02212	Yes	****	<0,0001	A-D		

NR Pre vs. NR Late	-0,02752	-0,02928 to -0,02575	Yes	****	<0,0001	A-G		
NR Pre vs. NR Extinction	-0,02989	-0,03193 to -0,02785	Yes	****	<0,0001	A-J		
R Pre vs. R Early	-0,04024	-0,06370 to -0,01679	Yes	****	<0,0001	B-E		
R Pre vs. R Late	-0,03799	-0,06406 to -0,01192	Yes	***	0,0001	B-H		
R Pre vs. R Extinction	-0,01623	-0,03841 to 0,005947	No	ns	0,4093	B-K		
R vs. NR Pre vs. R Early	-0,05630	-0,07507 to -0,03753	Yes	****	<0,0001	C-E		
R vs. NR Pre vs. R Late	-0,05405	-0,07600 to -0,03209	Yes	****	<0,0001	C-H		
R vs. NR Pre vs. R vs. NR Extinction	0,001304	-0,006802 to 0,009410	No	ns	>0,9999	C-L		
NR Late vs. R Late	-0,01718	-0,03859 to 0,004235	No	ns	0,2652	G-H		
R Late vs. R vs. NR Late	0,03839	0,01624 to 0,06053	Yes	****	<0,0001	H-I		
NR Late vs. R vs. NR Late	0,02121	0,01525 to 0,02716	Yes	****	<0,0001	G-I		
Test details	Mean 1	Mean 2	Mean Diff,	SE of diff,	n1	n2	t	DF
NR Pre vs. R Pre	0,01454	0,02125	-0,006707	0,004585	88244	638	1,463	644,6
NR Pre vs. R vs. NR Pre	0,01454	0,005191	0,009352	0,001583	88244	3793	5,908	4196
R Pre vs. R vs. NR Pre	0,02125	0,005191	0,01606	0,004825	638	3793	3,328	788,8
NR Early vs. R Early	0,03822	0,06149	-0,02327	0,005526	130299	785	4,211	789,3
NR Early vs. R vs. NR Early	0,03822	0,02012	0,01810	0,001419	130299	5407	12,75	6001
R Early vs. R vs. NR Early	0,06149	0,02012	0,04137	0,005687	785	5407	7,275	885,1
NR Extinction vs. R Extinction	0,04443	0,03748	0,006950	0,005026	57217	689	1,383	702,8
NR Extinction vs. R vs. NR Extinction	0,04443	0,003887	0,04054	0,002008	57217	3841	20,19	4402
R Extinction vs. R vs. NR Extinction	0,03748	0,003887	0,03359	0,005363	689	3841	6,264	907,3
NR Pre vs. NR Early	0,01454	0,03822	-0,02368	0,0004759	88244	130299	49,75	201321
NR Pre vs. NR Late	0,01454	0,04206	-0,02752	0,0005393	88244	94696	51,02	180660
NR Pre vs. NR Extinction	0,01454	0,04443	-0,02989	0,0006252	88244	57217	47,80	107646
R Pre vs. R Early	0,02125	0,06149	-0,04024	0,007165	638	785	5,617	1411
R Pre vs. R Late	0,02125	0,05924	-0,03799	0,007966	638	949	4,769	1551
R Pre vs. R Extinction	0,02125	0,03748	-0,01623	0,006774	638	689	2,396	1322
R vs. NR Pre vs. R Early	0,005191	0,06149	-0,05630	0,005728	3793	785	9,829	910,4
R vs. NR Pre vs. R Late	0,005191	0,05924	-0,05405	0,006704	3793	949	8,062	1056
R vs. NR Pre vs. R vs. NR Extinction	0,005191	0,003887	0,001304	0,002480	3793	3841	0,5258	7283
NR Late vs. R Late	0,04206	0,05924	-0,01718	0,006536	94696	949	2,628	955,4

R Late vs. R vs. NR Late	0,05924	0,02085	0,03839	0,006761	949	5885	5,678	1093
NR Late vs. R vs. NR Late	0,04206	0,02085	0,02121	0,001822	94696	5885	11,64	6522

Fig. 5a:

Kruskal-Wallis test	
P value	<0,0001
Exact or approximate P value?	Approximate
P value summary	****
Do the medians vary signif. (P < 0.05)?	Yes
Number of groups	6
Kruskal-Wallis statistic	248,2
Data summary	
Number of treatments (columns)	6
Number of values (total)	697

Number of families	1					
Number of comparisons per family	5					
Alpha	0,05					
Dunn's multiple comparisons test	**Mean rank diff,**	**Significant?**	**Summary**	**Adjusted P Value**	**A-?**	
Baseline vs. T-2	10,52	No	ns	>0,9999	B	T-2
Baseline vs. T-1	-23,27	No	ns	>0,9999	C	T-1
Baseline vs. T0	-294,6	Yes	****	<0,0001	D	T0
Baseline vs. T+1	-64,20	Yes	*	0,0124	E	T+1
Baseline vs. T+2	-57,06	No	ns	0,1393	F	T+2
Test details	Mean rank 1	Mean rank 2	Mean rank diff,	n1	n2	Z
Baseline vs. T-2	280,2	269,7	10,52	246	63	0,4133
Baseline vs. T-1	280,2	303,5	-23,27	246	103	1,100
Baseline vs. T0	280,2	574,9	-294,6	246	123	14,81
Baseline vs. T+1	280,2	344,4	-64,20	246	102	3,026
Baseline vs. T+2	280,2	337,3	-57,06	246	60	2,199

Supp. Fig 1d:

Two-way ANOVA	**Ordinary**				
Alpha	0,05				
Source of Variation	% of total variation	P value	P value summary	Significant?	
Interaction	4,100	0,1979	ns	No	
Row Factor	40,60	<0,0001	****	Yes	
Column Factor	7,002	<0,0001	****	Yes	
ANOVA table	SS (Type III)	DF	MS	F (DFn, DFd)	P value
Interaction	0,2373	10	0,02373	F (10, 167) = 1,370	P=0,1979
Row Factor	2,350	5	0,4700	F (5, 167) = 27,14	P<0,0001
Column Factor	0,4053	2	0,2027	F (2, 167) = 11,70	P<0,0001
Residual	2,892	167	0,01732		

Data summary					
Number of columns (Column Factor)	3				
Number of rows (Row Factor)	6				
Number of values	185				

Number of families	6							
Number of comparisons per family	3							
Alpha	0,05							
Holm-Šídák's multiple comparisons test	**Predicted (LS) mean diff,**	**Below threshold?**	**Summary**	**Adjusted P Value**				
H1								
non Illuminated vs. GFP control	-0,03961	No	ns	0,8847				
non Illuminated vs. Inhibition	-0,003207	No	ns	0,9560				
GFP control vs. Inhibition	0,03640	No	ns	0,8847				
H2								
non Illuminated vs. GFP control	-0,04560	No	ns	0,8120				
non Illuminated vs. Inhibition	-0,0007436	No	ns	0,9898				
GFP control vs. Inhibition	0,04486	No	ns	0,8120				
T1								
non Illuminated vs. GFP control	0,008866	No	ns	0,8836				
non Illuminated vs. Inhibition	0,1770	Yes	**	0,0095				
GFP control vs. Inhibition	0,1681	Yes	**	0,0095				
T2								
non Illuminated vs. GFP control	-0,005117	No	ns	0,9327				
non Illuminated vs. Inhibition	0,1617	Yes	*	0,0118				
GFP control vs. Inhibition	0,1669	Yes	*	0,0105				
T3								
non Illuminated vs. GFP control	0,06882	No	ns	0,4475				
non Illuminated vs. Inhibition	0,09415	No	ns	0,2869				
GFP control vs. Inhibition	0,02533	No	ns	0,6536				
T4								
non Illuminated vs. GFP control	-0,06204	No	ns	0,3064				
non Illuminated vs. Inhibition	0,1063	No	ns	0,1328				
GFP control vs. Inhibition	0,1683	Yes	**	0,0097				

Test details	Predicted (LS) mean 1	Predicted (LS) mean 2	Predicted (LS) mean diff,	SE of diff,	N1	N 2	t	DF
H1								
non Illuminated vs. GFP control	0,03461	0,07422	-0,03961	0,06047	9	10	0,6551	167,0

non Illuminated vs. Inhibition	0,03461	0,03782	-0,003207	0,05803	9	12	0,05526	167,0
GFP control vs. Inhibition	0,07422	0,03782	0,03640	0,05635	10	12	0,6460	167,0
H2								
non Illuminated vs. GFP control	0,03904	0,08464	-0,04560	0,06047	9	10	0,7541	167,0
non Illuminated vs. Inhibition	0,03904	0,03979	-0,0007436	0,05803	9	12	0,01281	167,0
GFP control vs. Inhibition	0,08464	0,03979	0,04486	0,05635	10	12	0,7961	167,0
T1								
non Illuminated vs. GFP control	0,3940	0,3851	0,008866	0,06047	9	10	0,1466	167,0
non Illuminated vs. Inhibition	0,3940	0,2170	0,1770	0,05915	9	11	2,992	167,0
GFP control vs. Inhibition	0,3851	0,2170	0,1681	0,05750	10	11	2,924	167,0
T2								
non Illuminated vs. GFP control	0,3701	0,3752	-0,005117	0,06047	9	10	0,08462	167,0
non Illuminated vs. Inhibition	0,3701	0,2084	0,1617	0,05803	9	12	2,787	167,0
GFP control vs. Inhibition	0,3752	0,2084	0,1669	0,05635	10	12	2,961	167,0
T3								
non Illuminated vs. GFP control	0,2848	0,2160	0,06882	0,06047	9	10	1,138	167,0
non Illuminated vs. Inhibition	0,2848	0,1906	0,09415	0,05803	9	12	1,622	167,0
GFP control vs. Inhibition	0,2160	0,1906	0,02533	0,05635	10	12	0,4495	167,0
T4								
non Illuminated vs. GFP control	0,2479	0,3099	-0,06204	0,06047	9	10	1,026	167,0
non Illuminated vs. Inhibition	0,2479	0,1416	0,1063	0,05803	9	12	1,832	167,0
GFP control vs. Inhibition	0,3099	0,1416	0,1683	0,05635	10	12	2,988	167,0

Supp Fig 2e (top):

Trial activity of all cells over days.

Kruskal-Wallis test	
P value	<0,0001
Exact or approximate P value?	Approximate
P value summary	****
Do the medians vary signif. (P < 0.05)?	Yes
Number of groups	6
Kruskal-Wallis statistic	87,45
Data summary	
Number of treatments (columns)	6
Number of values (total)	6596

Number of families	1					
Number of comparisons per family	5					
Alpha	0,05					

Dunn's multiple comparisons test	Mean rank diff,	Significant?	Summary	Adjusted P Value	A-?	
H1/2 vs. T1	-292,4	Yes	****	<0,0001	B	T1
H1/2 vs. T2	-488,4	Yes	****	<0,0001	C	T2
H1/2 vs. T3	-527,5	Yes	****	<0,0001	D	T3
H1/2 vs. T4	-302,7	Yes	****	<0,0001	E	T4
H1/2 vs. Ext	-379,8	Yes	****	<0,0001	F	Ext

Test details	Mean rank 1	Mean rank 2	Mean rank diff,	n1	n2	Z
H1/2 vs. T1	3006	3299	-292,4	1738	1042	4,456
H1/2 vs. T2	3006	3495	-488,4	1738	921	7,154
H1/2 vs. T3	3006	3534	-527,5	1738	969	7,855
H1/2 vs. T4	3006	3309	-302,7	1738	916	4,426
H1/2 vs. Ext	3006	3386	-379,8	1738	1010	5,731

Supp Fig 2e (bottom):

Non-Trial activity of all cells over days.

Kruskal-Wallis test	
P value	<0,0001
Exact or approximate P value?	Approximate
P value summary	****
Do the medians vary signif. (P < 0.05)?	Yes
Number of groups	6
Kruskal-Wallis statistic	175,3
Data summary	
Number of treatments (columns)	6
Number of values (total)	6540

Number of families	1					
Number of comparisons per family	5					
Alpha	0,05					

Dunn's multiple comparisons test	Mean rank diff,	Significant?	Summary	Adjusted P Value	A-?	
H1/2 vs. T1	-397,4	Yes	****	<0,0001	B	T1
H1/2 vs. T2	-843,1	Yes	****	<0,0001	C	T2
H1/2 vs. T3	-377,9	Yes	****	<0,0001	D	T3
H1/2 vs. T4	-755,8	Yes	****	<0,0001	E	T4
H1/2 vs. Ext	-656,5	Yes	****	<0,0001	F	Ext

Test details	Mean rank 1	Mean rank 2	Mean rank diff,	n1	n2	Z
H1/2 vs. T1	2827	3224	-397,4	1710	1014	5,310
H1/2 vs. T2	2827	3670	-843,1	1710	921	10,93
H1/2 vs. T3	2827	3205	-377,9	1710	969	4,978
H1/2 vs. T4	2827	3583	-755,8	1710	916	9,776
H1/2 vs. Ext	2827	3483	-656,5	1710	1010	8,761

Supp Fig 2f (top):

Trial activity of nonresponder vs. responder.

Two-way ANOVA	**Ordinary**				
Alpha	0,05				
Source of Variation	% of total variation	P value	P value summary	Significant?	
Interaction	2,423	<0,0001	****	Yes	
Day	3,999	<0,0001	****	Yes	
Cell Group	30,00	<0,0001	****	Yes	
ANOVA table	SS (Type III)	DF	MS	F (DFn, DFd)	P value
Interaction	8,852	5	1,770	F (5, 6528) = 47,04	P<0,0001
Day	14,61	5	2,922	F (5, 6528) = 77,64	P<0,0001
Cell Group	109,6	1	109,6	F (1, 6528) = 2913	P<0,0001
Residual	245,7	6528	0,03763		
Difference between column means					
Predicted (LS) mean of NR	0,06391				
Predicted (LS) mean of R	0,6088				
Difference between predicted means	-0,5449				
SE of difference	0,01010				
95% CI of difference	-0,5647 to -0,5251				
Data summary					
Number of columns (Cell Group)	2				
Number of rows (Day)	6				
Number of values	6540				

Number of families	2							
Number of comparisons per family	5							
Alpha	0,05							
Šídák's multiple comparisons test	**Predicted (LS) mean diff,**	**95,00% CI of diff,**	**Below threshold?**	**Summary**	**Adjusted P Value**			
NR								
H1/2 vs. T1	-0,03016	-0,05054 to -0,009772	Yes	***	0,0007			
H1/2 vs. T2	-0,03434	-0,05541 to -0,01327	Yes	***	0,0001			
H1/2 vs. T3	-0,07778	-0,09854 to -0,05703	Yes	****	<0,0001			
H1/2 vs. T4	-0,02320	-0,04423 to -0,002172	Yes	*	0,0228			
H1/2 vs. Ext.	-0,01806	-0,03861 to 0,002491	No	ns	0,1143			
R								

H1/2 vs. T1	-0,1649	-0,2453 to -0,08450	Yes	****	<0,0001			
H1/2 vs. T2	-0,3602	-0,4401 to -0,2802	Yes	****	<0,0001			
H1/2 vs. T3	-0,4595	-0,5366 to -0,3824	Yes	****	<0,0001			
H1/2 vs. T4	-0,3852	-0,4703 to -0,3000	Yes	****	<0,0001			
H1/2 vs. Ext.	-0,1563	-0,2296 to -0,08310	Yes	****	<0,0001			
Test details	Predicted (LS) mean 1	Predicted (LS) mean 2	Predicted (LS) mean diff,	SE of diff,	N1	N2	t	DF
NR								
H1/2 vs. T1	0,03332	0,06347	-0,03016	0,007934	1596	956	3,801	6528
H1/2 vs. T2	0,03332	0,06766	-0,03434	0,008200	1596	862	4,188	6528
H1/2 vs. T3	0,03332	0,1111	-0,07778	0,008078	1596	903	9,629	6528
H1/2 vs. T4	0,03332	0,05652	-0,02320	0,008184	1596	867	2,835	6528
H1/2 vs. Ext.	0,03332	0,05137	-0,01806	0,007997	1596	932	2,258	6528
R								
H1/2 vs. T1	0,3544	0,5193	-0,1649	0,03129	114	58	5,270	6528
H1/2 vs. T2	0,3544	0,7146	-0,3602	0,03111	114	59	11,58	6528
H1/2 vs. T3	0,3544	0,8139	-0,4595	0,03000	114	66	15,32	6528
H1/2 vs. T4	0,3544	0,7396	-0,3852	0,03314	114	49	11,62	6528
H1/2 vs. Ext.	0,3544	0,5108	-0,1563	0,02851	114	78	5,485	6528

Supp Fig 2f (bottom):

Non-Trial activity of nonresponder vs. responder.

Two-way ANOVA	**Ordinary**				
Alpha	0,05				
Source of Variation	% of total variation	P value	P value summary	Significant?	
Interaction	0,3270	0,0003	***	Yes	
Day	1,819	<0,0001	****	Yes	
Cell Group	2,951	<0,0001	****	Yes	
ANOVA table	SS (Type III)	DF	MS	F (DFn, DFd)	P value
Interaction	0,3942	5	0,07884	F (5, 6528) = 4,644	P=0,0003
Day	2,193	5	0,4387	F (5, 6528) = 25,84	P<0,0001
Cell Group	3,558	1	3,558	F (1, 6528) = 209,6	P<0,0001
Residual	110,8	6528	0,01698		
Difference between column means					
Predicted (LS) mean of NR	0,1135				
Predicted (LS) mean of R	0,2116				
Difference between predicted means	-0,09816				
SE of difference	0,006781				
95% CI of difference	-0,1115 to -0,08487				
Data summary					

Number of columns (Cell Group)	2				
Number of rows (Day)	6				
Number of values	6540				

Within each column, compare rows (simple effects within columns)								
Number of families	2							
Number of comparisons per family	5							
Alpha	0,05							
Šídák's multiple comparisons test	**Predicted (LS) mean diff,**	**95,00% CI of diff,**	**Below threshold ?**	**Summary**	**Adjusted P Value**			
NR								
H1/2 vs. T1	-0,07428	-0,08797 to -0,06059	Yes	****	<0,0001			
H1/2 vs. T2	-0,08028	-0,09443 to -0,06613	Yes	****	<0,0001			
H1/2 vs. T3	-0,04618	-0,06012 to -0,03224	Yes	****	<0,0001			
H1/2 vs. T4	-0,05798	-0,07210 to -0,04386	Yes	****	<0,0001			
H1/2 vs. Ext.	-0,05108	-0,06488 to -0,03728	Yes	****	<0,0001			
R								
H1/2 vs. T1	-0,04710	-0,1011 to 0,006896	No	ns	0,1191			
H1/2 vs. T2	-0,1223	-0,1760 to -0,06861	Yes	****	<0,0001			
H1/2 vs. T3	-0,08870	-0,1405 to -0,03692	Yes	****	<0,0001			
H1/2 vs. T4	-0,1365	-0,1937 to -0,07931	Yes	****	<0,0001			
H1/2 vs. Ext.	-0,08850	-0,1377 to -0,03931	Yes	****	<0,0001			

Test details	Predicted (LS) mean 1	Predicted (LS) mean 2	Predicted (LS) mean diff,	SE of diff,	N1	N2	t	DF
NR								
H1/2 vs. T1	0,06182	0,1361	-0,07428	0,005329	1596	956	13,94	6528
H1/2 vs. T2	0,06182	0,1421	-0,08028	0,005507	1596	862	14,58	6528
H1/2 vs. T3	0,06182	0,1080	-0,04618	0,005425	1596	903	8,512	6528
H1/2 vs. T4	0,06182	0,1198	-0,05798	0,005497	1596	867	10,55	6528
H1/2 vs. Ext.	0,06182	0,1129	-0,05108	0,005371	1596	932	9,510	6528
R								
H1/2 vs. T1	0,1311	0,1782	-0,04710	0,02101	114	58	2,241	6528
H1/2 vs. T2	0,1311	0,2534	-0,1223	0,02090	114	59	5,853	6528
H1/2 vs. T3	0,1311	0,2198	-0,08870	0,02015	114	66	4,401	6528
H1/2 vs. T4	0,1311	0,2676	-0,1365	0,02226	114	49	6,133	6528
H1/2 vs. Ext.	0,1311	0,2196	-0,08850	0,01915	114	78	4,623	6528

Supp. Fig. 5c:

Kruskal-Wallis test	
P value	<0,0001
Exact or approximate P value?	Approximate
P value summary	****
Do the medians vary signif. (P < 0.05)?	Yes
Number of groups	6
Kruskal-Wallis statistic	141,2
Data summary	
Number of treatments (columns)	6
Number of values (total)	590

Number of families	1					
Number of comparisons per family	5					
Alpha	0,05					
Dunn's multiple comparisons test	**Mean rank diff,**	**Significant?**	**Summary**	**Adjusted P Value**	**A-?**	
H1/2 vs. T1	-124,1	Yes	****	<0,0001	B	T1
H1/2 vs. T2	-112,3	Yes	****	<0,0001	C	T2
H1/2 vs. T3	-143,1	Yes	****	<0,0001	D	T3
H1/2 vs. T4	-211,7	Yes	****	<0,0001	E	T4
H1/2 vs. Extinction	-192,0	Yes	****	<0,0001	F	Extinction
Test details	Mean rank 1	Mean rank 2	Mean rank diff,	n1	n2	Z
H1/2 vs. T1	192,2	316,3	-124,1	209	74	5,406
H1/2 vs. T2	192,2	304,6	-112,3	209	80	5,036
H1/2 vs. T3	192,2	335,3	-143,1	209	52	5,441
H1/2 vs. T4	192,2	404,0	-211,7	209	87	9,781
H1/2 vs. Extinction	192,2	384,2	-192,0	209	88	8,905

Supp. Fig. 5d:

Kruskal-Wallis test	
P value	<0,0001
Exact or approximate P value?	Approximate
P value summary	****
Do the medians vary signif. (P < 0.05)?	Yes
Number of groups	6
Kruskal-Wallis statistic	672,0
Data summary	
Number of treatments (columns)	6
Number of values (total)	3857

Number of families	1					
Number of comparisons per family	5					
Alpha	0,05					
Dunn's multiple comparisons test	**Mean rank diff,**	**Significant?**	**Summary**	**Adjusted P Value**	**A-?**	

H1/2 vs. T1	-992,8	Yes	****	<0,0001	B	T1
H1/2 vs. T2	-956,2	Yes	****	<0,0001	C	T2
H1/2 vs. T3	-1256	Yes	****	<0,0001	D	T3
H1/2 vs. T4	-1135	Yes	****	<0,0001	E	T4
H1/2 vs. Extinction	-1194	Yes	****	<0,0001	F	Extinction
Test details	Mean rank 1	Mean rank 2	Mean rank diff,	n1	n2	Z
H1/2 vs. T1	1063	2056	-992,8	830	645	16,99
H1/2 vs. T2	1063	2019	-956,2	830	613	16,13
H1/2 vs. T3	1063	2319	-1256	830	537	20,37
H1/2 vs. T4	1063	2198	-1135	830	547	18,52
H1/2 vs. Extinction	1063	2257	-1194	830	685	20,78

Supp. Fig. 6a:

Two-way ANOVA	**Ordinary**				
Alpha	0,05				
Source of Variation	% of total variation	P value	P value summary	Significant?	
Interaction	0,7079	<0,0001	****	Yes	
Day	1,740	<0,0001	****	Yes	
Celltype	0,7195	<0,0001	****	Yes	
ANOVA table	SS (Type III)	DF	MS	F (DFn, DFd)	P value
Interaction	4297	5	859,4	F (5, 11704) = 17,06	P<0,0001
Day	10563	5	2113	F (5, 11704) = 41,94	P<0,0001
Celltype	4367	1	4367	F (1, 11704) = 86,69	P<0,0001
Residual	589626	11704	50,38		
Difference between column means					
Predicted (LS) mean of Nonresponder	3,331				
Predicted (LS) mean of Responder	5,750				
Difference between predicted means	-2,420				
SE of difference	0,2599				
95% CI of difference	-2,929 to -1,910				
Data summary					
Number of columns (Celltype)	2				
Number of rows (Day)	6				
Number of values	11716				

Number of families	1							
Number of comparisons per family	6							
Alpha	0,05							

Šídák's multiple comparisons test	Predicted (LS) mean diff,	95,00% CI of diff,	Below threshold?	Summary	Adjusted P Value			
Nonresponder - Responder								
Baseline	0,1770	-1,060 to 1,414	No	ns	0,9994			
T1	-0,7620	-2,514 to 0,9900	No	ns	0,8255			
T2	-2,977	-4,726 to -1,228	Yes	****	<0,0001			
T3	-5,919	-7,668 to -4,170	Yes	****	<0,0001			
T4	-4,738	-6,487 to -2,989	Yes	****	<0,0001			
Extinction	-0,3000	-2,049 to 1,449	No	ns	0,9982			

Test details	Predicted (LS) mean 1	Predicted (LS) mean 2	Predicted (LS) mean diff,	SE of diff,	N1	N2	t	DF
Nonresponder - Responder								
Baseline	2,056	1,879	0,1770	0,4700	3120	246	0,3766	11704
T1	3,044	3,806	-0,7620	0,6658	1495	123	1,145	11704
T2	3,827	6,804	-2,977	0,6647	1560	123	4,478	11704
T3	4,211	10,13	-5,919	0,6647	1560	123	8,904	11704
T4	3,330	8,068	-4,738	0,6647	1560	123	7,128	11704
Extinction	3,515	3,815	-0,3000	0,6647	1560	123	0,4513	11704

Supp. Fig. 6b:

Brown-Forsythe ANOVA test	
F* (DFn, DFd)	0,5447 (8,000, 11252)
P value	0,8235
P value summary	ns
Significant diff. among means (P < 0.05)?	No
Welch's ANOVA test	
W (DFn, DFd)	0,5607 (8,000, 4738)
P value	0,8108
P value summary	ns
Significant diff. among means (P < 0.05)?	No
Data summary	
Number of treatments (columns)	9
Number of values (total)	304888

Supp. Fig. 6c:

Kruskal-Wallis test	
P value	<0,0001
Exact or approximate P value?	Approximate
P value summary	****
Do the medians vary signif. (P < 0.05)?	Yes
Number of groups	4
Kruskal-Wallis statistic	83,52
Data summary	
Number of treatments (columns)	4
Number of values (total)	263

Number of families	1					

Number of comparisons per family	4					
Alpha	0,05					
Dunn's multiple comparisons test	**Mean rank diff,**	**Significant?**	**Summary**	**Adjusted P Value**		
T-1 vs. T0	-71,62	Yes	****	<0,0001	A-B	
T-1 vs. T+1	-17,37	No	ns	>0,9999	A-C	
T0 vs. T+1	54,25	Yes	**	0,0010	B-C	
T0 vs. T0 Training Responder	-42,05	Yes	***	0,0009	B-E	
Test details	Mean rank 1	Mean rank 2	Mean rank diff,	n1	n2	Z
T-1 vs. T0	57,00	128,6	-71,62	28	70	4,217
T-1 vs. T+1	57,00	74,37	-17,37	28	42	0,9374
T0 vs. T+1	128,6	74,37	54,25	70	42	3,660
T0 vs. T0 Training Responder	128,6	170,7	-42,05	70	123	3,698

Supp. Fig. 6d:**Kruskal-Wallis test**	
P value	<0,0001
Exact or approximate P value?	Approximate
P value summary	****
Do the medians vary signif. (P < 0.05)?	Yes
Number of groups	6
Kruskal-Wallis statistic	251,6
Data summary	
Number of treatments (columns)	6
Number of values (total)	629

Number of families	1					
Number of comparisons per family	5					
Alpha	0,05					
Dunn's multiple comparisons test	**Mean rank diff,**	**Significant ?**	**Summary**	**Adjusted P Value**	**A-?**	
Baseline vs. T-2	3,275	No	ns	>0,9999	B	T-2
Baseline vs. T-1	-19,65	No	ns	>0,9999	C	T-1
Baseline vs. T0	-273,3	Yes	****	<0,0001	D	T0
Baseline vs. T+1	-43,66	No	ns	0,1380	E	T+1
Baseline vs. T+2	-25,48	No	ns	>0,9999	F	T+2
Test details	Mean rank 1	Mean rank 2	Mean rank diff,	n1	n2	Z
Baseline vs. T-2	255,8	252,5	3,275	222	60	0,1419
Baseline vs. T-1	255,8	275,5	-19,65	222	95	1,011
Baseline vs. T0	255,8	529,1	-273,3	222	111	14,82
Baseline vs. T+1	255,8	299,5	-43,66	222	90	2,203
Baseline vs. T+2	255,8	281,3	-25,48	222	51	1,034

8 Publication bibliography

Acsády, László; Kamondi, A.; Sík, A.; Freund, T.; Buzsáki, G. (1998): GABAergic cells are the major postsynaptic targets of mossy fibers in the rat hippocampus. In *The Journal of Neuroscience* 18 (9), pp. 3386–3403. DOI: 10.1523/JNEUROSCI.18-09-03386.1998.

Amaral, D. G.; Witter, M. P. (1989): The three-dimensional organization of the hippocampal formation: A review of anatomical data. In *Neuroscience* 31 (3), pp. 571–591. DOI: 10.1016/0306-4522(89)90424-7.

Amaral, David G. (1999): Introduction: What is where in the medial temporal lobe? In *Hippocampus* 9 (1), pp. 1–6. DOI: 10.1002/(SICI)1098-1063(1999)9:1<1::AID-HIPO1>3.0.CO;2-T.

Amaral, David G.; Kurz, J. (1985): An analysis of the origins of the cholinergic and noncholinergic septal projections to the hippocampal formation of the rat. In *The Journal of comparative neurology* 240 (1), pp. 37–59. DOI: 10.1002/cne.902400104.

Amaral, David G.; Scharfman, Helen E.; Lavenex, Pierre (2007): The dentate gyrus: fundamental neuroanatomical organization (dentate gyrus for dummies). In H. E. Scharfman (Ed.): DENTATE GYRUS: A COMPHREHENSIVE GUIDE TO STRUCTURE, FUNCTION, AND CLINICAL IMPLICATIONS, vol. 163. SARA BURGERHARTSTRAAT 25, PO BOX 211, 1000 AE AMSTERDAM, NETHERLANDS: ELSEVIER SCIENCE BV (Progress in Brain Research), 3+.

Andersen, Per (2007): The hippocampus book. Oxford, New York: Oxford University Press.

Andersen, Per; Bliss, T. V.; Skrede, K. K. (1971): Lamellar organization of hippocampal pathways. In *Exp Brain Res* 13 (2), pp. 222–238. DOI: 10.1007/BF00234087.

Andersen, Per; Holmqvist, B.; Voorhoeve, P. E. (1966): Excitatory synapses on hippocampal apical dendrites activated by entorhinal stimulation. In *Acta physiologica Scandinavica* 66 (4), pp. 461–472. DOI: 10.1111/j.1748-1716.1966.tb03224.x.

Berron, David; Schütze, Hartmut; Maass, Anne; Cardenas-Blanco, Arturo; Kuijf, Hugo J.; Kumaran, Dharshan; Düzel, Emrah (2016): Strong Evidence for Pattern Separation in Human Dentate Gyrus. In *J. Neurosci.* 36 (29), pp. 7569–7579. DOI: 10.1523/JNEUROSCI.0518-16.2016.

Blackstad, T. W.; Brink, K.; Hem, J.; Jeune, B. (1970): Distribution of hippocampal mossy fibers in the rat. An experimental study with silver impregnation methods. In *The Journal of comparative neurology* 138 (4), pp. 433–449. DOI: 10.1002/cne.901380404.

Bliss, T. V. P.; Lømo, T. (1973): Long-lasting potentiation of synaptic transmission in the dentate area of the anaesthetized rabbit following stimulation of the perforant path. In *The Journal of physiology* 232 (2), pp. 331–356. DOI: 10.1113/jphysiol.1973.sp010273.

Bonthius, Daniel J.; McKim, Ross; Koele, Lindsey; Harb, Harb; Karacay, Bahri; Mahoney, Jo; Pantazis, Nicholas J. (2004): Use of frozen sections to determine neuronal number in the murine hippocampus and neocortex using the optical disector and optical fractionator. In *Brain research. Brain research protocols* 14 (1), pp. 45–57. DOI: 10.1016/j.brainresprot.2004.09.003.

Bragin, A.; Jandó, G.; Nádasdy, Z.; van Landeghem, M.; Buzsáki, G. (1995): Dentate EEG spikes and associated interneuronal population bursts in the hippocampal hilar region of the rat. In *Journal of neurophysiology* 73 (4), pp. 1691–1705. DOI: 10.1152/jn.1995.73.4.1691.

Bramham, C. R. (1998): Phasic boosting of medial perforant path-evoked granule cell output time-locked to spontaneous dentate EEG spikes in awake rats. In *Journal of neurophysiology* 79 (6), pp. 2825–2832. DOI: 10.1152/jn.1998.79.6.2825.

Bramham, C. R.; Errington, M. L.; Bliss, T. V. (1988): Naloxone blocks the induction of long-term potentiation in the lateral but not in the medial perforant pathway in the anesthetized rat. In *Brain research* 449 (1-2), pp. 352–356. DOI: 10.1016/0006-8993(88)91052-9.

Buckmaster, P. S.; Strowbridge, B. W.; Schwartzkroin, P. A. (1993): A comparison of rat hippocampal mossy cells and CA3c pyramidal cells. In *Journal of neurophysiology* 70 (4), pp. 1281–1299. DOI: 10.1152/jn.1993.70.4.1281.

Burwell, R. D.; Witter, M. P.; Amaral, D. G. (1995): Perirhinal and postrhinal cortices of the rat: a review of the neuroanatomical literature and comparison with findings from the monkey brain. In *Hippocampus* 5 (5), pp. 390–408. DOI: 10.1002/hipo.450050503.

Burwell, Rebecca D.; Witter, Menno P. (2002): Basic anatomy of the parahippocampal region in monkeys and rats.

Buzsáki, G.; Draguhn, A. (2004): Neuronal oscillations in cortical networks. In *Science (New York, N.Y.)* 304 (5679), pp. 1926–1929. DOI: 10.1126/science.1099745.

Buzsáki, György (2015): Hippocampal sharp wave-ripple: A cognitive biomarker for episodic memory and planning. In *Hippocampus* 25 (10), pp. 1073–1188. DOI: 10.1002/hipo.22488.

Buzsáki, György; Moser, Edvard I. (2013): Memory, navigation and theta rhythm in the hippocampal-entorhinal system. In *Nature neuroscience* 16 (2), pp. 130–138. DOI: 10.1038/nn.3304.

Charvet, Christine J.; Finlay, Barbara L. (2018): Comparing Adult Hippocampal Neurogenesis Across Species: Translating Time to Predict the Tempo in Humans. In *FRONTIERS IN NEUROSCIENCE* 12, p. 706. DOI: 10.3389/fnins.2018.00706.

Claiborne, B. J.; Amaral, David G.; Cowan, W. M. (1986): A light and electron microscopic analysis of the mossy fibers of the rat dentate gyrus. In *The Journal of comparative neurology* 246 (4), pp. 435–458. DOI: 10.1002/cne.902460403.

Claiborne, B. J.; Amaral, David G.; Cowan, W. M. (1990): Quantitative, three-dimensional analysis of granule cell dendrites in the rat dentate gyrus. In *The Journal of comparative neurology* 302 (2), pp. 206–219. DOI: 10.1002/cne.903020203.

Clark, R. E.; Lavond, D. G. (1996): Neural unit activity in the trigeminal complex with interpositus or red nucleus inactivation during classical eyeblink conditioning. In *Behavioral neuroscience* 110 (1), pp. 13–21. DOI: 10.1037//0735-7044.110.1.13.

Csicsvari, J.; Hirase, H.; Mamiya, A.; Buzsáki, G. (2000): Ensemble patterns of hippocampal CA3-CA1 neurons during sharp wave-associated population events. In *Neuron* 28 (2), pp. 585–594. DOI: 10.1016/s0896-6273(00)00135-5.

Dana, Hod; Chen, Tsai-Wen; Hu, Amy; Shields, Brenda C.; Guo, Caiying; Looger, Loren L. et al. (2014): Thy1-GCaMP6 transgenic mice for neuronal population imaging in vivo. In *PloS one* 9 (9), e108697. DOI: 10.1371/journal.pone.0108697.

Danielson, Nathan B.; Kaifosh, Patrick; Zaremba, Jeffrey D.; Lovett-Barron, Matthew; Tsai, Joseph; Denny, Christine A. et al. (2016): Distinct Contribution of Adult-Born Hippocampal Granule Cells to Context Encoding. In *Neuron* 90 (1), pp. 101–112. DOI: 10.1016/j.neuron.2016.02.019.

Deller, T.; Martinez, A.; Nitsch, R.; Frotscher, M. (1996): A novel entorhinal projection to the rat dentate gyrus: direct innervation of proximal dendrites and cell bodies of granule cells and GABAergic neurons. In *The Journal of Neuroscience* 16 (10), pp. 3322–3333. DOI: 10.1523/JNEUROSCI.16-10-03322.1996.

Deshmukh, Sachin S.; Knierim, James J. (2011): Representation of non-spatial and spatial information in the lateral entorhinal cortex. In *FRONTIERS IN BEHAVIORAL NEUROSCIENCE* 5, p. 69. DOI: 10.3389/fnbeh.2011.00069.

Desmond, J. E.; Moore, J. W. (1991): Single-unit activity in red nucleus during the classically conditioned rabbit nictitating membrane response. In *NEUROSCIENCE RESEARCH* 10 (4), pp. 260–279. DOI: 10.1016/0168-0102(91)90083-B.

Dvorak, Dino; Chung, Ain; Park, Eun Hye; Fenton, André Antonio (2021): Dentate spikes and external control of hippocampal function. In *Cell reports* 36 (5), p. 109497. DOI: 10.1016/j.celrep.2021.109497.

Eichenbaum, H. (2014): Time cells in the hippocampus: a new dimension for mapping memories. In *NATURE REVIEWS NEUROSCIENCE* 15 (11), pp. 732–744. DOI: 10.1038/nrn3827.

Flores, Luke C.; Disterhoft, John F. (2009): Caudate nucleus is critically involved in trace eyeblink conditioning. In *J. Neurosci.* 29 (46), pp. 14511–14520. DOI: 10.1523/JNEUROSCI.3119-09.2009.

Flores, Luke C.; Disterhoft, John F. (2013): Caudate nucleus in retrieval of trace eyeblink conditioning after consolidation. In *J. Neurosci.* 33 (7), pp. 2828–2836. DOI: 10.1523/JNEUROSCI.2326-12.2013.

Freund, T. F.; Buzsáki, G. (1996): Interneurons of the hippocampus. In *Hippocampus* 6 (4), pp. 347–470. DOI: 10.1002/(SICI)1098-1063(1996)6:4<347::AID-HIPO1>3.0.CO;2-I.

Gaarskjaer, F. B. (1978): Organization of the mossy fiber system of the rat studied in extended hippocampi. I. Terminal area related to number of granule and pyramidal cells. In *The Journal of comparative neurology* 178 (1), pp. 49–72. DOI: 10.1002/cne.901780104.

Gaarskjaer, F. B. (1986): The organization and development of the hippocampal mossy fiber system. In *Brain research* 396 (4), pp. 335–357. DOI: 10.1016/0165-0173(86)90004-4.

Galvez, Roberto; Weible, Aldis P.; Disterhoft, John F. (2007): Cortical barrel lesions impair whisker-CS trace eyeblink conditioning. In *Learning & memory (Cold Spring Harbor, N.Y.)* 14 (1), pp. 94–100. DOI: 10.1101/lm.418407.

Gertz, S. D.; Lindenberg, R.; Piavis, G. W. (1972): Structural variations in the rostral human hippocampus. In *The Johns Hopkins medical journal* 130 (6), pp. 367–376.

Gruart, A.; Blázquez, P.; Delgado-García, J. M. (1995): Kinematics of spontaneous, reflex, and conditioned eyelid movements in the alert cat. In *Journal of neurophysiology* 74 (1), pp. 226–248. DOI: 10.1152/jn.1995.74.1.226.

Gruart, A.; Delgado-Garcia, J. M. (2007): Activity-dependent changes of the hippocampal CA3-CA1 synapse during the acquisition of associative learning in conscious mice. In *GENES BRAIN AND BEHAVIOR* 6, pp. 24–31. DOI: 10.1111/j.1601-183X.2007.00319.x.

Gruart, A.; Schreurs, B. G.; del Toro, E. D.; Delgado-García, J. M. (2000): Kinetic and frequency-domain properties of reflex and conditioned eyelid responses in the rabbit. In *Journal of neurophysiology* 83 (2), pp. 836–852. DOI: 10.1152/jn.2000.83.2.836.

Gruart, Agnès; Muñoz, María Dolores; Delgado-García, José M. (2006): Involvement of the CA3-CA1 synapse in the acquisition of associative learning in behaving mice. In *The Journal of Neuroscience* 26 (4), pp. 1077–1087. DOI: 10.1523/JNEUROSCI.2834-05.2006.

Hafting, Torkel; Fyhn, Marianne; Molden, Sturla; Moser, May-Britt; Moser, Edvard I. (2005): Microstructure of a spatial map in the entorhinal cortex. In *Nature* 436 (7052), pp. 801–806. DOI: 10.1038/nature03721.

Hainmueller, Thomas; Bartos, Marlene (2018): Parallel emergence of stable and dynamic memory engrams in the hippocampus. In *Nature* 558 (7709), pp. 292–296. DOI: 10.1038/s41586-018-0191-2.

Hainmueller, Thomas; Bartos, Marlene (2020): Dentate gyrus circuits for encoding, retrieval and discrimination of episodic memories. In *Nature reviews. Neuroscience* 21 (3), pp. 153–168. DOI: 10.1038/s41583-019-0260-z.

Hargreaves, Eric L.; Rao, Geeta; Lee, Inah; Knierim, James J. (2005): Major dissociation between medial and lateral entorhinal input to dorsal hippocampus. In *Science (New York, N.Y.)* 308 (5729), pp. 1792–1794. DOI: 10.1126/science.1110449.

Hashimotodani, Yuki; Nasrallah, Kaoutsar; Jensen, Kyle R.; Chávez, Andrés E.; Carrera, Daniel; Castillo, Pablo E. (2017): LTP at Hilar Mossy Cell-Dentate Granule Cell Synapses Modulates Dentate Gyrus Output by Increasing Excitation/Inhibition Balance. In *Neuron* 95 (4), 928-943.e3. DOI: 10.1016/j.neuron.2017.07.028.

Hattori, Shoai; Chen, Lillian; Weiss, Craig; Disterhoft, John F. (2015): Robust hippocampal responsivity during retrieval of consolidated associative memory. In *Hippocampus* 25 (5), pp. 655–669. DOI: 10.1002/hipo.22401.

Headley, Drew B.; Kanta, Vasiliki; Paré, Denis (2017): Intra- and interregional cortical interactions related to sharp-wave ripples and dentate spikes. In *Journal of neurophysiology* 117 (2), pp. 556–565. DOI: 10.1152/jn.00644.2016.

Henze, Darrell A.; Wittner, Lucia; Buzsáki, György (2002): Single granule cells reliably discharge targets in the hippocampal CA3 network in vivo. In *Nat Neurosci* 5 (8), pp. 790–795. DOI: 10.1038/nn887.

Hofer, Katharina T.; Kandrács, Ágnes; Ulbert, István; Pál, Ildikó; Szabó, Csilla; Héja, László; Wittner, Lucia (2015): The hippocampal CA3 region can generate two distinct types of sharp wave-ripple complexes, in vitro. In *Hippocampus* 25 (2), pp. 169–186. DOI: 10.1002/hipo.22361.

Hosp, Jonas A.; Strüber, Michael; Yanagawa, Yuchio; Obata, Kunihiko; Vida, Imre; Jonas, Peter; Bartos, Marlene (2014): Morpho-physiological criteria divide dentate gyrus interneurons into classes. In *Hippocampus* 24 (2), pp. 189–203. DOI: 10.1002/hipo.22214.

Høydal, Øyvind Arne; Skytøen, Emilie Ranheim; Andersson, Sebastian Ola; Moser, May-Britt; Moser, Edvard I. (2019): Object-vector coding in the medial entorhinal cortex. In *Nature* 568 (7752), pp. 400–404. DOI: 10.1038/s41586-019-1077-7.

Huang, Lawrence; Ledochowitsch, Peter; Knoblich, Ulf; Lecoq, Jérôme; Murphy, Gabe J.; Reid, R. Clay et al. (2021): Relationship between simultaneously recorded spiking activity and fluorescence signal in GCaMP6 transgenic mice. In *eLife* 10. DOI: 10.7554/eLife.51675.

Hunsaker, Michael R.; Kesner, Raymond P. (2013): The operation of pattern separation and pattern completion processes associated with different attributes or domains of memory. In *NEUROSCIENCE AND BIOBEHAVIORAL REVIEWS* 37 (1), pp. 36–58. DOI: 10.1016/j.neubiorev.2012.09.014.

Hunsaker, Michael R.; Mooy, Graham G.; Swift, Jesse S.; Kesner, Raymond P. (2007): Dissociations of the medial and lateral perforant path projections into dorsal DG, CA3, and CA1 for spatial and nonspatial (visual object) information processing. In *Behavioral neuroscience* 121 (4), pp. 742–750. DOI: 10.1037/0735-7044.121.4.742.

Igarashi, K. M.; Ito, H. T.; Moser, E. I.; Moser, M. B. (2014a): Functional diversity along the transverse axis of hippocampal area CA1. In *FEBS LETTERS* 588 (15), pp. 2470–2476. DOI: 10.1016/j.febslet.2014.06.004.

Igarashi, Kei M.; Lu, Li; Colgin, Laura L.; Moser, May-Britt; Moser, Edvard I. (2014b): Coordination of entorhinal-hippocampal ensemble activity during associative learning. In *Nature* 510 (7503), pp. 143–147. DOI: 10.1038/nature13162.

Ishizuka, N.; Cowan, W. M.; Amaral, David G. (1995): A quantitative analysis of the dendritic organization of pyramidal cells in the rat hippocampus. In *The Journal of comparative neurology* 362 (1), pp. 17–45. DOI: 10.1002/cne.903620103.

Ishizuka, N.; Weber, J.; Amaral, David G. (1990): Organization of intrahippocampal projections originating from CA3 pyramidal cells in the rat. In *The Journal of comparative neurology* 295 (4), pp. 580–623. DOI: 10.1002/cne.902950407.

Izquierdo, I.; Furini, C. R.G.; Myskiw, J. C. (2016): FEAR MEMORY. In *PHYSIOLOGICAL REVIEWS* 96 (2), pp. 695–750. DOI: 10.1152/physrev.00018.2015.

Jung, M. W.; McNaughton, B. L. (1993): Spatial selectivity of unit activity in the hippocampal granular layer. In *Hippocampus* 3 (2), pp. 165–182. DOI: 10.1002/hipo.450030209.

Kandel, E. R.; Schwartz, J. H.; Jessel, T. M. (2000): Principles of Neural Science. 4th Edition.

Kaneko, T.; Thompson, R. F. (1997): Disruption of trace conditioning of the nictitating membrane response in rabbits by central cholinergic blockade. In *Psychopharmacology* 131 (2), pp. 161–166. DOI: 10.1007/s002130050279.

Kesner, R. P. (2013a): A process analysis of the CA3 subregion of the hippocampus. In *Front. Cell. Neurosci.* 7. DOI: 10.3389/fncel.2013.00078.

Kesner, Raymond P. (2013b): An analysis of the dentate gyrus function. In *BEHAVIOURAL BRAIN RESEARCH* 254 (SI), pp. 1–7. DOI: 10.1016/j.bbr.2013.01.012.

Kesner, Raymond P. (2018): An analysis of dentate gyrus function (an update). In *BEHAVIOURAL BRAIN RESEARCH* 354 (SI), pp. 84–91. DOI: 10.1016/j.bbr.2017.07.033.

Kesner, Raymond P.; Taylor, James O.; Hoge, Jennifer; Andy, Ford (2015): Role of the dentate gyrus in mediating object-spatial configuration recognition. In *Neurobiology of learning and memory* 118, pp. 42–48. DOI: 10.1016/j.nlm.2014.11.004.

Kim, J. J.; Clark, R. E.; Thompson, R. F. (1995): Hippocampectomy impairs the memory of recently, but not remotely, acquired trace eyeblink conditioned responses. In *Behavioral neuroscience* 109 (2), pp. 195–203. DOI: 10.1037//0735-7044.109.2.195.

Kimberly M. Christian and Richard F. Thompson (2003): Neural Substrates of Eyeblink Conditioning: Acquisition and Retention. In *Learning & Memory*.

Klinzing, Jens G.; Niethard, Niels; Born, Jan (2019): Mechanisms of systems memory consolidation during sleep. In *Nature neuroscience* 22 (10), pp. 1598–1610. DOI: 10.1038/s41593-019-0467-3.

Kneisler, T. B.; Dingledine, R. (1995a): Synaptic input from CA3 pyramidal cells to dentate basket cells in rat hippocampus. In *The Journal of physiology* 487 (1), pp. 125–146. DOI: 10.1113/jphysiol.1995.sp020866.

Kneisler, Tracy B.; Dingledine, Raymond (1995b): Synaptic input from CA3 pyramidal cells to dentate basket cells in rat hippocampus. In *Journal of Physiology*.

Köhler, C. (1985): Intrinsic projections of the retrohippocampal region in the rat brain. I. The subicular complex. In *The Journal of comparative neurology* 236 (4), pp. 504–522. DOI: 10.1002/cne.902360407.

Komorowski, Robert W.; Manns, Joseph R.; Eichenbaum, Howard (2009): Robust conjunctive item-place coding by hippocampal neurons parallels learning what happens where. In *The Journal of Neuroscience* 29 (31), pp. 9918–9929. DOI: 10.1523/JNEUROSCI.1378-09.2009.

Kronforst-Collins, M. A.; Disterhoft, J. F. (1998): Lesions of the caudal area of rabbit medial prefrontal cortex impair trace eyeblink conditioning. In *Neurobiology of learning and memory* 69 (2), pp. 147–162. DOI: 10.1006/nlme.1997.3818.

La Prida, L. M. de (2020): Potential factors influencing replay across CA1 during sharp-wave ripples. In *PHILOSOPHICAL TRANSACTIONS OF THE ROYAL SOCIETY B-BIOLOGICAL SCIENCES* 375 (1799). DOI: 10.1098/rstb.2019.0236.

Le Duigou, Caroline; Simonnet, Jean; Teleñczuk, Maria T.; Fricker, Desdemona; Miles, Richard (2014): Recurrent synapses and circuits in the CA3 region of the hippocampus: an associative network. In *Front. Cell. Neurosci.* 7, p. 262. DOI: 10.3389/fncel.2013.00262.

Lee, Inah; Kesner, Raymond P. (2004): Encoding versus retrieval of spatial memory: double dissociation between the dentate gyrus and the perforant path inputs into CA3 in the dorsal hippocampus. In *Hippocampus* 14 (1), pp. 66–76. DOI: 10.1002/hipo.10167.

Lehtonen, Suvi-Maaria; Waselius, Tomi; Penttonen, Markku; Nokia, Miriam S. (2022): Hippocampal responses to electrical stimulation of the major input pathways are modulated by dentate spikes. In *Hippocampus* 32 (11-12), pp. 808–817. DOI: 10.1002/hipo.23470.

Leutgeb, Jill K.; Leutgeb, Stefan; Moser, May-Britt; Moser, Edvard I. (2007): Pattern separation in the dentate gyrus and CA3 of the hippocampus. In *Science (New York, N.Y.)* 315 (5814), pp. 961–966. DOI: 10.1126/science.1135801.

Leutgeb, Stefan; Leutgeb, Jill K.; Barnes, Carol A.; Moser, Edvard I.; McNaughton, Bruce L.; Moser, May-Britt (2005): Independent codes for spatial and episodic memory in hippocampal neuronal ensembles. In *Science (New York, N.Y.)* 309 (5734), pp. 619–623. DOI: 10.1126/science.1114037.

Li, X. G.; Somogyi, P.; Ylinen, A.; Buzsáki, G. (1994): The hippocampal CA3 network: an in vivo intracellular labeling study. In *The Journal of comparative neurology* 339 (2), pp. 181–208. DOI: 10.1002/cne.903390204.

Lincoln, J. S.; McCormick, D. A.; Thompson, R. F. (1982): Ipsilateral cerebellar lesions prevent learning of the classically conditioned nictitating membrane/eyelid response. In *Brain research* 242 (1), pp. 190–193. DOI: 10.1016/0006-8993(82)90510-8.

Lisman, J. E. (1999): Relating hippocampal circuitry to function: recall of memory sequences by reciprocal dentate-CA3 interactions. In *Neuron* 22 (2), pp. 233–242. DOI: 10.1016/s0896-6273(00)81085-5.

Liu, Xin; Terada, Satoshi; Ramezani, Mehrdad; Kim, Jeong-Hoon; Lu, Yichen; Grosmark, Andres et al. (2022): E-Cannula reveals anatomical diversity in sharp-wave ripples as a driver for the recruitment of distinct hippocampal assemblies. In *Cell reports* 41 (1), p. 111453. DOI: 10.1016/j.celrep.2022.111453.

Liu, Yunzhe; Dolan, Raymond J.; Kurth-Nelson, Zeb; Behrens, Timothy E. J. (2019): Human Replay Spontaneously Reorganizes Experience. In *CELL* 178 (3), 640-652.e14. DOI: 10.1016/j.cell.2019.06.012.

MacDonald, Christopher J.; Lepage, Kyle Q.; Eden, Uri T.; Eichenbaum, Howard (2011): Hippocampal "time cells" bridge the gap in memory for discontiguous events. In *Neuron* 71 (4), pp. 737–749. DOI: 10.1016/j.neuron.2011.07.012.

Madroñal, Noelia; Delgado-García, José M.; Fernández-Guizán, Azahara; Chatterjee, Jayanta; Köhn, Maja; Mattucci, Camilla et al. (2016): Rapid erasure of hippocampal memory following inhibition of dentate gyrus granule cells. In *Nature communications* 7, p. 10923. DOI: 10.1038/ncomms10923.

Markus, E. J.; Qin, Y. L.; Leonard, B.; Skaggs, W. E.; McNaughton, B. L.; Barnes, Carol A. (1995): Interactions between location and task affect the spatial and directional firing of hippocampal neurons. In *The Journal of Neuroscience* 15 (11), pp. 7079–7094. DOI: 10.1523/JNEUROSCI.15-11-07079.1995.

Marr, D. (1971): Simple memory: a theory for archicortex. In *Philosophical transactions of the Royal Society of London. Series B, Biological sciences* 262 (841), pp. 23–81. DOI: 10.1098/rstb.1971.0078.

Matthew D. McEchron and John F. Disterhoft (1997): Sequence of Single Neuron Changes in CA1 Hippocampus of Rabbits During Acquisition of Trace Eyeblink Conditioned Responses.

McCormick, D. A.; Thompson, R. F. (1984): Cerebellum: essential involvement in the classically conditioned eyelid response. In *Science (New York, N.Y.)* 223 (4633), pp. 296–299. DOI: 10.1126/science.6701513.

McLaughlin, Joselyn; Skaggs, Helen; Churchwell, John; Powell, D. A. (2002): Medial prefrontal cortex and pavlovian conditioning: trace versus delay conditioning. In *Behavioral neuroscience* 116 (1), pp. 37–47. Available online at https://pubmed.ncbi.nlm.nih.gov/11895181/.

Meier, Kolja; Merseburg, Andrea; Isbrandt, Dirk; Marguet, Stephan Lawrence; Morellini, Fabio (2020): Dentate Gyrus Sharp Waves, a Local Field Potential Correlate of Learning in the Dentate Gyrus of Mice. In *The Journal of neuroscience : the official journal of the Society for Neuroscience* 40 (37), pp. 7105–7118. DOI: 10.1523/JNEUROSCI.2275-19.2020.

Miller, Lisa N.; Weiss, Craig; Disterhoft, John F. (2019): Genetic Ablation of Neural Progenitor Cells Impairs Acquisition of Trace Eyeblink Conditioning. In *eNeuro* 6 (5). DOI: 10.1523/ENEURO.0251-19.2019.

Miller, Lisa N.; Weiss, Craig; Disterhoft, John F. (2022): Learning-related changes in cellular activity within mouse dentate gyrus during trace eyeblink conditioning. In *Hippocampus* 32 (10), pp. 776–794. DOI: 10.1002/hipo.23468.

Modi, Mehrab N.; Dhawale, Ashesh K.; Bhalla, Upinder S. (2014): CA1 cell activity sequences emerge after reorganization of network correlation structure during associative learning. In *eLife* 3, e01982. DOI: 10.7554/eLife.01982.

Moita, Marta A. P.; Rosis, Svetlana; Zhou, Yu; LeDoux, Joseph E.; Blair, Hugh T. (2004): Putting fear in its place: remapping of hippocampal place cells during fear conditioning. In *The Journal of Neuroscience* 24 (31), pp. 7015–7023. DOI: 10.1523/JNEUROSCI.5492-03.2004.

Morris, R. G.; Garrud, P.; Rawlins, J. N.; O'Keefe, J. (1982): Place navigation impaired in rats with hippocampal lesions. In *Nature* 297 (5868), pp. 681–683. DOI: 10.1038/297681a0.

Moser, Edvard I.; Kropff, Emilio; Moser, May-Britt (2008): Place cells, grid cells, and the brain's spatial representation system. In *ANNUAL REVIEW OF NEUROSCIENCE* 31, pp. 69–89. DOI: 10.1146/annurev.neuro.31.061307.090723.

Mosko, S.; Lynch, G.; Cotman, C. W. (1973): The distribution of septal projections to the hippocampus of the rat. In *The Journal of comparative neurology* 152 (2), pp. 163–174. DOI: 10.1002/cne.901520204.

Mount and Sridhar (2021): Distinct neuronal populations contribute to trace conditioning and extinction learning in the hippocampal CA1. In *eLife*.

Moyer, J. R.; Deyo, R. A.; Disterhoft, J. F. (1990): Hippocampectomy disrupts trace eye-blink conditioning in rabbits. In *Behavioral neuroscience* 104 (2), pp. 243–252. DOI: 10.1037//0735-7044.104.2.243.

Moyer, James R.; Deyo, Richard A.; Disterhoft, John F. (2015): Hippocampectomy disrupts trace eye-blink conditioning in rabbits. In *Behavioral neuroscience* 129 (4), pp. 523–532. DOI: 10.1037/bne0000079.

Moyer, JR; Thompson, L. T.; Disterhoft, J. F. (1996): Trace eyeblink conditioning increases CA1 excitability in a transient and learning-specific manner. In *The Journal of Neuroscience* 16 (17), pp. 5536–5546.

Múnera, A.; Gruart, A.; Muñoz, M. D.; Fernández-Mas, R.; Delgado-García, J. M. (2001): Hippocampal pyramidal cell activity encodes conditioned stimulus predictive value during classical conditioning in alert cats. In *Journal of neurophysiology* 86 (5), pp. 2571–2582. DOI: 10.1152/jn.2001.86.5.2571.

Naber, P. A.; Da Lopes Silva, F. H.; Witter, M. P. (2001): Reciprocal connections between the entorhinal cortex and hippocampal fields CA1 and the subiculum are in register with the projections from CA1 to the subiculum. In *Hippocampus* 11 (2), pp. 99–104. DOI: 10.1002/hipo.1028.

Neubrandt, Máté; Oláh, Viktor János; Brunner, János; Marosi, Endre Levente; Soltesz, Ivan; Szabadics, János (2018): Single Bursts of Individual Granule Cells Functionally Rearrange Feedforward Inhibition. In *J. Neurosci.* 38 (7), pp. 1711–1724. DOI: 10.1523/JNEUROSCI.1595-17.2018.

Neunuebel, Joshua P.; Knierim, James J. (2012): Spatial firing correlates of physiologically distinct cell types of the rat dentate gyrus. In *J. Neurosci.* 32 (11), pp. 3848–3858. DOI: 10.1523/JNEUROSCI.6038-11.2012.

Nokia, Miriam S.; Gureviciene, Irina; Waselius, Tomi; Tanila, Heikki; Penttonen, Markku (2017): Hippocampal electrical stimulation disrupts associative learning when targeted at dentate spikes. In *The Journal of physiology* 595 (14), pp. 4961–4971. DOI: 10.1113/JP274023.

Nokia, Miriam S.; Penttonen, Markku (2022): Rhythmic Memory Consolidation in the Hippocampus. In *FRONTIERS IN NEURAL CIRCUITS* 16, p. 885684. DOI: 10.3389/fncir.2022.885684.

Nokia, Miriam S.; Penttonen, Markku; Wikgren, Jan (2010): Hippocampal ripple-contingent training accelerates trace eyeblink conditioning and retards extinction in rabbits. In *The Journal of neuroscience : the official journal of the Society for Neuroscience* 30 (34), pp. 11486–11492. DOI: 10.1523/JNEUROSCI.2165-10.2010.

O'Keefe, John (1976): Place units in the hippocampus of the freely moving rat. In *Experimental Neurology* 51 (1), pp. 78–109. DOI: 10.1016/0014-4886(76)90055-8.

Oliva, Azahara; Fernández-Ruiz, Antonio; Buzsáki, György; Berényi, Antal (2016): Role of Hippocampal CA2 Region in Triggering Sharp-Wave Ripples. In *Neuron* 91 (6), pp. 1342–1355. DOI: 10.1016/j.neuron.2016.08.008.

O'Reilly, R. C.; McClelland, J. L. (1994): Hippocampal conjunctive encoding, storage, and recall: avoiding a trade-off. In *Hippocampus* 4 (6), pp. 661–682. DOI: 10.1002/hipo.450040605.

Oswald, B. B.; Knuckley, B.; Maddox, S. A.; Powell, D. A. (2007): Ibotenic acid lesions to ventrolateral thalamic nuclei disrupts trace and delay eyeblink conditioning in rabbits. In *BEHAVIOURAL BRAIN RESEARCH* 179 (1), pp. 111–117. DOI: 10.1016/j.bbr.2007.01.016.

Pastalkova, Eva; Itskov, Vladimir; Amarasingham, Asohan; Buzsáki, György (2008): Internally generated cell assembly sequences in the rat hippocampus. In *Science (New York, N.Y.)* 321 (5894), pp. 1322–1327. DOI: 10.1126/science.1159775.

Patzke, Nina; Spocter, Muhammad A.; Karlsson, Karl Æ.; Bertelsen, Mads F.; Haagensen, Mark; Chawana, Richard et al. (2015): In contrast to many other mammals, cetaceans have relatively small hippocampi that appear to lack adult neurogenesis. In *Brain Struct Funct* 220 (1), pp. 361–383. DOI: 10.1007/s00429-013-0660-1.

Penick, S.; Solomon, P. R. (1991): Hippocampus, context, and conditioning. In *Behavioral neuroscience* 105 (5), pp. 611–617. DOI: 10.1037//0735-7044.105.5.611.

Penttonen, Markku; Kamondi, Anita; Sik, Attila; Acsády, László; Buzsáki, György (1997): Feed-forward and feed-back activation of the dentate gyrus in vivo during dentate spikes and sharp wave bursts. In *Hippocampus* 7 (4), pp. 437–450. DOI: 10.1002/(SICI)1098-1063(1997)7:4<437::AID-HIPO9>3.0.CO;2-F.

Pilz, Gregor-Alexander; Carta, Stefano; Stäuble, Andreas; Ayaz, Asll; Jessberger, Sebastian; Helmchen, Fritjof (2016): Functional Imaging of Dentate Granule Cells in the Adult Mouse Hippocampus. In *J. Neurosci.* 36 (28), pp. 7407–7414. DOI: 10.1523/JNEUROSCI.3065-15.2016.

Pnevmatikakis, Eftychios A.; Giovannucci, Andrea (2017): NoRMCorre: An online algorithm for piecewise rigid motion correction of calcium imaging data. In *Journal of Neuroscience Methods* 291, pp. 83–94. DOI: 10.1016/j.jneumeth.2017.07.031.

Pnevmatikakis, Eftychios A.; Soudry, Daniel; Gao, Yuanjun; Machado, Timothy A.; Merel, Josh; Pfau, David et al. (2016): Simultaneous Denoising, Deconvolution, and Demixing of Calcium Imaging Data. In *Neuron* 89 (2), pp. 285–299. DOI: 10.1016/j.neuron.2015.11.037.

Pofahl, Martin; Nikbakht, Negar; Haubrich, André N.; Nguyen, Theresa; Masala, Nicola; Distler, Fabian et al. (2021): Synchronous activity patterns in the dentate gyrus during immobility. In *eLife* 10. DOI: 10.7554/eLife.65786.

Powell, Donald A.; Churchwell, John (2002): Mediodorsal thalamic lesions impair trace eyeblink conditioning in the rabbit. In *Learning & memory (Cold Spring Harbor, N.Y.)* 9 (1), pp. 10–17. DOI: 10.1101/lm.45302.

Pyapali, G. K.; Sik, A.; Penttonen, M.; Buzsaki, G.; Turner, D. A. (1998): Dendritic properties of hippocampal CA1 pyramidal neurons in the rat: Intracellular staining in vivo and in vitro. In *The Journal of comparative neurology* 391 (3), pp. 335–352. DOI: 10.1002/(SICI)1096-9861(19980216)391:3<335::AID-CNE4>3.0.CO;2-2.

Radic, Tijana; Al-Qaisi, Omar; Jungenitz, Tassilo; Beining, Marcel; Schwarzacher, Stephan W. (2015): Differential Structural Development of Adult-Born Septal Hippocampal Granule Cells in the Thy1-GFP Mouse, Nuclear Size as a New Index of Maturation. In *PloS one* 10 (8), e0135493. DOI: 10.1371/journal.pone.0135493.

Rolls, E. T. (2013a): A quantitative theory of the functions of the hippocampal CA3 network in memory. In *Front. Cell. Neurosci.* 7. DOI: 10.3389/fncel.2013.00098.

Rolls, Edmund T. (1996): A theory of hippocampal function in memory. In *Hippocampus* 6 (6), pp. 601–620. DOI: 10.1002/(SICI)1098-1063(1996)6:6<601::AID-HIPO5>3.0.CO;2-J.

Rolls, Edmund T. (2013b): The mechanisms for pattern completion and pattern separation in the hippocampus. In *Front. Syst. Neurosci.* 7, p. 74. DOI: 10.3389/fnsys.2013.00074.

Rolls, Edmund T. (2018): The storage and recall of memories in the hippocampo-cortical system. In *CELL AND TISSUE RESEARCH* 373 (3), pp. 577–604. DOI: 10.1007/s00441-017-2744-3.

Rolls, Edmund T.; Kesner, Raymond P. (2006): A computational theory of hippocampal function, and empirical tests of the theory. In *Progress in neurobiology* 79 (1), pp. 1–48. DOI: 10.1016/j.pneurobio.2006.04.005.

Ryou, J. W.; Cho, S. Y.; Kim, H. T. (2001): Lesions of the entorhinal cortex impair acquisition of hippocampal-dependent trace conditioning. In *Neurobiology of learning and memory* 75 (2), pp. 121–127. DOI: 10.1006/nlme.2000.3966.

Sakon, John J.; Suzuki, Wendy A. (2019): A neural signature of pattern separation in the monkey hippocampus. In *Proceedings of the National Academy of Sciences of the United States of America* 116 (19), pp. 9634–9643. DOI: 10.1073/pnas.1900804116.

Sasaki, Takuya; Piatti, Verónica C.; Hwaun, Ernie; Ahmadi, Siavash; Lisman, John E.; Leutgeb, Stefan; Leutgeb, Jill K. (2018): Dentate network activity is necessary for spatial working memory by supporting CA3 sharp-wave ripple generation and prospective firing of CA3 neurons. In *Nat Neurosci* 21 (2), pp. 258–269. DOI: 10.1038/s41593-017-0061-5.

Schade Powers, Alice; Coburn-Litvak, Pamela; Evinger, Craig (2010): Conditioned eyelid movement is not a blink. In *Journal of neurophysiology* 103 (2), pp. 641–647. DOI: 10.1152/jn.00631.2009.

Scharfman, H. E. (2007a): The dentate gyrus. A Comprehensive Guide to Structure, Function, and Clinical Implications (163).

Scharfman, Helen E. (2007b): The CA3 “backprojection” to the dentate gyrus. In : The Dentate Gyrus: A Comprehensive Guide to Structure, Function, and Clinical Implications, vol. 163: Elsevier (Progress in Brain Research), pp. 627–637.

Scharfman, Helen E. (2016): The enigmatic mossy cell of the dentate gyrus. In *NATURE REVIEWS NEUROSCIENCE* 17 (9), pp. 562–575. DOI: 10.1038/nrn.2016.87.

Scharfman, Helen E. (2018): Advances in understanding hilar mossy cells of the dentate gyrus. In *CELL AND TISSUE RESEARCH* 373 (3, SI), pp. 643–652. DOI: 10.1007/s00441-017-2750-5.

Schmaltz, L. W.; Theios, J. (1972): Acquisition and extinction of a classically conditioned response in hippocampectomized rabbits (Oryctolagus cuniculus). In *Journal of comparative and physiological psychology* 79 (2), pp. 328–333. DOI: 10.1037/h0032531.

Scoville, W. B.; Milner, B. (1957): Loss of recent memory after bilateral hippocampal lesions. In *Journal of neurology, neurosurgery, and psychiatry* 20 (1), pp. 11–21. DOI: 10.1136/jnnp.20.1.11.

Sears, L. L.; Logue, S. F.; Steinmetz, J. E. (1996): Involvement of the ventrolateral thalamic nucleus in rabbit classical eyeblink conditioning. In *BEHAVIOURAL BRAIN RESEARCH* 74 (1-2), pp. 105–117. DOI: 10.1016/0166-4328(96)00171-4.

Seki, M.; Kobayashi, C.; Takahashi, N.; Matsuki, N.; Ikegaya, Y. (2012): Synchronized spike waves in immature dentate gyrus networks. In *The European journal of neuroscience* 35 (5), pp. 673–681. DOI: 10.1111/j.1460-9568.2012.07995.x.

Senzai, Yuta; Buzsáki, György (2017): Physiological Properties and Behavioral Correlates of Hippocampal Granule Cells and Mossy Cells. In *Neuron* 93 (3), 691-704.e5. DOI: 10.1016/j.neuron.2016.12.011.

Shi, Yulin; Grieco, Steven F.; Holmes, Todd C.; Xu, Xiangmin (2019): Development of Local Circuit Connections to Hilar Mossy Cells in the Mouse Dentate Gyrus. In *eNeuro* 6 (2). DOI: 10.1523/ENEURO.0370-18.2019.

Shi, Yulin; Ikrar, Taruna; Olivas, Nicholas D.; Xu, Xiangmin (2014): Bidirectional global spontaneous network activity precedes the canonical unidirectional circuit organization in the developing hippocampus. In *The Journal of comparative neurology* 522 (9), pp. 2191–2208. DOI: 10.1002/cne.23528.

Shors, Tracey J.; Townsend, David A.; Zhao, Mingrui; Kozorovitskiy, Yevgenia; Gould, Elizabeth (2002): Neurogenesis may relate to some but not all types of hippocampal-dependent learning. In *Hippocampus* 12 (5), pp. 578–584. DOI: 10.1002/hipo.10103.

Sik, A.; Penttonen, M.; Buzsáki, G. (1997): Interneurons in the hippocampal dentate gyrus: an in vivo intracellular study. In *The European journal of neuroscience* 9 (3), pp. 573–588. DOI: 10.1111/j.1460-9568.1997.tb01634.x.

Sik, A.; Penttonen, M.; Ylinen, A.; Buzsáki, G. (1995): Hippocampal CA1 interneurons: an in vivo intracellular labeling study. In *The Journal of Neuroscience* 15 (10), pp. 6651–6665. DOI: 10.1523/JNEUROSCI.15-10-06651.1995.

Sik, A.; Ylinen, A.; Penttonen, M.; Buzsáki, G. (1994): Inhibitory CA1-CA3-hilar region feedback in the hippocampus. In *Science (New York, N.Y.)* 265 (5179), pp. 1722–1724. DOI: 10.1126/science.8085161.

Solomon, P. R.; Groccia-Ellison, M. E.; Flynn, D.; Mirak, J.; Edwards, K. R.; Dunehew, A.; Stanton, M. E. (1993): Disruption of human eyeblink conditioning after central cholinergic

blockade with scopolamine. In *Behavioral neuroscience* 107 (2), pp. 271–279. DOI: 10.1037//0735-7044.107.2.271.

Soltesz, I.; Bourassa, J.; Deschênes, M. (1993): The behavior of mossy cells of the rat dentate gyrus during theta oscillations in vivo. In *Neuroscience* 57 (3), pp. 555–564. DOI: 10.1016/0306-4522(93)90005-z.

Soriano, E.; Frotscher, M. (1989): A GABAergic axo-axonic cell in the fascia dentata controls the main excitatory hippocampal pathway. In *Brain research* 503 (1), pp. 170–174. DOI: 10.1016/0006-8993(89)91722-8.

Spalding, Kirsty L.; Bergmann, Olaf; Alkass, Kanar; Bernard, Samuel; Salehpour, Mehran; Huttner, Hagen B. et al. (2013): Dynamics of hippocampal neurogenesis in adult humans. In *CELL* 153 (6), pp. 1219–1227. DOI: 10.1016/j.cell.2013.05.002.

Squire, Larry R. (1998): Memory systems. In *Comptes Rendus de l'Académie des Sciences - Series III - Sciences de la Vie* 321 (2-3), pp. 153–156. DOI: 10.1016/s0764-4469(97)89814-9.

Squire, Larry R. (2004): Memory systems of the brain: A brief history and current perspective. In *Neurobiology of learning and memory* 82 (3), pp. 171–177. DOI: 10.1016/j.nlm.2004.06.005.

Steinmetz, Adam B.; Harmon, Thomas C.; Freeman, John H. (2013): Visual cortical contributions to associative cerebellar learning. In *Neurobiology of learning and memory* 104, pp. 103–109. DOI: 10.1016/j.nlm.2013.06.005.

Steinmetz, J. E. (2000): Brain substrates of classical eyeblink conditioning: a highly localized but also distributed system. In *BEHAVIOURAL BRAIN RESEARCH* 110 (1-2), pp. 13–24. DOI: 10.1016/s0166-4328(99)00181-3.

Steward, O.; Scoville, S. A. (1976): Cells of origin of entorhinal cortical afferents to the hippocampus and fascia dentata of the rat. In *The Journal of comparative neurology* 169 (3), pp. 347–370. DOI: 10.1002/cne.901690306.

Strange, B. A.; Fletcher, P. C.; Henson, R. N.; Friston, K. J.; Dolan, R. J. (1999): Segregating the functions of human hippocampus. In *Proceedings of the National Academy of Sciences of the United States of America* 96 (7), pp. 4034–4039. DOI: 10.1073/pnas.96.7.4034.

Strange, B. A.; Witter, M. P.; Lein, E. S.; Moser, E. I. (2014): Functional organization of the hippocampal longitudinal axis. In *NATURE REVIEWS NEUROSCIENCE* 15 (10), pp. 655–669. DOI: 10.1038/nrn3785.

Struble, R. G.; Desmond, N. L.; Levy, W. B. (1978): Anatomical evidence for interlamellar inhibition in the fascia dentata. In *Brain research* 152 (3), pp. 580–585. DOI: 10.1016/0006-8993(78)91113-7.

Sun, Yanjun; Grieco, Steven F.; Holmes, Todd C.; Xu, Xiangmin (2017): Local and Long-Range Circuit Connections to Hilar Mossy Cells in the Dentate Gyrus. In *eNeuro* 4 (2), ENEURO.0097-17.2017. DOI: 10.1523/ENEURO.0097-17.2017.

Suter, Eugénie E.; Weiss, Craig; Disterhoft, John F. (2013): Perirhinal and postrhinal, but not lateral entorhinal, cortices are essential for acquisition of trace eyeblink conditioning. In *Learning & memory (Cold Spring Harbor, N.Y.)* 20 (2), pp. 80–84. DOI: 10.1101/lm.028894.112.

Suter, Eugénie E.; Weiss, Craig; Disterhoft, John F. (2018): Differential responsivity of neurons in perirhinal cortex, lateral entorhinal cortex, and dentate gyrus during time-bridging learning. In *Hippocampus* 29 (6), pp. 511–526. DOI: 10.1002/hipo.23041.

Swaminathan, Aarti; Wichert, Ines; Schmitz, Dietmar; Maier, Nikolaus (2018): Involvement of Mossy Cells in Sharp Wave-Ripple Activity In Vitro. In *Cell reports* 23 (9), pp. 2541–2549. DOI: 10.1016/j.celrep.2018.04.095.

Swanson, L. W. (1977): The anatomical organization of septo-hippocampal projections. In *Ciba Foundation symposium* (58), pp. 25–48. DOI: 10.1002/9780470720394.ch4.

Swanson, L. W.; Wyss, J. M.; Cowan, W. M. (1978): An autoradiographic study of the organization of intrahippocampal association pathways in the rat. In *The Journal of comparative neurology* 181 (4), pp. 681–715. DOI: 10.1002/cne.901810402.

Szabo, Gergely G.; Du, Xi; Oijala, Mikko; Varga, Csaba; Parent, Jack M.; Soltesz, Ivan (2017): Extended Interneuronal Network of the Dentate Gyrus. In *Cell reports* 20 (6), pp. 1262–1268. DOI: 10.1016/j.celrep.2017.07.042.

Takehara, Kaori; Kawahara, Shigenori; Kirino, Yutaka (2003): Time-dependent reorganization of the brain components underlying memory retention in trace eyeblink conditioning. In *J. Neurosci.* 23 (30), pp. 9897–9905. DOI: 10.1523/JNEUROSCI.23-30-09897.2003.

Takehara, Kaori; Kawahara, Shigenori; Takatsuki, Kanako; Kirino, Yutaka (2002): Time-limited role of the hippocampus in the memory for trace eyeblink conditioning in mice. In *Brain research* 951 (2), pp. 183–190. DOI: 10.1016/s0006-8993(02)03159-1.

Takehara-Nishiuchi, Kaori (2018): The Anatomy and Physiology of Eyeblink Classical Conditioning. In *Current topics in behavioral neurosciences* 37, pp. 297–323. DOI: 10.1007/7854_2016_455.

Takehara-Nishiuchi, Kaori; Kawahara, Shigenori; Kirino, Yutaka (2005): NMDA receptor-dependent processes in the medial prefrontal cortex are important for acquisition and the early stage of consolidation during trace, but not delay eyeblink conditioning. In *Learning & memory (Cold Spring Harbor, N.Y.)* 12 (6), pp. 606–614. DOI: 10.1101/lm.5905.

Tanninen, Stephanie E.; Yu, XiaoTian; Giritharan, Thamy; Tran, Lina; Bakir, Rami; Volle, Julien et al. (2015): Cholinergic, but not NMDA, receptors in the lateral entorhinal cortex mediate acquisition in trace eyeblink conditioning. In *Hippocampus* 25 (11), pp. 1456–1464. DOI: 10.1002/hipo.22466.

Terada, Satoshi; Geiller, Tristan; Liao, Zhenrui; O'Hare, Justin; Vancura, Bert; Losonczy, Attila (2022): Adaptive stimulus selection for consolidation in the hippocampus. In *Nature* 601 (7892), pp. 240–244. DOI: 10.1038/s41586-021-04118-6.

Tolman, E. C. (1948): Cognitive maps in rats and men. In *Psychological review* 55 (4), pp. 189–208. DOI: 10.1037/h0061626.

Treves, A.; Tashiro, A.; Witter, M. P.; Moser, E. I. (2008): What is the mammalian dentate gyrus good for? In *Neuroscience* 154 (4), pp. 1155–1172. DOI: 10.1016/j.neuroscience.2008.04.073.

Tseng, W.; Guan, R.; Disterhoft, J. F.; Weiss, C. (2004): Trace eyeblink conditioning is hippocampally dependent in mice. In *Hippocampus* 14 (1), pp. 58–65. DOI: 10.1002/hipo.10157.

van Dijk, Milenna Tamara; Fenton, André Antonio (2018): On How the Dentate Gyrus Contributes to Memory Discrimination. In *Neuron* 98 (4), 832-845.e5. DOI: 10.1016/j.neuron.2018.04.018.

Vertes, Robert P.; McKenna, James Timothy (2000): Collateral projections from the supramammillary nucleus to the medial septum and hippocampus. In *Synapse* 38 (3), pp. 281–293. DOI: 10.1002/1098-2396(20001201)38:3<281::AID-SYN7>3.0.CO;2-6.

Vivar, Carmen; Potter, Michelle C.; Choi, Jiwon; Lee, Ji-young; Stringer, Thomas P.; Callaway, Edward M. et al. (2012): Monosynaptic inputs to new neurons in the dentate gyrus. In *Nat Commun* 3 (1). DOI: 10.1038/ncomms2101.

Walker, Adam G.; Steinmetz, Joseph E. (2008): Hippocampal lesions in rats differentially affect long- and short-trace eyeblink conditioning. In *Physiology & behavior* 93 (3), pp. 570–578. DOI: 10.1016/j.physbeh.2007.10.018.

Wang, Cheng; Chen, Xiaojing; Lee, Heekyung; Deshmukh, Sachin S.; Yoganarasimha, D.; Savelli, Francesco; Knierim, James J. (2018): Egocentric coding of external items in the lateral entorhinal cortex. In *Science (New York, N.Y.)* 362 (6417), pp. 945–949. DOI: 10.1126/science.aau4940.

Wang, J.; Bast, T.; Wang, Y. C.; Zhang, W. N. (2015): Hippocampus and Two-Way Active Avoidance Conditioning: Contrasting Effects of Cytotoxic Lesion and Temporary Inactivation. In *Hippocampus* 25 (12), pp. 1517–1531. DOI: 10.1002/hipo.22471.

Weible, A. P.; McEchron, M. D.; Disterhoft, J. F. (2000): Cortical involvement in acquisition and extinction of trace eyeblink conditioning. In *Behavioral neuroscience* 114 (6), pp. 1058–1067. DOI: 10.1037//0735-7044.114.6.1058.

Weiss, C.; Bouwmeester, H.; Power, J. M.; Disterhoft, J. F. (1999): Hippocampal lesions prevent trace eyeblink conditioning in the freely moving rat. In *BEHAVIOURAL BRAIN RESEARCH* 99 (2), pp. 123–132. DOI: 10.1016/s0166-4328(98)00096-5.

White, I. M.; Miller, D. P.; White, W.; Dike, G. L.; Rebec, G. V.; Steinmetz, J. E. (1994): Neuronal activity in rabbit neostriatum during classical eyelid conditioning. In *Experimental brain research* 99 (2), pp. 179–190. DOI: 10.1007/BF00239585.

Wilson, Donald A. (2009): Pattern separation and completion in olfaction. In *Annals of the New York Academy of Sciences* 1170, pp. 306–312. DOI: 10.1111/j.1749-6632.2009.04017.x.

Witter, M. P.; Groenewegen, H. J.; Da Lopes Silva, F. H.; Lohman, A. H. (1989): Functional organization of the extrinsic and intrinsic circuitry of the parahippocampal region. In *Progress in neurobiology* 33 (3), pp. 161–253. DOI: 10.1016/0301-0082(89)90009-9.

Witter, Menno P. (2007a): Intrinsic and extrinsic wiring of CA3: indications for connectional heterogeneity. In *Learning & memory (Cold Spring Harbor, N.Y.)* 14 (11), pp. 705–713. DOI: 10.1101/lm.725207.

Witter, Menno P. (2007b): The perforant path: projections from the entorhinal cortex to the dentate gyrus. In H. E. Scharfman (Ed.): DENTATE GYRUS: A COMPHREHENSIVE GUIDE TO STRUCTURE, FUNCTION, AND CLINICAL IMPLICATIONS, vol. 163. SARA BURGERHARTSTRAAT 25, PO BOX 211, 1000 AE AMSTERDAM, NETHERLANDS: ELSEVIER SCIENCE BV (Progress in Brain Research), pp. 43–61.

Wittner, Lucia; Henze, Darrell A.; Záborszky, László; Buzsáki, György (2007): Three-dimensional reconstruction of the axon arbor of a CA3 pyramidal cell recorded and filled in vivo. In *Brain Struct Funct* 212 (1), pp. 75–83. DOI: 10.1007/s00429-007-0148-y.

Wood, E. R.; Dudchenko, P. A.; Eichenbaum, H. (1999): The global record of memory in hippocampal neuronal activity. In *Nature* 397 (6720), pp. 613–616. DOI: 10.1038/17605.

Woodruff-Pak, Diana S.; Disterhoft, John F. (2008): Where is the trace in trace conditioning? In *Trends in neurosciences* 31 (2), pp. 105–112. DOI: 10.1016/j.tins.2007.11.006.

Woods, Nicholas I.; Stefanini, Fabio; Apodaca-Montano, Daniel L.; Tan, Isabelle M. C.; Biane, Jeremy S.; Kheirbek, Mazen A. (2020): The Dentate Gyrus Classifies Cortical Representations of Learned Stimuli. In *Neuron* 107 (1), 173-184.e6. DOI: 10.1016/j.neuron.2020.04.002.

Wyss, J. M.; Swanson, L. W.; Cowan, W. M. (1979): Evidence for an input to the molecular layer and the stratum granulosum of the dentate gyrus from the supramammillary region of the hypothalamus. In *Anat Embryol* 156 (2), pp. 165–176. DOI: 10.1007/BF00300012.

X.-G. Li, P. Somogyi, A. Ylinen, AND G. Buzsáki (1994): The hippocampal CA3 network: An in vivo intracellular labeling study. In *The Journal of comparative neurology*.

Xu, X. M.; Sun, Y. J.; Holmes, T. C.; Lopez, A. J. (2016): Noncanonical Connections Between the Subiculum and Hippocampal CA1. In *The Journal of comparative neurology* 524 (17), pp. 3666–3673. DOI: 10.1002/cne.24024.

Yeo, C. H.; Hesslow, G. (1998): Cerebellum and conditioned reflexes. In *TRENDS IN COGNITIVE SCIENCES* 2 (9), pp. 322–330. DOI: 10.1016/s1364-6613(98)01219-4.

Young, B. J.; Fox, G. D.; Eichenbaum, H. (1994): Correlates of hippocampal complex-spike cell activity in rats performing a nonspatial radial maze task. In *The Journal of Neuroscience* 14 (11 Pt 1), pp. 6553–6563. DOI: 10.1523/JNEUROSCI.14-11-06553.1994.

Yu, C. L.; Li, J. N.; Gan, P.; Wang, L. P.; Yang, Y. X.; Yu, D. F. et al. (2021): Developing of Focal Ischemia in the Hippocampus or the Amygdala Reveals a Regional Compensation Rule for FearMemory Acquisition. In *eNeuro* 8 (2). DOI: 10.1523/ENEURO.0398-20.2021.

Zhang, Xiaomin; Schlögl, Alois; Jonas, Peter (2020): Selective Routing of Spatial Information Flow from Input to Output in Hippocampal Granule Cells. In *Neuron* 107 (6), 1212-1225.e7. DOI: 10.1016/j.neuron.2020.07.006.